Utah State University

DigitalCommons@USU

All Graduate Theses and Dissertations | Graduate Studies

5-2016

A Spatiotemporal Mountain Pine Beetle Outbreak Model Predicting Severity, Cycle Period, and Invasion Speed

Jacob P. Duncan
Utah State University

Follow this and additional works at: https://digitalcommons.usu.edu/etd

 Part of the Ecology and Evolutionary Biology Commons, and the Mathematics Commons

Recommended Citation

Duncan, Jacob P., "A Spatiotemporal Mountain Pine Beetle Outbreak Model Predicting Severity, Cycle Period, and Invasion Speed" (2016). *All Graduate Theses and Dissertations*. 4729.
https://digitalcommons.usu.edu/etd/4729

This Dissertation is brought to you for free and open access by the Graduate Studies at DigitalCommons@USU. It has been accepted for inclusion in All Graduate Theses and Dissertations by an authorized administrator of DigitalCommons@USU. For more information, please contact digitalcommons@usu.edu.

A SPATIOTEMPORAL MOUNTAIN PINE BEETLE OUTBREAK MODEL

PREDICTING SEVERITY, CYCLE PERIOD, AND INVASION SPEED

by

Jacob P. Duncan

A dissertation submitted in partial fulfillment
of the requirements for the degree

of

DOCTOR OF PHILOSOPHY

in

Mathematical Sciences

Approved:

James Powell Major Professor	Brynja Kohler Committee Member
Luis Gordillo Committee Member	Barbara Bentz Committee Member
Nghiem Nguyen Committee Member	Mark McLellan Vice President of Research Dean of Graduate Studies

UTAH STATE UNIVERSITY
Logan, Utah

2016

Copyright © Jacob P. Duncan 2016

All Rights Reserved

ABSTRACT

A Spatiotemporal Mountain Pine Beetle Outbreak Model

Predicting Severity, Cycle Period, and Invasion Speed

by

Jacob P. Duncan, Doctor of Philosophy

Utah State University, 2016

Major Professor: Dr. James Powell
Department: Mathematics and Statistics

The mountain pine beetle (MPB, *Dendroctonus ponderosae*), a tree-killing bark beetle, has historically been part of the normal disturbance regime in lodgepole pine (*Pinus contorta*) forests. In recent years, warm winters and summers have allowed MPB populations to achieve synchronous emergence and successful attacks, resulting in widespread population outbreaks and resultant tree mortality across western North America. We develop an age-structured forest demographic model that incorporates temperature-dependent MPB infestations: the Susceptible-Infested-Juvenile (SIJ) model. Stability of fixed points is analyzed as a function of population growth rates, and indicates the existence of periodic outbreaks that intensify as growth rates increase. We devise analytical methods to predict outbreak severity and duration as well as outbreak return time.

To assess the vulnerability of natural resources to climate change, we develop a thermally-driven mechanistic model to predict MPB population growth rates using a distributional model of beetle phenology in conjunction with criteria for successful tree colonization. The model uses projected daily minimum and maximum temperatures for the years 2025 to 2085 generated by three separate global climate models. Growth rates are calculated each year for an area defined by latitude range 42° N to 49° N and longitude range 108° W to 117° W on a Cartesian grid of approximately 4km

resolution. Using these growth rates, we analyze how the optimal thermal window for beetle development is changing with respect to elevation as a result of climate change induced warming. We also use our combined model to evaluate if thermal regimes exist that would promote life cycle bivoltinism and discuss how yearly growth rates would change as a result.

Outbreaks of MPB are largely driven by host tree stand demographics and spatial effects of beetle dispersal. We augment the SIJ model to account for the spatial effects of MPB dispersal throughout a forest landscape by coupling it with a Gaussian redistribution kernel. The new model generates a train of sustained solitary waves of infestation that move through a forest with constant speed. We convert the resulting integrodifference equation into a partial differential equation and search for travelling wave solutions. The resulting differential equation provides predictions of the shape of an outbreak wave profile and of peak infestation as functions of wave speed, which can be calculated analytically. These results culminate in the derivation of an explicit formula for predicting the severity of an outbreak based on the net reproductive rate of MPB and host searching efficiency.

(152 pages)

PUBLIC ABSTRACT

A Spatiotemporal Mountain Pine Beetle Outbreak Model

Predicting Severity, Cycle Period, and Invasion Speed

by

Jacob P. Duncan, Doctor of Philosophy

Utah State University, 2016

Major Professor: Dr. James Powell
Department: Mathematics and Statistics

The mountain pine beetle (MPB, *Dendroctonus ponderosae*), a tree-killing bark beetle, has historically been part of the normal disturbance regime in lodgepole pine (*Pinus contorta*) forests. In recent years, warm winters and summers have allowed MPB populations to achieve synchronous emergence and successful attacks, resulting in widespread population outbreaks and resultant tree mortality across western North America. We develop an age-structured forest demographic model that incorporates temperature-dependent MPB infestations: the Susceptible-Infested-Juvenile (SIJ) model. Stability of equilibria is analyzed as a function of population growth rates, and indicates the existence of periodic outbreaks that intensify as growth rates increase. We devise methods to predict outbreak severity and duration as well as outbreak return time.

To assess the vulnerability of natural resources to climate change, we develop a thermally-driven mechanistic model to predict MPB population growth rates using a distributional model of beetle phenology in conjunction with criteria for successful tree colonization. The model uses projected daily minimum and maximum temperatures for the years 2025 to 2085 generated by three separate global climate models. Growth rates are calculated each year for an area defined by latitude range 42° N to 49° N and longitude range 108° W to 117° W on a rectangular grid with approximately 4km

resolution. Using these growth rates, we analyze how the optimal thermal window for beetle development is changing with respect to elevation as a result of climate change induced warming. We also use our combined model to evaluate if thermal regimes exist that would promote two generations per year and discuss how yearly growth rates would change as a result.

Outbreaks of MPB are largely driven by host tree stand demographics and spatial effects of beetle dispersal. We augment the SIJ model to account for the spatial effects of MPB dispersal throughout a forest landscape by coupling it with a probability distribution for beetle location after dispersal. The new model generates a train of solitary waves of infestation that move through a forest with constant speed. We move from a discrete to a continuous modelling framework and search for travelling wave solutions which results in predictions of the shape of an outbreak wave profile and of peak infestation as functions of wave speed, which can be calculated analytically. These results culminate in the derivation of an explicit formula for predicting the severity of an outbreak based on the net reproductive rate of MPB and host searching efficiency.

(152 pages)

ACKNOWLEDGMENTS

I would like to thank my advisor, James Powell, for his generous academic, research, and financial support throughout the course of my PhD program. I have grown more intellectually and professionally in the last four years than in all my previous years combined on account of his guidance in refining my mathematical thinking, and approaches to research and teaching. Barbara Bentz deserves a special thanks for sharing her entomology/forest-ecology expertise and for giving me field experience opportunities. Many thanks to USU Mathematical Biology professors Luis Gordillo, Brynja Kohler, and Michael Cortez for help and support provided in my research.

Immeasurable thanks and gratitude is owed my wife Michelle for her full and continuous support, and without whom none of this work would have been possible. I am forever grateful to you Michelle. Thanks to my Mom for moral support and letting me teach her the quadratic formula circa 1998. Thanks to my Dad for his moral and financial support, and for teaching me Ohm's law and building a homemade electromagnet-telegraph with me for the fourth grade science fair. My interest in math and science began with and was strengthened by Uncle Tim showing me the "fractal video", *Fermat's Last Theorem* from Uncle Bill, and the star machine from Uncle Rick. Finally, for their contributions in sparking my scientific curiosity, thanks to Grandpa Schwartz for showing me the inner workings of the telephone company switching system, and to Grandpa Duncan for teaching me some trigonometry in surveying the Grace Lake property. You all are as much a part of this accomplishment as I.

Jacob Duncan

Contents

LIST OF TABLES

LIST OF FIGURES

Chapter 1

INTRODUCTION

Outbreaks of the phytophagous mountain pine beetle (*Dendroctonus ponderosae*) have significant detrimental impacts on forest ecosystems as well as potentially severe economic effects. Mountain pine beetle (MPB) can cause millions of acres of pine tree mortality and millions of dollars in damages over the course of a single outbreak. Current outbreaks are responsible for elevated mortality in pine forests across the western United States and Canada (Meddens et al., 2012), generating a high volume of fuel and increased potential for forest fires. A mathematical formulation of the biological mechanisms responsible for infestation epidemics is paramount in predicting the severity and frequency of outbreaks based on environmental parameters. These predictions can provide forest managers with useful information to guide management strategies in mitigating the negative effects of outbreaks.

Until recently, MPB has played a natural role in forest succession, removing aged and decrepit trees which accelerated the development of a more vibrant forest. Although outbreaks of MPB have historically been normative (Mattson, 1996) in lodgepole pine (*Pinus contorta*) forests, recent outbreaks have been far more severe and expansive than in previous decades due in part to warming climate (Bentz et al., 2010). Warmer annual minimum temperatures have increased the destructive outbreak insects' overwintering survival and furthermore, allowed for survival at higher than normal elevation in MPB-vulnerable five-needle pine tree habitats (Weed et al., 2015).

Some species of conifers have evolved significant defensive responses to bark beetle attacks such as the secretion of resin to impede a beetle's ability to bore into a host tree (Amman and Cole, 1983). It is necessary for MPB to mass attack a tree to successfully overcome these anti-predator adaptations (Berryman et al., 1985). Therefore, beetles must emerge from host trees nearly simultaneously to achieve such a high-density rapid attack. MPB are poikilothermic and as such, the ability to achieve synchronous emergence is a direct function of temperature (Bentz et al., 1991; Safranyik et al., 1975).

Thus, increasing temperatures due to global climate change are a significant factor in explaining the elevated severity of recent outbreaks. Furthermore, temperature variation throughout the life history of MPB plays a major role in determining adult emergence numbers and timing (Bentz et al., 2014). Higher, more temporally concentrated adult MPB emergence translates to higher population growth rates which can have disastrous effects on pine forest ecosystems.

MPB population growth rates have a direct effect on the severity of outbreaks in terms of total host tree mortality (Duncan et al., 2015). Growth rates depend on the seasonal efficiency with which individuals develop and progress through the stages of their life history. As ectotherms, MPB developmental rates in various life stages are dictated almost exclusively by temperature. Several thermally-driven phenological models have been constructed that predict development times for life stage emergence (Bentz et al., 1991; Bentz and Mullens, 1999; Powell et al., 2000; Gilbert et al., 2004). Powell and Bentz (2009) used a distributional model of MPB phenology to generate adult emergence time distributions from hourly tree phloem temperatures. They connected the temperature-dependent phenology model to a mathematical description of criteria for successful infestation and colonization of a tree. Based on the number of trees successfully infested in a certain year and in the following year, they estimated the MPB population growth rate for that year. However, this mechanistic approach has not yet been applied in future climate scenarios to assess potential outbreak damage in forests at the landscape level across elevational gradients.

Population growth rates have a direct effect on the spatial spread of infestation. There is a clear analogy between waves of disease in human and animal populations (Anderson and May, 1979a,b, 1982) and waves of infestation in forests; an extensive literature on infectious disease models with demographic structure also exists (Hethcote, 1994, 2000; Keeling, 1999; Riley, 2007). Heavilin et al. (2007) and Heavilin and Powell (2008) built several MPB outbreak models in the spirit of the classic SIR (Susceptible - Infected - Recovered) infectious disease model (Kermack and McKendrick, 1927). Generally speaking, the intensity of an outbreak wave depends on factors set at the beginning of the wave: number of susceptible individuals, infectivity of the disease, and removal rate of infected individuals. Recovery time between outbreaks depends on how rapidly the birth rate can repopulate the susceptible class of individuals to a level that allows for exponential growth of infectives.

Though class structured, these epidemiological models fall short of capturing the long recovery period of a forest affected by a MPB outbreak. A stand of pines is considered recovering when most trees are juvenile and not large enough to facilitate successful MPB infestation. It takes 50 to 100 years for a lodgepole pine to reach sufficient size to be susceptible to MPB attack. The models of Heavilin et al. (2007), for instance, have just one juvenile latency compartment. In order to model the dynamics of a cycle with an extended recovery period and make realistic predictions of outbreak severity, it is necessary to incorporate several latency classes.

Along with temperature-dependent phenology and host tree stand demographic structure, a primary driver of the irruptive nature of MPB population dynamics is the spatial effect of beetle dispersal (Bjornstad et al., 2002; Aukema et al., 2008). While the models of Heavilin and Powell (2008) are successful in capturing the advance of infestation across a forest landscape by addressing MPB dispersal, their model-generated waves of infected trees do not persist indefinitely as in realistic forests. Abramson et al. (2003), who modeled the spread of the hantavirus infection in deer mice using a continuous SIR type epidemiological model coupled with a diffusion term for spatial dispersal of infectives, showed that travelling waves of infection can persist indefinitely. However, a continuous (e.g. differential equation) model is not appropriate for insect infestations on account of the discrete nature of insect life cycles. In particular, MPB typically completes one generation per year which necessitates discrete-time modelling with difference equations.

There is a substantial amount of literature proving the existence of travelling waves generated by disease outbreak models (for example, Ruan and Xiao (2004)). On the other hand, methods for predicting the impact of a propagating wave on hosts are few. The speed of an invading wave of infestation plays a critical role in determining the intensity of an outbreak. Kot et al. (1996) as well as Neubert and Caswell (1996) have discussed methods for calculating invasion speeds for unstructured and structured invasive populations respectively. Sherratt (1994, 1998) derived explicit predictions of the amplitude and speed of periodic (invasion) wave trains generated by oscillatory reaction-diffusion equations. However, methods for predicting the intensity of travelling periodic invasion waves arising from structured discrete-time demographic models conjoined with continuous-space dispersal components have not hitherto been developed.

In chapter two of this dissertation we construct a system of difference equations that model the populations of trees susceptible to MPB colonization, infested trees, and

age classes of juvenile trees which are not susceptible to MPB attacks: the Susceptible - Infested - Juvenile (SIJ) model. The system has a trivial fixed point (no infestation) and a fixed point corresponding to an incipient epidemic. Stability analysis (as a function of MPB population growth rate) reveals that the incipient epidemic fixed point is a center for periodic orbits which is consistent with periodic irruptive population behavior exhibited by MPB. We divide a cycle into components of MPB outbreak and forest recovery which can be approximated temporally to construct an estimate of cycle duration. We then develop an analytic approximation of infestation with time and use it to define three measures of outbreak severity - maximum infestation, total infestation, and outbreak duration - and devise approximations for each.

Chapter three examines the potential impact of MPB populations on pine forests under future climate scenarios by predicting yearly population growth rates from climate model projected temperature signals. We develop a thermally-driven model (the R-model) for predicting population growth rates for decades of climate model projected temperature signals over an area in the northern U.S. Rocky Mountains. Our mechanistic R-model predicts growth rates using a distributional model of beetle phenology (Sharpe et al., 1977) with specific life stage developmental rate functions developed in Régnière et al. (2012) in conjunction with the criteria for successful infestation and colonization of trees outlined by Powell and Bentz (2009). Daily minimum and maximum temperatures were obtained for the years 2025 to 2085 using Multivariate Adaptive Constructed Analogs (MACA) statistical downscaling method (Abatzoglou and Brown, 2013; Abatzoglou, 2013). Projected future temperatures were generated using three separate global climate models each with two different emissions scenario representative concentration pathways (Vuuren et al., 2011; Thomson et al., 2011).

We calculate MPB growth rates each year for an area defined by latitude range 42° N to 49° N and longitude range 108° W to 117° W on a Cartesian grid of approximately 4km resolution. Using these growth rates, we analyze how the optimal thermal window for MPB development is changing with respect to elevation as a result of climate change induced warming. We also use our combined model to evaluate if thermal regimes exist that would allow for bivoltine life cycles (two generations per year) and discuss how yearly growth rates would change as a result.

Finally, in the fourth chapter we augment our existing SIJ model to account for the spatial effects of MPB dispersal throughout a forest landscape. The structured demographic SIJ model becomes a system of integrodifference equations upon coupling

it with a Gaussian redistribution kernel to emulate MPB dispersal each summer in their search for new susceptible host trees. Redistributing MPB across a landscape in which previously infested trees may not be reinfested for 50 to 100 years (via mortality and seedling regrowth to susceptible size) generates a train of sustained solitary waves of infestation that move through a forest with constant speed. At a stationary point in the forest, a passing wave manifests temporally as an outbreak at the stand level.

We use a WKB approximation in conjunction with the method of steepest descent to evaluate the convolution integral in the IDE for infested trees. This enables a transition to a continuous setting by converting the resulting difference equation to a second order nonlinear partial differential equation (PDE). A search for travelling wave solutions of the PDE results in predictions of the shape of an outbreak wave profile and of its peak (maximum infestation) as functions of the speed of the wave. Following an approach similar to that of Neubert and Caswell (1996), we calculate an estimate of the rate of invasion that depends solely on model parameters. We are left with an explicit formula for predicting the severity of an outbreak based on MPB population growth rate and host searching efficiency. This prediction compares favorably with peak impact observations taken during a recent outbreak in the Sawtooth National Recreation Area (SNRA) of central Idaho.

Chapter 2

A MODEL FOR MOUNTAIN PINE BEETLE OUTBREAKS IN AN AGE-STRUCTURED FOREST: PREDICTING SEVERITY AND OUTBREAK-RECOVERY CYCLE PERIOD

2.1 Introduction

The mountain pine beetle (*Dendroctonus ponderosae*) is an aggressive, tree killing beetle whose hosts span the genus *Pinus*. Some species of conifers have evolved significant defensive responses to bark beetle attacks such as the secretion of resin to impede a beetle's ability to bore into a host tree (Amman and Cole, 1983). It is necessary for mountain pine beetle (MPB) to mass attack a tree to successfully overcome these anti-predator adaptations (Berryman et al., 1985). Therefore, beetles must emerge from host trees nearly simultaneously to achieve such a high-density rapid attack. MPB are poikilothermic and as such, the ability to achieve synchronous emergence is a direct function of temperature (Safranyik et al., 1975; Bentz et al., 1991). Increasing temperatures due to global climate change are a significant factor in explaining why outbreaks of MPB have been severe and expansive in recent decades (Bentz et al., 2010). While MPB outbreaks constitute a natural disturbance regime for forests, recent outbreaks are responsible for elevated mortality in lodgepole pine tree (*Pinus contorta*) forests across the western United States and Canada (Meddens et al., 2012), generating a high volume of fuel and increased potential for forest fires. Furthermore, it is predicted that the current MPB outbreak in Canada will release 270 megatons of carbon dioxide into the atmosphere (Kurz et al., 2008). This is a substantial contribution to the greenhouse effect and subsequently to warmer average temperatures, which played a role in triggering the outbreak to begin with.

It is natural to think of MPB outbreak-recovery cycles observed in forests across western North America as "waves of disease" (Anderson and May, 1979a,b, 1982). Heavilin et al. (2007) and Heavilin and Powell (2008) constructed several "red-top" models in the spirit of the classic SIR (Susceptible-Infected-Recovered) infectious disease model

(Kermack and McKendrick, 1927). Generally speaking, the intensity of an outbreak wave depends on factors set at the beginning of the wave: number of susceptible individuals, infectivity of the disease, and removal rate of infected individuals. Recovery time between outbreaks depends on how rapidly the birth rate can repopulate the susceptible class of individuals to a level that allows for exponential growth of infectives.

These models, however, fall short of capturing the long recovery period of a forest affected by a MPB outbreak. A stand of pines is considered recovering when most trees are juvenile and not large enough to facilitate successful MPB infestation. It takes 50 to 100 years for a lodgepole pine to reach sufficient size to be susceptible to MPB attack. Heavilin's red-top models have just one juvenile latency compartment. In order to model the dynamics of a cycle with an extended recovery period and make realistic predictions of outbreak severity, it is necessary to incorporate several latency classes. Our model makes use of a Leslie matrix (Leslie, 1945) to endow a lodgepole pine stand with age structure thereby eliminating the problem of an insufficiently long recovery time.

The ability to predict when an outbreak will occur, how long it will last, and the expected number of trees killed is crucial for forest management and understanding the biological impacts of warming climate. To date, methods for predicting such values/quantities do not exist. In this paper we construct a system of difference equations that model the populations of trees infested by MPB, healthy uninfested trees, and age classes of juvenile trees which are not susceptible to MPB attacks.

The system has a trivial fixed point (no infestation) and a fixed point corresponding to an incipient epidemic. Stability analysis (as a function of MPB population growth rate) reveals that this incipient epidemic fixed point is a center for periodic orbits which is consistent with periodic irruptive population behavior exhibited by MPB. We divide a cycle into components of MPB outbreak and forest recovery which can be approximated temporally to construct an estimate of cycle duration. We develop an analytic approximation of infestation with time and use it to define three measures of outbreak severity - maximum infestation, total infestation, and outbreak duration - and devise accurate approximations for each.

Powell and Bentz (2009) showed that the infectivity of MPB depends directly on yearly temperatures at an hourly scale. Their method for predicting MPB growth rates (and therefore infectivity) we call the R-model. The R-model is based on a distributional (cohort) model for MPB phenology (Sharpe et al., 1977) and in particular, specific

life stage developmental rates as functions of temperature (Régnière et al., 2012). Using historical daily temperatures together with projected future temperatures obtained from Multivariate Adaptive Constructed Analogs (MACA) for the Sawtooth National Recreation Area (SNRA), the R-model generates MPB growth rates for each year from 1950 to 2100. Using these growth rates, we predict potential severity of future outbreaks reflecting the effects of changing climate.

Finally, since our model overestimates the outbreak cycle period when compared to observations, we explore possible mechanisms for lowering predicted cycle period including spatial variability, demographic variability, infestation forcing, and parametric variation and forcing. A spatial component is added by allowing for disjunct, weakly coupled lodgepole pine stands. We find that incorporating spatial variability can produce outbreak frequencies in the range of observed values. Variability in initial stand demographic produces age cohorts that double outbreak frequency. Realistic outbreak-recovery cycle periods can also be produced by adding constant infestation forcing.

2.2 Model Development and Dynamics

MPB lays its eggs in the phloem layer of pine trees. Adult attack of live trees and egg-laying typically occurs in mid to late summer. Eggs hatch and the larvae feed on the phloem while developing into mature MPB, which eventually results in the death of the host tree (Amman and Schmitz, 1988). As the tree dies, needles turn red (these trees are called "red tops" or "red snags") by the following summer when MPB emerge and begin searching for new hosts. Two to three years later, needles turn gray ("gray snags") and begin to fall off the tree. Lodgepole pine trees are shade intolerant and therefore need light to regenerate. Like other early succession species, regeneration often occurs following a disturbance, such as a MPB outbreak or fire. The death of trees opens up the forest floor to sunlight and frees up resources previously unavailable to seedlings (Schmidt and Alexander, 1985).

Below we present a structured model for forest infestation, including susceptibles, snags, and nonsusceptible juveniles, with birth rates proportional to space freed up for seedlings as snags lose their needles and juveniles succumb to natural mortality.

2.2.1 Host Tree Demographics

MPB cannot successfully infest trees smaller than 10 cm in diameter at breast height (DBH) since the phloem layer is too small to support beetle development. Furthermore, beetles developing in small trees have lower growth rates and brood production increases

with DBH (Safranyik, 2003). We assume a lower DBH threshold of 20 cm for infestations that lead to significant mass adult emergence. Thus, trees below a given age will be considered nonsusceptible and this age, NJ, is the number of juvenile age classes. For example, if trees have fixed (optimal) radial growth rate of 2 mm/year (Heath et al. 1990), juvenile trees age 50 or younger are not susceptible to MPB attacks, and we take $NJ = 50$. As trees get older than approximately 120 years of age their phloem layer becomes too thin for MPB reproduction (Safranyik et al., 1975). However, we assume simply that trees older than NJ are fully susceptible. The population of juvenile trees in the k^{th} age class in year n is given by $j_{k,n}$ while the total population of juveniles from all NJ age classes is represented by J_n.

We let S_n denote the population of healthy adult trees that are susceptible to MPB infestation in year n and I_n represent the number of infested trees in year n, measured in stems. For convenience, juveniles $j_{k,n}$ and J_n are measured in number of stems in adult equivalents. E.g., if 5 juvenile trees in the 10^{th} age class shade as much of the forest floor as 1 adult tree, then those 5 juveniles contribute only 1 to the population of the 10^{th} age class. See Tables 2.1 and 2.2 for a summary of variables, parameters, units and estimated nominal values. Figure 2.1 shows a life-cycle diagram of the model. Our model assumes that the forest consists of five types of trees: juveniles, adult susceptible trees, infested trees I_n, as well as red snags I_{n-1}, and gray snags I_{n-2}. The snag classes must be included because they still shade the forest floor, delaying initiation of juvenile recruitment.

In the spring, juvenile trees in an age class either survive with probability s and graduate to the next age class, or die with probability $d = 1 - s$ and contribute to empty forest floor where new seedlings can grow next year (Fig. 2.2), assuming constant survivorship across age classes. Total juvenile mortality in year n is dJ_n and

$$j_{k+1,n+1} = sj_{k,n}, \ k = 1, .., NJ - 1. \tag{2.1}$$

The total number of trees in the juvenile latency class is given by

$$J_n = \sum_{k=1}^{NJ} j_{k,n}. \tag{2.2}$$

Successful infestation kills the host tree and lodgepole pines lose nearly all their needles two years after infestation. Thus, I_{n-2}, I_{n-3}, ... have no impact on the forest in

TABLE 2.1: Variables and parameters. Powell and Bentz (2009) estimated R, β, and T from data taken during a recent outbreak in central Idaho. Based on optimal radial trunk growth rate, $NJ = 50$ is an approximation of when a lodgepole pine has enough girth to support MPB colonization. We take $d = 0.01$ for juvenile lodgepole pine tree mortality.

Variables	**Description**	**Units**
S_n	Susceptible (to MPB colonization) tree population in year n	Number of stems
I_n	Infested (by MPB) tree population in year n	Number of stems
$j_{k,n}$	Juvenile tree population of the k^{th} age class in year n	Number of stems (in adult equivalents)
J_n	Total Juvenile tree population (age NJ or younger)	Number of stems (in adult equivalents)
Parameters	**Description**	**Units/Nominal Values**
T	Total number of trees in the forest	$T = 110,000$ stems (in adult equivalents)
NJ	Number of juvenile age classes	$NJ = 50$ age classes
d	Natural mortality rate for juveniles	$d = 0.01$ per year
$s = 1 - d$	Natural juvenile survivorship	$s = 0.99$ per year
R	Temperature dependent MPB pop. growth rate	$R = 1.8$ per year
β	Failure rate for MPB host search process	$\beta = 10.8 \times 10^{-6}$ per stem

TABLE 2.2: Parameters we seek to estimate with the model. Measures of the intensity of an outbreak are OD, I_{max}, and F.

Variables to Approximate	**Description**	**Units**
OD	Outbreak duration	Years
I_{max}	Maximum impact in a single year	Number of stems
F	Total trees impacted by outbreak	Number of stems
RT	Recovery time for susceptible trees in post-outbreak recovery	Years
P	Outbreak-recovery cycle period	Years

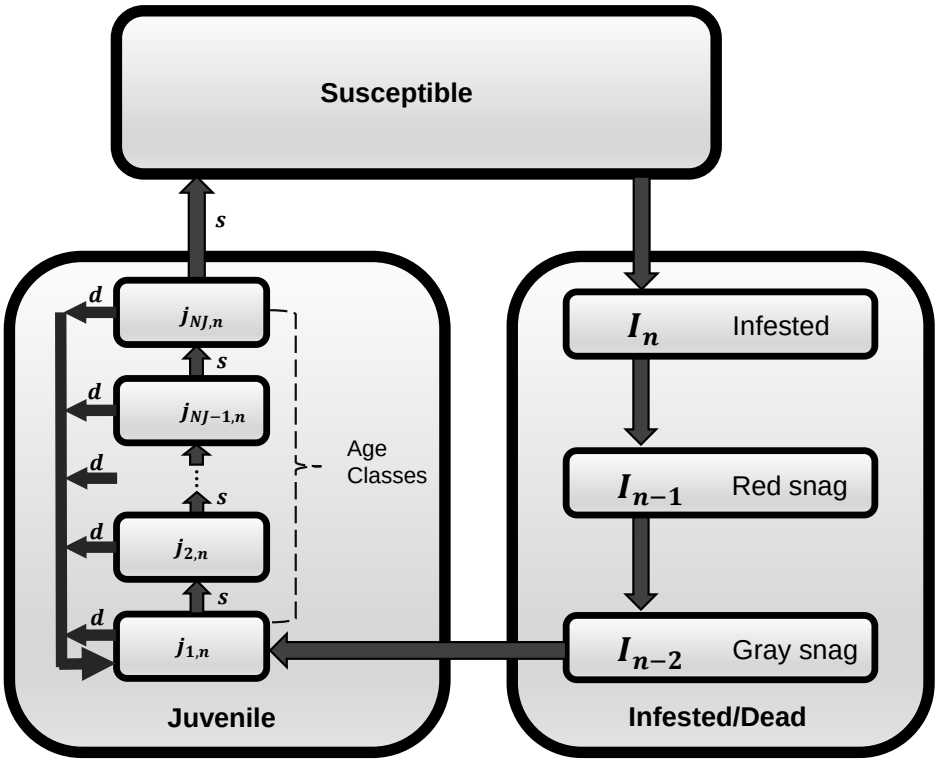

FIGURE 2.1: Life-cycle diagram. Natural juvenile mortality, d, opens up forest floor space to new seedling growth. Likewise, infestation mortality translates to seedling growth (after a once infested tree spends two years as a snag). Juvenile age class survivorship $s = 1 - d$ is constant. Fifty year old trees that survive the year graduate (mature) into the class of susceptibles. A red snag is a tree that became infested in year $n - 1$ and whose needles are now red. A gray snag is a tree that became infested in year $n - 2$ and whose needles are now gray.

terms of shading. Since lodgepole pine trees are not shade tolerant, seeds only germinate in gaps in the forest floor left by MPB infestation or other natural mortality. Hence, assuming there is always an ample supply of seeds on the ground, seedlings sprout in the unshaded areas of the forest and empty space (in terms of adult tree equivalents) is directly converted into 1^{st} age class juveniles (Fig. 2.2),

$$j_{1,n+1} = dJ_n + I_{n-2}. \tag{2.3}$$

In mid to late summer, beetles emerge from infested trees, search for new hosts, and attack. A Ricker-type model is used for newly infested trees (Powell and Bentz, 2009),

$$I_{n+1} = RI_n e^{-\beta(\text{current number of nonsusceptible trees})}.$$

Here R is the number of trees that will become infested next year for each infested

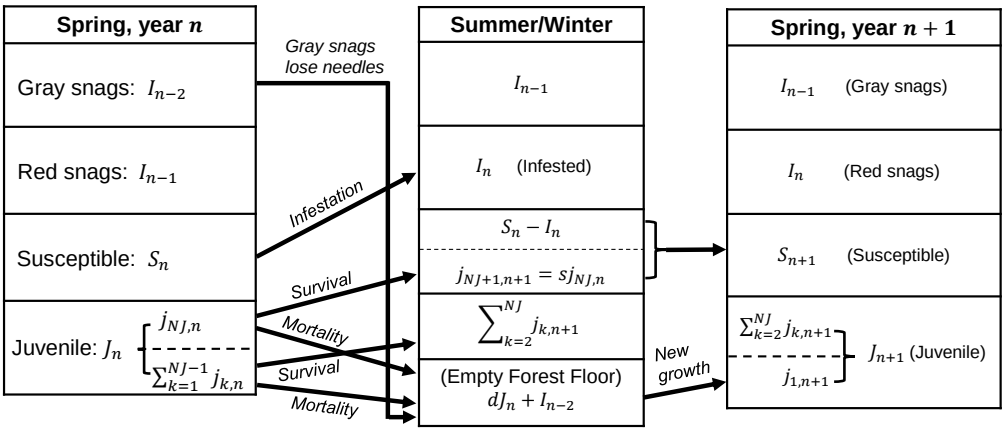

FIGURE 2.2: In spring, juvenile trees either die and leave empty spaces on the forest floor, or survive and graduate to the next age class. Surviving NJ year old juvenile trees transition to the class of MPB susceptible trees. In summer, a susceptible tree either becomes infested by MPB or avoids infestation and remains in the class of susceptible trees. Over the winter, two year old snags lose all their needles creating a gap in the forest floor. In spring, seedlings sprout in any open forest floor space created by natural juvenile mortality or MPB infestation mortality.

tree this year which we also interpret as MPB population growth rate. The exponential factor represents the probability of infesting beetles encountering new susceptible trees in a Poisson search process with failure rate per tree β. Since juveniles and snags are not susceptible, we have

$$I_{n+1} = RI_n e^{-\beta(J_{n+1}+I_n+I_{n-1})}.$$

We may also view β as being inversely proportional to the number of uninfested trees in the stand. That is, when the number of nonsusceptible trees is greater than $\frac{\ln R}{\beta}$ a MPB epidemic cannot propagate. Hence, $\frac{1}{\beta}$ scales the size of a noninfectious cohort of trees, as we will see in detail below. When all trees are susceptible, the exponential factor becomes one and the population of infested trees grows exponentially. On the other hand, as the forest becomes more and more infested, the exponential term tends to zero.

In spring, the population of susceptible trees will be its previous value, minus the number of trees that became infested last summer, plus the number of NJ year old juveniles that survived and matured into adult susceptible trees,

$$S_{n+1} = S_n - I_n + sj_{NJ,n}. \tag{2.4}$$

Total number of tree equivalents T, (inventoried in spring), is conserved from year to year reflecting finite floor space and therefore stand carrying capacity,

$$T = J_{n+1} + S_{n+1} + I_n + I_{n-1} \tag{2.5}$$

which allows for a more convenient form of the infestation equation,

$$I_{n+1} = RI_n e^{-\beta(T - S_n + I_n - sj_{NJ,n})}. \tag{2.6}$$

Putting everything together, equations (2.1)-(2.6) make up a system of nonlinear difference equations that can model all lodgepole pine populations in a stand:

$$\begin{aligned} j_{1,n+1} &= dJ_n + I_{n-2}, \\ j_{k+1,n+1} &= sj_{k,n},\ k = 1, .., NJ - 1, \\ S_{n+1} &= S_n - I_n + sj_{NJ,n}, \\ I_{n+1} &= RI_n e^{-\beta(T - S_n + I_n - sj_{NJ,n})}. \end{aligned}$$

2.2.2 Phases of Outbreak and Recovery

Due to its disturbance-based nature of regeneration, lodgepole pine often grows in even-aged stands. When initialized with uniformly susceptible trees, the combined model reliably falls into outbreak-recovery cycles (Fig. 2.3). A cycle consists of an outbreak followed by three stages of forest recovery, each of which we describe and analyze separately to derive approximations of outbreak severity and recovery time.

Phase 1: Outbreak

As the cycle begins, we initially see endemic beetle populations transition to incipient epidemic level. This leads to an exponential increase in infested trees while susceptible tree numbers plummet due to infestation mortality. Meanwhile the juvenile tree population increases to fill gaps in the forest floor left by dead susceptible trees. As the outbreak ensues, it reaches a peak at which point infestation begins to decay exponentially and approach zero. Our model assumes that an infested tree takes up space and shades the forest floor (denying any would-be seedlings from sprouting) for two years following infestation. Thus the length of this phase is $OD + 2$, where OD is the (unknown) outbreak duration.

Phase 2: Footprint Progression

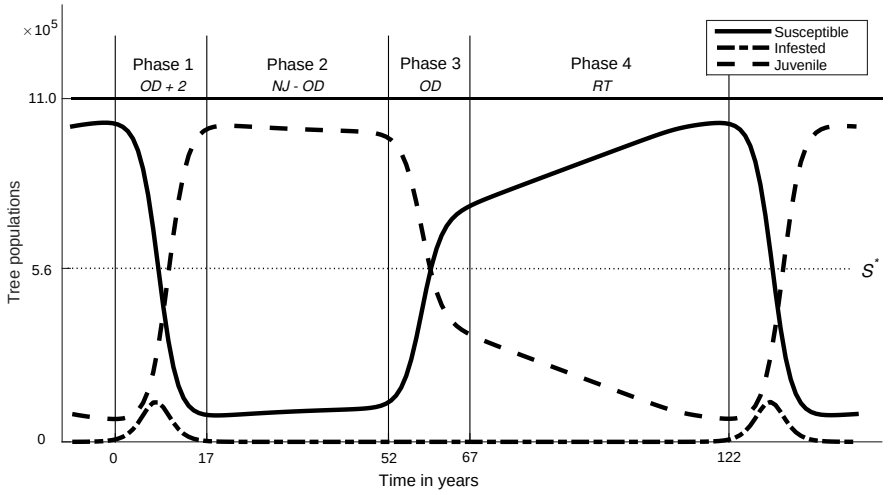

FIGURE 2.3: **The outbreak-recovery cycle**: Simulation output showing tree populations over one full period. The cycle can be naturally divided into four phases with corresponding time durations. NJ and OD denote the number of juvenile age classes and outbreak duration respectively. The length of phase 4 is denoted by RT and S^* is the fixed point for the population of susceptible trees. Specific times and populations are generated by the model with parameters obtained from a recent MPB outbreak in central Idaho (Powell and Bentz, 2009).

This phase can be described as the first stage of forest recovery. The forest experiences mass juvenile tree growth released by the outbreak. This surge of juveniles, called the outbreak footprint, progresses through the age classes until maturing into adult susceptible trees after NJ years. Phase 2 begins at the end of the outbreak and ends when outbreak-generated juveniles graduate to susceptibility. The time duration of footprint progression is then $NJ - OD$.

Phase 3: Footprint Graduation

At this time in the cycle, juveniles in the outbreak footprint that survived natural mortality over the course of phase 2 begin to graduate to the class of adult susceptible trees. This second stage of forest recovery can be thought of as the inverse outbreak and therefore takes the same amount of time as the outbreak itself, OD.

Phase 4: Full Recovery

In this final stage of forest recovery, there is still a significant number of juvenile trees due to intrinsic mortality as the footprint juveniles progress through the age classes in phase 2. These juveniles need to mature before the forest is completely recovered. We denote the (unknown) time required for this recovery by RT. MPB host density in the forest is maximal at the end of this phase, setting the stage for another outbreak.

2.2.3 Stability Analysis

As with waves of disease (Anderson and May, 1979a,b, 1982), outbreak cycles are organized by oscillations around unstable equilibria. We will show that observed MPB population growth rates fall in the range of values that produce such instability and hence tree population oscillation with periodic infestation outbreaks.

Fixed Points

The model system has two fixed points. The first, trivial, fixed point is one in which there is no infestation and all trees in the forest are adult susceptible trees, i.e $I_n = J_n = 0$ and $S_n = T$ for all time n. The other, incipient epidemic, fixed point is

$$J^* = \frac{(1-D)\ln R}{\beta K},$$

$$S^* = T - \frac{\ln R}{\beta}, \tag{2.7}$$

and

$$I^* = \frac{dD\ln R}{\beta K}$$

where $D = s^{NJ}$ and $K = 1 + D - 2sD$. Stability analysis reveals that there is an exchange of stability (as MPB growth rates increase) from the trivial to the incipient epidemic state, which loses stability through a Hopf bifurcation to periodic solutions (outbreaks). The incipient epidemic fixed point, with parameter values given in Table 4.1, is a center for periodic orbits.

At the incipient epidemic fixed point, there is relatively small (but nonzero) constant infestation whereby the number of newly infested trees each year exactly equals the number of juvenile trees that mature into adult trees, meaning that the same number of trees flow into the class of susceptible trees as flow out. Thus, if $I_n > I^*$ then $S_n > S_{n+1}$ (susceptibles are decreasing) and if $I_n < I^*$, $S_n < S_{n+1}$ (susceptibles are increasing). Therefore, the forest is in outbreak state when $I_n > I^*$. We will use these facts to connect the incipient outbreak fixed point to the outbreak waves it organizes after its Hopf bifurcation.

Spectral Radius of Jacobian

Next we analyze the stability of each fixed point by calculating the maximum (in modulus) eigenvalue, (denoted by λ_{max} for the trivial fixed point and λ^*_{max} for the incipient epidemic fixed point), of the Jacobian of the system as a function of temperature

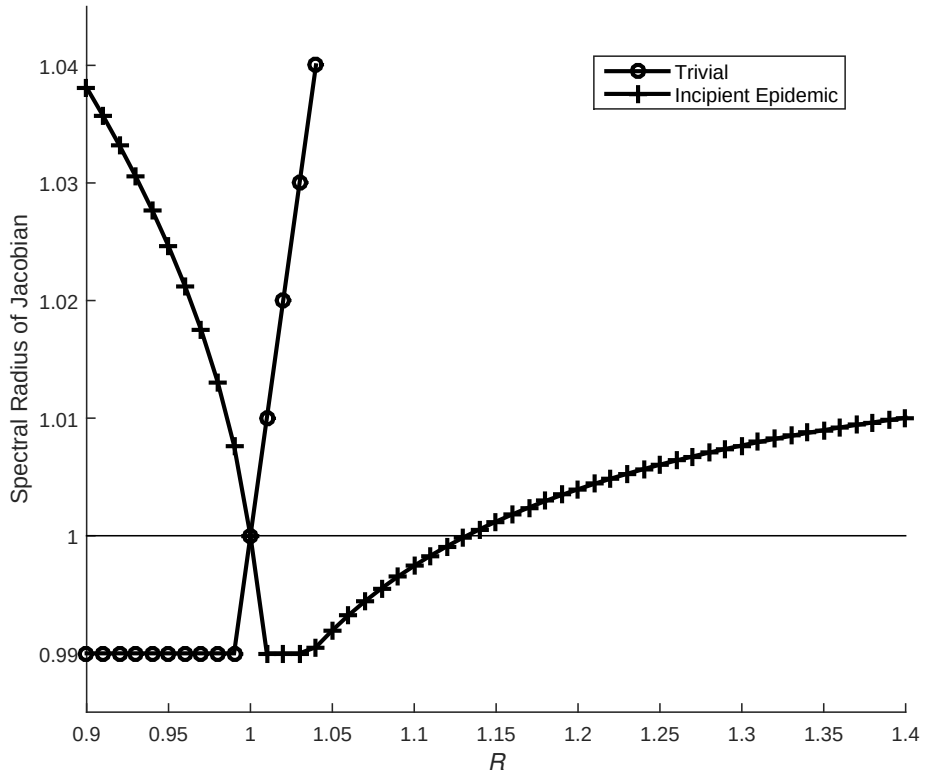

FIGURE 2.4: Stability of each fixed point is determined by the maximum (modulus) eigenvalue of the Jacobian of the system as a function of temperature dependent MPB population growth rate R

dependent MPB growth rate R (Fig. 2.4). The trivial fixed point is asymptotically stable ($|\lambda_{max}| < 1$) for all $R < 1$ while the incipient epidemic infestation fixed point is unstable ($|\lambda^*_{max}| > 1$). If infestation is not large enough ($R < 1$), any outbreak dies out. As growth rates move into the range $1 < R < 1.133$ (approx.), the incipient epidemic fixed point becomes asymptotically stable while the trivial fixed point losses stability. For growth rates in this interval, oscillations decay in amplitude and populations converge to the incipient epidemic fixed point. For large MPB growth rates, ($R > 1.133$), the incipient outbreak fixed point experiences a Hopf bifurcation and both fixed points are unstable. The system exhibits sustained oscillation and we see periodic outbreaks much like that of a realistic forest with a MPB presence (Fig. 2.3). Note that the value of R estimated by Powell and Bentz (2009) is in this interval ($R \approx 1.8$). It is for this range of growth rates that we shall develop analytic approximations for outbreak intensity, duration and return time.

2.3 Approximating Outbreak Severity and Cycle Period

It is our goal to derive analytic approximations of outbreak severity and duration as well as the duration of the entire outbreak-recovery cycle. We begin by deriving a continuous function that approximates infestation levels during the outbreak phase. Using this function we can approximate maximum infestation I_{max}, outbreak duration OD, and subsequently outbreak footprint F from given parameter values. Then we construct a linear approximation of the susceptible population in phase 4 and use it to estimate the length of phase 4, RT. Lastly, with approximations of OD and RT we piece together the lengths of each of the four phases to get an approximation for the cycle period P.

2.3.1 Phase 1 (Outbreak)

Just before an outbreak, the forest consists of mostly adult susceptible trees, a small number of pre-outbreak juveniles, and a negligible number of infested trees (Fig. 2.5). When S_n reaches the threshold S_{max}, infestation approaches the incipient epidemic level I^* and so the outbreak begins. With nearly the entire forest susceptible, the number of infested trees grows exponentially. However, as susceptible trees die and give way to new juvenile trees which are not susceptible, the outbreak slows until I_n reaches a maximum I_{max} (when $S_n \approx S^*$). As the population of susceptible trees decreases to its minimum S_{min}, infestation decays exponentially as there is no longer a sufficient number of host trees available for MPB colonization. Note that when $S_n \approx S_{min}$, $I_n \approx I^*$; this signifies the end of the outbreak.

The Outbreak Curve

The model equation for infested trees (2.6) can be written as

$$I_{n+1} = RI_n e^{-\beta(T-S_{n+1})}. \tag{2.8}$$

Taking logarithms and rearranging yields

$$\beta S_{n+1} = \beta T - \ln R + \ln I_{n+1} - \ln I_n \tag{2.9}$$

which we re-index as

$$\beta S_n = \beta T - \ln R + \ln I_n - \ln I_{n-1}. \tag{2.10}$$

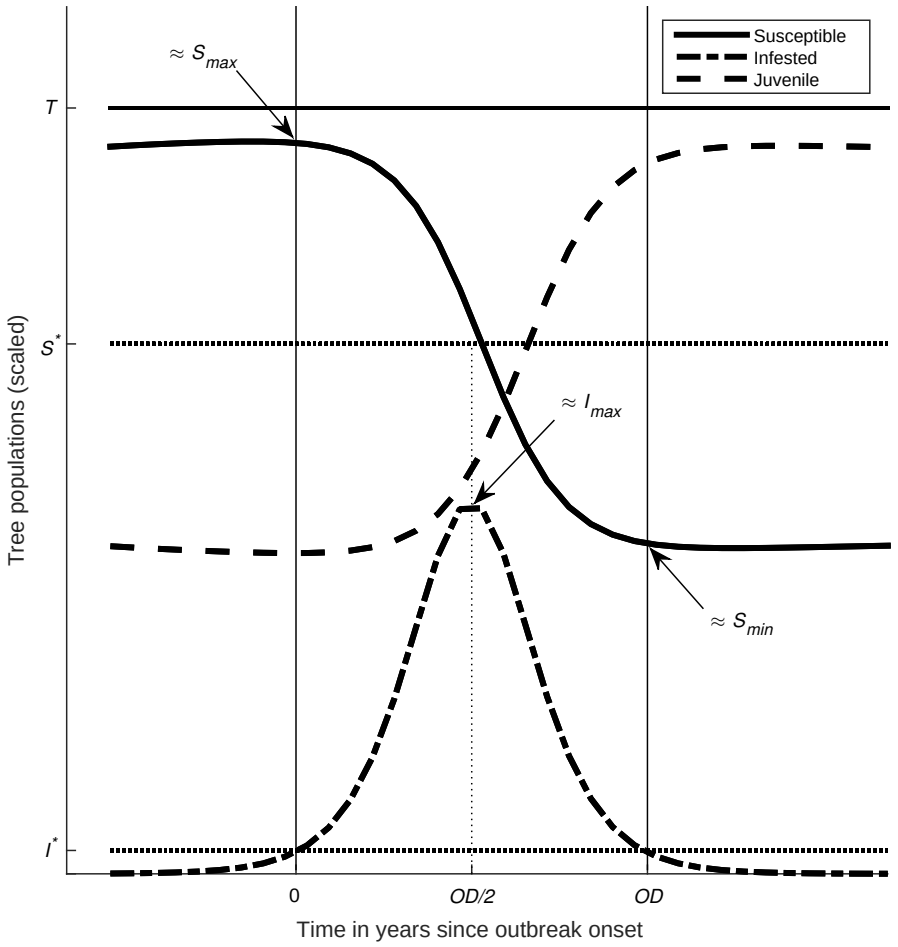

FIGURE 2.5: The system is in outbreak phase when $I_n > I^*$. Equivalently, the outbreak begins when $S_n \approx S_{max}$ and ends when $S_n \approx S_{min}$. The population of susceptible trees will be roughly at its fixed point when the outbreak peaks, i.e. $S_n \approx S^*$ when $I_n = I_{max}$. (Population values have been scaled to illustrate details.)

Subtracting (2.10) from (2.9) gives

$$\beta(S_{n+1} - S_n) = \ln I_{n+1} - 2\ln I_n + \ln I_{n-1}. \tag{2.11}$$

Since J_n is small at the onset of an outbreak and trees killed by MPB infestation are converted to seedlings which take $NJ - 1$ years to mature into the NJ^{th} age class, $sj_{NJ,n}$ is small during an outbreak and can be neglected. Thus $S_{n+1} \approx S_n - I_n$ and (2.11) becomes

$$-\beta I_n = \ln I_{n+1} - 2\ln I_n + \ln I_{n-1}$$

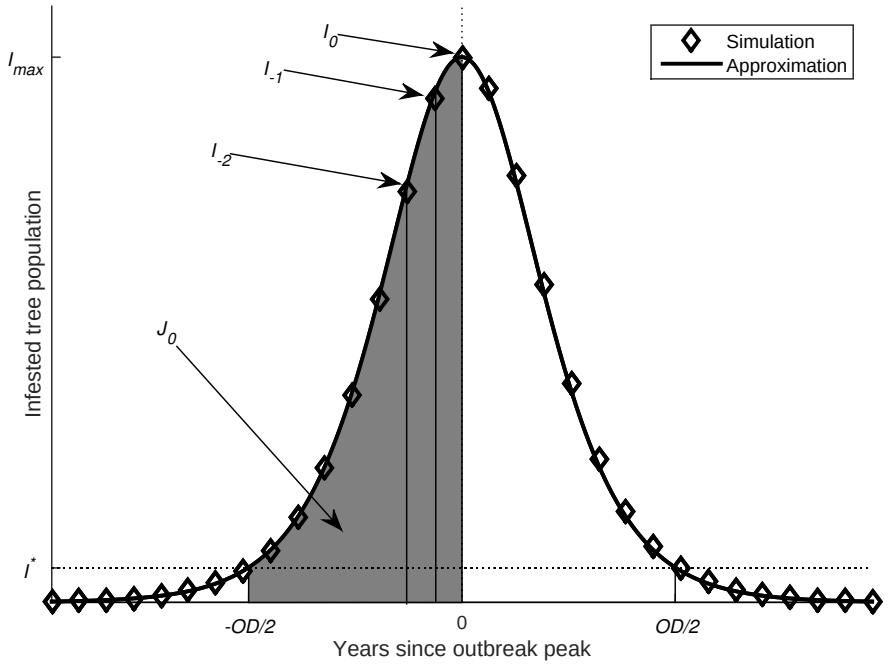

FIGURE 2.6: The outbreak curve approximation $\hat{I}$ is nearly indistinguishable from simulation output of infested tree populations ($r^2 = 0.999148$). The first half of the outbreak footprint (represented by the gray shaded area under the sech-squared approximation) is the total number of trees killed by outbreak infestation up to the time of peak outbreak. The snags I_{-1} and I_{-2} are contained in this area as well as all new juvenile growth, J_0, sparked by infestation mortality (under the assumption of no pre-outbreak juveniles).

whose solution is

$$I_n = I_{max}\ \mathrm{sech}^2\left(\sqrt{\frac{I_{max}\beta}{2}}n\right) \equiv \hat{I}(n) \tag{2.12}$$

for $I_0 = I_{max}$ and $I_{-n} = I_n$ (we use $\hat{I}$ to denote our approximation of infestation during the outbreak phase). Note that we define time zero for this approximation as the time of outbreak peak.

The approximation, $\hat{I}$, and actual outbreak infestation values are practically indistinguishable (Fig. 2.6). Next we use the sech-squared function to approximate the outbreak footprint F, maximum infestation I_{max}, and length of outbreak, OD. Estimates of S_{max} and S_{min} will also be derived.

Measures of Outbreak Intensity

To find expressions for S_{max} and S_{min} in terms of I_{max}, we apply matching conditions on (2.8) and (2.12) at the tails of the outbreak curve. Just before an outbreak,

$n << 0$ and from (2.12) we have

$$\frac{\hat{I}(n+1)}{\hat{I}(n)} \approx e^{\rho} \tag{2.13}$$

where $\rho = \sqrt{2I_{max}\beta}$. Similarly, at the end of an outbreak $n >> 0$ and

$$\frac{\hat{I}(n+1)}{\hat{I}(n)} \approx e^{-\rho}. \tag{2.14}$$

At the onset of an outbreak, $S_{n+1} \approx S_{max}$ and it follows from (2.8) that

$$\frac{I_{n+1}}{I_n} \approx Re^{-\beta(T-S_{max})}. \tag{2.15}$$

Similarly, at the end of an outbreak, $S_{n+1} \approx S_{min}$ and

$$\frac{I_{n+1}}{I_n} \approx Re^{-\beta(T-S_{min})}. \tag{2.16}$$

Equating the right hand sides of (2.13) and (2.15) leads to an approximation for S_{max},

$$S_{max} \approx S^* + \sqrt{\frac{2I_{max}}{\beta}}. \tag{2.17}$$

Similarly, after equating right hand sides of (2.14) and (2.16) we have

$$S_{min} \approx S^* - \sqrt{\frac{2I_{max}}{\beta}}. \tag{2.18}$$

From these approximations we see that the fixed point for susceptible trees is midway between the extremes of S_n,

$$S^* \approx \frac{S_{max} + S_{min}}{2}. \tag{2.19}$$

Assuming that pre-outbreak juveniles are negligible, the total tree population at outbreak peak can be approximated using equation (2.5) by

$$T = S_0 + J_0 + I_{-1} + I_{-2} \approx S^* + \int_{-\frac{OD}{2}}^{0} \hat{I}(t)dt,$$

since S_0 is approximately S^* and J_0, I_{-1}, and I_{-2} are accounted for in the integral, which represents the first half of the outbreak footprint (Fig. 2.6). Thus we have

$$T \approx S^* + \sqrt{\frac{2I_{max}}{\beta}} \tanh\left(\sqrt{\frac{I_{max}\beta}{8}} OD\right). \tag{2.20}$$

Given that $S^* = T - \frac{\ln R}{\beta}$ from equation (2.7), we solve (2.20) for OD,

$$OD \approx 2\sqrt{\frac{2}{I_{max}\beta}} \tanh^{-1}\left(\frac{\ln R}{\sqrt{2I_{max}\beta}}\right). \tag{2.21}$$

With the assumption that $\hat{I}(-\frac{OD}{2}) \approx I^*$ at the onset of an outbreak, we get a closed form approximation of maximum infestation I_{max} in terms of model parameters alone,

$$I_{max} \approx I^* + \frac{\ln^2 R}{2\beta}. \tag{2.22}$$

Substituting this into (2.21) gives us the expected outbreak duration OD as a function of MPB growth rate R, search efficiency β, and lodgepole pine tree mortality d. Observe that we can now approximate total tree mortality due to MPB outbreak (outbreak footprint, F) by

$$F \approx \int_{-\frac{OD}{2}}^{\frac{OD}{2}} \hat{I}(t)dt = \frac{2\ln R}{\beta}, \tag{2.23}$$

which we use as the primary measure of outbreak intensity.

2.3.2 Phase 2 (Footprint Progression)

An outbreak generates a wave of new juvenile trees which progress through the age classes until maturing into adult susceptibles. This footprint wave diminishes in amplitude due to natural juvenile mortality. Footprint trees that die are converted back into seedlings the following year via equation (2.3) of the model (Fig. 2.2). Just after outbreak the size of the footprint is approximately equal to F. After a year, the footprint has lost dF trees and therefore has population $F - dF = sF$. Next year the footprint is reduced by $d \cdot$(current population) $= d(sF)$ and has new population $sF - d(sF) = s^2F$. Thus the size of the footprint just before it graduates into the class of susceptible trees is

$$s^{NJ-OD}F, \tag{2.24}$$

noting that the exponent is the duration of phase 2.

2.3.3 Phase 3 (Footprint Graduation)

This second stage of forest recovery can be described as an inverse outbreak. That is, $NJ + 2$ years after the start of an outbreak, juvenile trees that grew up in the spaces left by outbreak tree mortality begin to mature into adult trees. A wave of trees, $s^{NJ-OD}F$, enters the class of susceptible trees and takes OD years to fully graduate. The population of susceptible trees rebounds to a level above its fixed point and nearly that of the healthy forest just before outbreak while the number of juvenile trees drops by the same amount to a level below its fixed point.

Measures of Outbreak Intensity

Measures of Outbreak Intensity At this interchange of population levels when the susceptible tree population is crossing its fixed point, infestation is at its lowest point in the cycle. It takes $NJ+2+\frac{1}{2}OD$ years after the start of an outbreak for S_n to surpass S^* (Fig. 2.3). It is here where we splice together the sech-squared approximation curve for the previous outbreak with the sech-squared approximation curve for the next outbreak (Fig. 2.7).

Infestation at Outset of Footprint Graduation

We now approximate the level of infestation at the outset of phase 3 ($NJ+2+OD$ years after outbreak onset) using the sech-squared function, $\hat{I}$. By the approximate symmetry of I_n with respect to $n = NJ+2+\frac{1}{2}OD$ (the middle of phase 3), $I_{NJ+2+OD} \approx I_{NJ+2}$. Thus we may use the previous outbreak curve approximation, the sech-squared function (equation 2.12), evaluated at time $NJ + 2 - \frac{1}{2}OD$, to estimate infestation at the end of phase 3 (Fig. 2.7). Time zero for equation (2.12) is when the outbreak is at its maximum so it is necessary to shift time inputs by $-\frac{1}{2}OD$. We approximate the population of infested trees at the onset of phase 4 (denoted by $\tilde{I}$) by

$$\hat{I}(m) = I_{max}\ \mathrm{sech}^2\left(\sqrt{\frac{I_{max}\beta}{2}}m\right) \equiv \tilde{I}, \tag{2.25}$$

where $m = NJ + 2 - \frac{1}{2}OD$.

2.3.4 Phase 4 (Full Recovery)

Just after the footprint enters the susceptible class, there is still a substantial number of juvenile trees due to mortality within the footprint as it progressed through the age classes. These must recycle before the population of susceptibles returns completely to its pre-outbreak level.

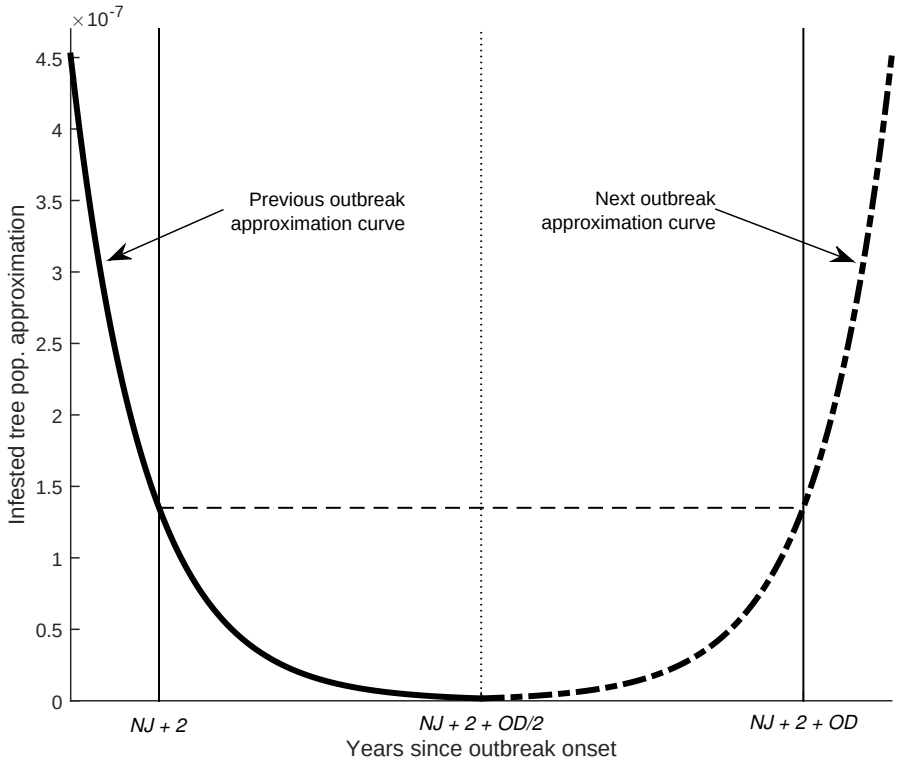

FIGURE 2.7: Minimum infestation occurs $NJ + 2 + \frac{1}{2}OD$ years after the start of an outbreak when S_n intersects S^*. We connect the sech-squared approximation of the last outbreak with the sech-squared approximation of the next outbreak at this point. Since I_n is approximately symmetric with respect to time $NJ+2+\frac{1}{2}OD$, $I_{NJ+2+OD} \approx I_{NJ+2}$

.

Linear Approximation of the Susceptible Population

We assume that juveniles spawned by footprint mortality are evenly distributed across age classes as indicated by simulations. Total footprint mortality during phase 2 is $(1 - s^{NJ-OD})F$ (see (2.24)), so the number of juveniles that graduate to susceptible trees each year (during phase 4) is approximately

$$\frac{(1 - s^{NJ-OD})F}{NJ} \equiv a.$$

During phase 3, the susceptible population increases from approximately S_{min} to $S_{min} + s^{NJ-OD}F$ as surviving footprint juveniles graduate, assuming juveniles not involved in the outbreak are negligible. Hence at the onset of phase 4, the susceptible population is approximately

$$S_{min} + s^{NJ-OD}F \equiv \tilde{S}.$$

We construct a linear approximation of S_n during phase 4:

$$\hat{S}(n) = \tilde{S} + an \tag{2.26}$$

where n is years after phase 4 begins.

Estimate of Phase 4 Recovery Time

Recovery time in phase 4 can now be estimated using the linear approximation of susceptibles to connect the end of recovery with the beginning of outbreak, when infestation reaches its fixed point. We solve

$$I_n = RI_{n-1}e^{-\beta(T-S_n)} = I^* \tag{2.27}$$

for n using the linear approximation $\hat{S}$ in place of S_n, and $\tilde{I}$ for I_0,

$$I_1 \approx R\tilde{I}e^{-\beta(T-S_1)},$$

$$I_2 \approx R(R\tilde{I}e^{-\beta(T-S_1)})e^{-\beta(T-S_2)}$$

$$= R^2\tilde{I}e^{-\beta(2T-(S_1+S_2))},$$

$$\vdots$$

$$I_n \approx R^n\tilde{I}e^{-\beta(nT-(S_1+\ldots+S_n))}.$$

Now using (2.26),

$$S_1 + \ldots + S_n \approx n\tilde{S} + a\frac{n(n+1)}{2}.$$

Thus (2.27) is equivalent to

$$R^n\tilde{I}e^{-\beta n[T-(\tilde{S}+a\frac{n+1}{2})]} = I^*,$$

which has the solution

$$n = \frac{-c_1 + \sqrt{c_1^2 - 4c_2c_0}}{2c_2} \approx RT,$$

where $c_0 = \frac{1}{\beta}\ln\frac{\tilde{I}}{I_*}$, $c_1 = \frac{a}{2} + \tilde{S} - S^*$, and $c_2 = \frac{a}{2}$.

Outbreak-Recovery Cycle Period

With our estimates of outbreak duration OD and phase 4 recovery time RT, it is now possible to construct an approximation of the cycle period that depends only on

model parameters:

$$\begin{aligned} P &= (OD+2)+(NJ-OD)+(OD)+(RT). \\ &= OD+2+NJ+RT \end{aligned} \tag{2.28}$$

It is necessary to add 2 years for the period in which infested trees linger called snag lag.

2.4 Results

We have developed analytic approximations of all measures of outbreak severity: outbreak duration OD, maximum infestation I_{max}, and footprint F. We also have estimates of the timing parameters: phase 4 recovery time RT, and outbreak return time P. In what follows we compare our approximations with model simulation outputs and with outbreak observations from central Idaho.

2.4.1 Outbreak Severity: Footprint Approximation vs. Simulation

The outbreak footprint depends on both outbreak duration and peak infestation. Therefore we need only analyze the outbreak footprint in assessing how well we can predict outbreak severity. Figure 2.8 compares the approximation of outbreak footprint F from equation (2.23) with footprint values obtained from simulation. Our approximation captures the general trend of increasing F with increasing R and has a 15 percent relative error for the parameterized value $R = 1.8$. That the approximation is an overestimate is essentially due to the fact that we integrated the continuous function $\hat{I}$ to approximate the first half of the footprint in (2.20). The integral is an underestimate since

$$\int_{-\frac{OD}{2}}^{0} \hat{I}(t)dt \leq \sum_{n=\lfloor -\frac{OD}{2} \rfloor}^{0} \hat{I}(n),$$

(Fig. 2.6) which implies (2.20) can actually be written as

$$T \geq S^* + \int_{-\frac{OD}{2}}^{0} \hat{I}(t)dt.$$

This leads to an overestimate of I_{max} (see (2.21) and (2.22)) and hence an overestimate of F (see (2.12) and (2.23)). The approximation of outbreak duration (2.21) (in conjunction with (2.22)) indicates that outbreaks get shorter as MPB growth rates increase which would reduce footprint size. On the other hand, maximum infestation increases considerably, which overall causes the footprint to increase considerably as well (Fig.

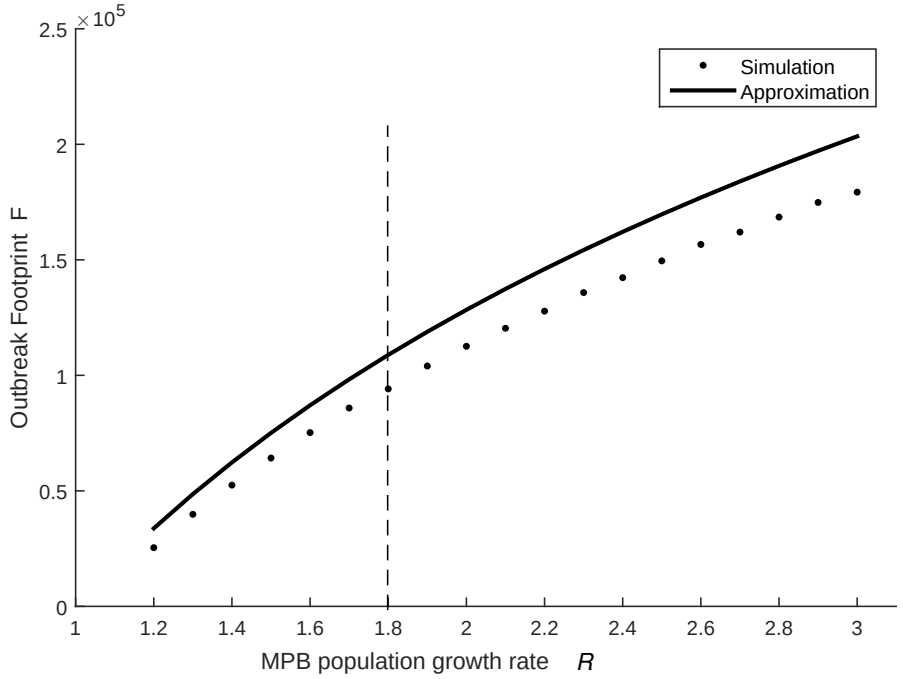

FIGURE 2.8: Our approximation of the outbreak footprint captures the positive association between R and F. We see a consistent 15 percent relative error due to integration of the continuous sech-squared function instead of summation of actual infestation values in our approximation of total forest size (2.20).

2.8). We conclude that outbreaks get worse with increasing R values.

2.4.2 Outbreak-Recovery Cycle Period: Approximation vs. Simulation

The graph in Figure 2.9 shows periods from simulation and from the approximation (2.28) for varying MPB growth rates. There is a 0.3 percent relative error for $R = 1.8$ which is only about half a year. With the parameter values from Powell and Bentz (2009), our model predicts a period of about 121 years. It seems likely that outbreak return time should decrease with higher MPB growth rates. However, contrary to our initial intuition, we find that as R increases, the period of the outbreak-recovery cycle does not decrease but rather stabilizes and approaches a constant value. This is due to a mutual cancelation of two effects: as R increases, outbreak duration decreases which

1. shortens the overall cycle period;

2. decreases the minimum of I_n (in phase 3) causing the time required for I_n to reach I^* to increase, that is, RT increases and subsequently the overall cycle period is lengthened.

Next we compare MPB infestation predicted by the model with actual infestation observed in a forest landscape between 1990 and 2010.

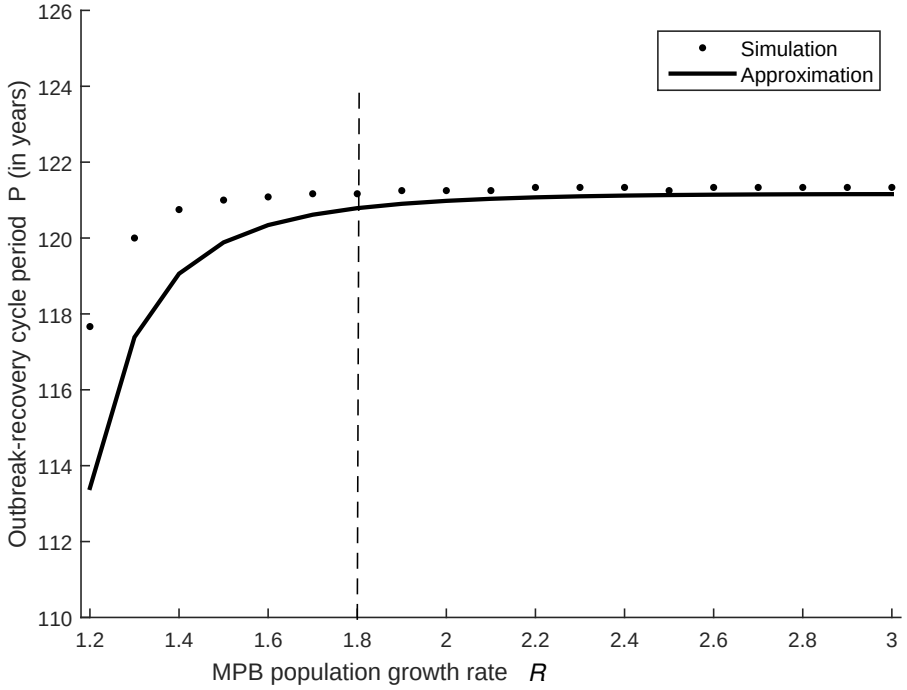

FIGURE 2.9: The approximation of the outbreak-recovery cycle period does a good job of matching the general trend of how the period increases and saturates at some value near 121 years as MPB growth rate increases.

2.4.3 Sawtooth National Recreation Area

In reality, R varies from year to year due to changing beetle phenology in response to varying temperatures as was described by Powell and Bentz (2009). We employ the R-model devised by Powell and Bentz (2009) to predict yearly MPB population growth rates from temperature signals for the Sawtooth National Recreation Area (SNRA) in central Idaho for each year from 1950 to 2099. From this string of growth rates we use our approximation of outbreak footprint to calculate yearly potential outbreak severities.

The R-Model and Temperature Signals

The R-model is based on a distributional model for MPB phenology (Sharpe et al., 1977) and in particular, specific life stage developmental rates as functions of temperature (Régnière et al., 2012). The model takes as input a series of 410 daily high and low temperatures starting on JD 200 (July 24th, the historical average time when beetles begin attacking trees) to produce completion times for each life stage and ultimately a distribution of adult beetle emergence times (the following year). From this distribution of emergence times, net survivorship of eggs, and beetle fecundity, the R-model calculates the number of *effective beetles* for year n, E_n, in the distribution that exceed the

daily attack threshold to achieve successful mass attack for an individual tree:

$$E_n = \int_{181}^{243} \max(s_E f P_n(t) - A, 0) dt,$$

where f is the number of eggs laid for all females in a tree, s_E is the fraction of those eggs surviving to emergence, A is the number of MPB required on a daily basis to successfully infest a tree, and $P_n(t)$ is the density of adult emergence associated with a tree in year n. Limits of integration, 181 and 243, correspond to reasonable limits on seasonality; development of eggs laid earlier than June 30 or later than August 31 will not be in the proper life stage (larvae) to survive fall and winter cold temperatures (Bentz and Mullens, 1999; Régnière and Bentz, 2007). The MPB growth rate for the year, R_n, is the product of the number of emerging effective beetles per infested tree and the parameter α describing the number of potential new infestations per effective beetle,

$$R_n = \alpha E_n.$$

Details of the R-model appear in Powell and Bentz (2009).

We generate a sequence of yearly growth rates using the R-model for historical as well as projected daily minimum/maximum temperatures for the SNRA located approximately 44° N, 115° W. Temperatures from 1950 to 2100 were obtained from the University of Idaho using Multivariate Adaptive Constructed Analogs (MACA: Abatzoglou and Brown (2013); Abatzoglou (2013)) statistical downscaling method. Projected temperatures were generated by the National Center of Atmospheric Research global climate model CCSM4 using the representative concentration pathway RCP4.5 which assumes a future scenario of moderate climate action (Vuuren et al., 2011; Thomson et al., 2011).

Projected Outbreak Severities

Using this sequence of growth rates, we calculate predicted outbreak footprints with equation (2.23) for each year based on the beetle growth rate for that year (Fig. 2.10). We also calculate outbreak footprints for each year using the average growth rate from the previous 15 years since the approximate outbreak duration is 15 years for the growth rate $R = 1.8$. Our simulations indicate that outbreaks (should they occur) will increase dramatically in severity around the year 2001. In fact, a major outbreak did occur in the SNRA between 1995 and 2010 and was the worst in recorded history for that area. It should be noted that just after the spike in outbreak severity (around

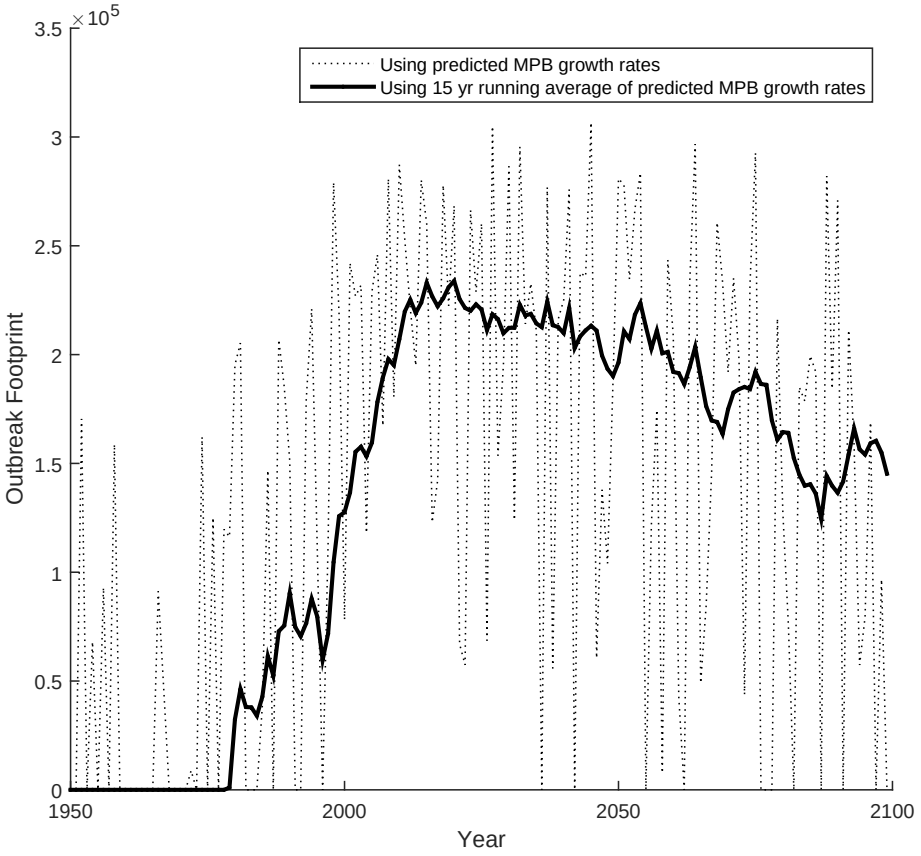

FIGURE 2.10: Based on MPB growth rates generated by the R-model of Powell and Bentz (2009) using temperatures from MACA (Abatzoglou and Brown, 2013; Abatzoglou, 2013), our approximation of outbreak severity (footprint) for the SNRA increases rapidly around the year 2001 which agrees well with the fact that an outbreak of unprecedented size took place around that time. Note: We set footprints corresponding to $R < 1$ equal to zero.

2015), footprint predictions begin to wane slightly over time. Warming during the last half of the twentieth century has likely created a temperature regime that supports MPB seasonality considerably more than in previous years for this particular elevation (2624 meters). However, as temperatures continue to increase we may see that beetles at this elevation are completing their life stages too quickly which could hinder seasonality. Thus, as warming continues, the optimal developmental window for MPB may be moving to higher elevations causing projected impacts in the SNRA to diminish from their initial peak.

2.5 Mechanisms for Creating Realistic Outbreak Frequencies

Model simulations and analytic approximations both predict an outbreak-recovery cycle period of around 120 years. If a majority of lodgepole pine in a stand are killed,

a 120 year outbreak return time is a reasonable approximation since re-growth to a MPB-susceptible girth takes 50 to 100 years. MPB outbreak frequency, however, can be variable and in some stand types was estimated to be between 20 and 50 years (Amman and Schmitz, 1988; Axelson et al., 2009; Campbell et al., 2004). There are several possible explanations for short cycle periods including spatial variability, demographic variability, endemic infestation forcing, and parametric variability. Next we explore these factors in the context of our model.

2.5.1 Spatial Variability and MPB Dispersal

As a first attempt at reducing model predicted outbreak return time, we account for possible effects of spatial variability by modifying the model to include two weakly coupled stands of lodgepole pine trees. In the SNRA, another MPB host (whitebark pine, *Pinus albicaulis*) occurs at higher elevations than lodgepole pine. The two host species are separated by a band of non-host conifers (Powell and Bentz, 2014). Subpopulations of conspecific hosts may also be separated by geographic barriers such as lakes, rivers, or mountain ranges. However, disconnected populations can still be coupled by long range migration (dispersal) when populations are high (Bleiker et al., 2014; Aukema et al., 2006). We model migration between stands as

$$I_n^{(1)} = I_n^{(1)} + e_2 I_n^{(2)} - e_1 I_n^{(1)}$$

$$I_n^{(2)} = I_n^{(2)} + e_1 I_n^{(1)} - e_2 I_n^{(2)}$$

where $I^{(1)}$ and $I^{(2)}$ denote the populations of infested trees in stands 1 and 2 respectively. The rate at which infestation flows from stand 1 to stand 2 is e_1 whereas e_2 is the rate of flow from stand 2 to stand 1. Each stand is modeled by its own set of equations (2.3) - (2.8) and we consider the total infestation in both stands for analyzing periodicity. This yields more realistic outbreak-recovery cycle periods. For example, with flow parameters $e_1 = 0.05$ and $e_2 = 0.000015$, the period is reduced to about 46 years which is in the range of observed outbreak return times (Fig. 2.11).

2.5.2 Demographic Variability

Another period-reducing mechanism is demographic variability. Since MPB prefer larger diameter trees, significant proportions of smaller stems are spared from infestation in an outbreak (Amman and Schmitz, 1988). This can cause age structure fragmentation leading to multiple cohorts of juvenile trees. We set the initial distribution of juveniles

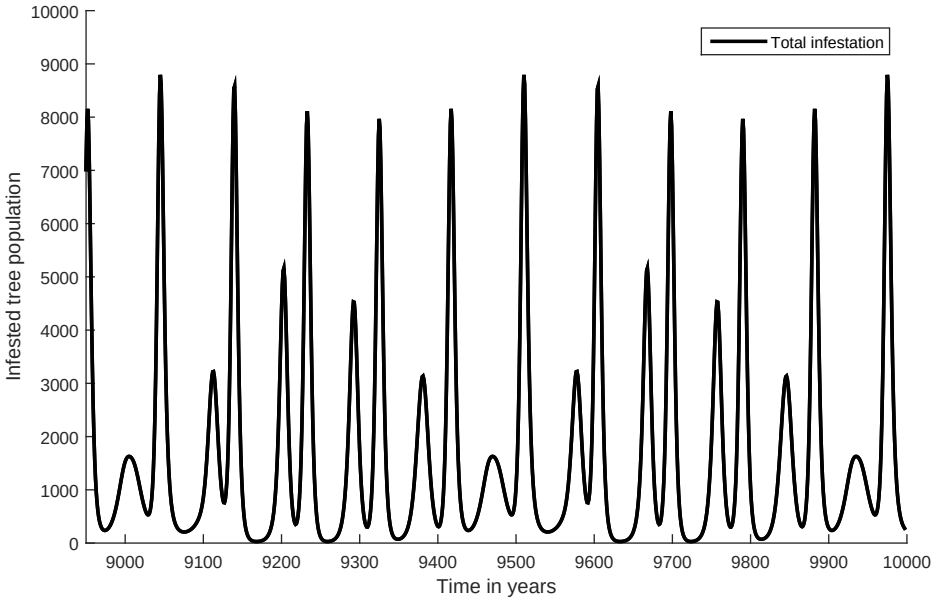

FIGURE 2.11: Total infestation in two weakly coupled lodgepole pine stands. With this coupling ($e_1 = 0.05$, $e_2 = 0.000015$), the outbreak-recovery cycle period gets reduced to the more realistic value of 46 years.

so that there are two footprint waves which doubles the frequency of outbreaks. To accomplish this it is necessary to increase the number of juvenile age classes NJ in order to fit the two footprint waves into the juvenile class. We have used $NJ = 50$ based on ideal conditions for lodgepole pine tree growth. A more realistic value of NJ is 80 years (Amman and Schmitz, 1988). With two age cohorts, one of susceptible trees fueling an outbreak and the other cohort of juveniles being spared, the cycle period is effectively reduced to about 55 years (Fig. 2.12).

2.5.3 Infestation Forcing

If we incorporate constant MPB infestation forcing into the model, the period decreases significantly. This additional beetle presence is realistic according Hrinkevich and Lewis (2011) who suggest that "stands maintain a nearly continuous supply of endemic beetle populations." It is likely that there are small MPB populations in any given stand, sustained by down but not yet dead trees or possibly by immigration (Bleiker et al., 2014). This endemic presence of beetles reduces the time in phase 4 required for infestation to reach its fixed point. We implement endemic infestation forcing by modifying model equation (2.8) as follows:

$$I_{n+1} = RI_n e^{-\beta(T - S_n + I_n - sj_{50,n})} + G$$

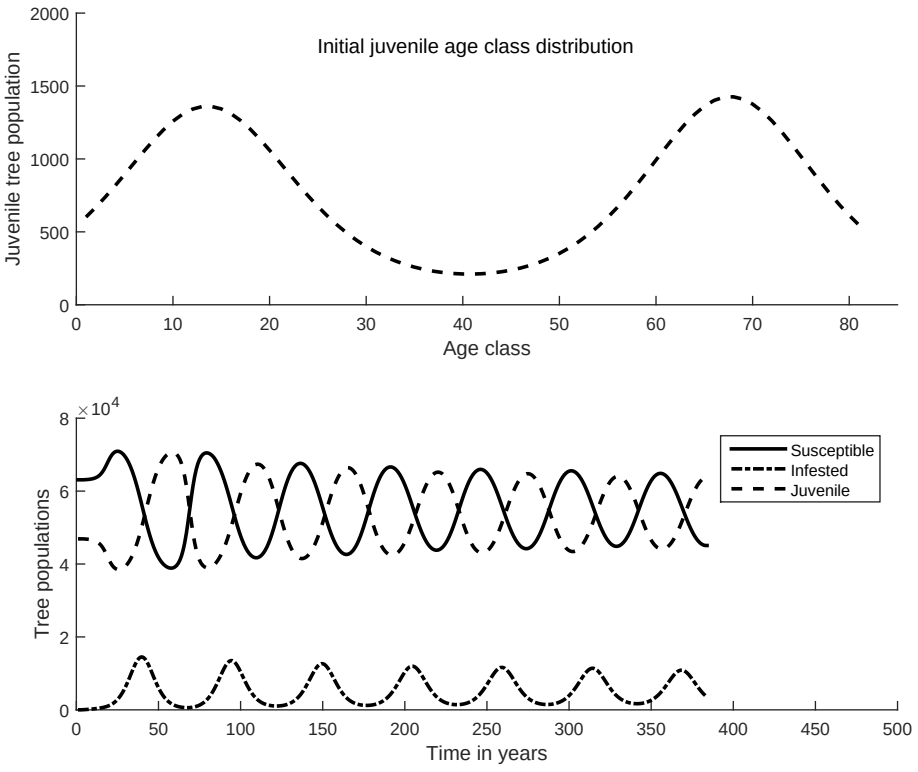

FIGURE 2.12: With enough age classes, ($NJ = 80$), the system can be forced into a state with twice its natural frequency by initiating the juvenile class with two footprint waves. The period of this oscillation is about 55 years which is close to observed outbreak return times.

where G is a constant forcing term. For small G both fixed points perturb and the cycle period decreases as G increases, reaching a minimum value around 68 years for $G \approx 48$ infested trees, and then begins to increase again (Fig. 2.13). When $G < 48$, both fixed points are unstable for nominal parameters. However, when $G > 48$ the incipient epidemic fixed point becomes stable and sustained oscillations are impossible.

2.5.4 Parametric Variation and Forcing

Stochastic MPB Growth Rates

Random variation in yearly MPB growth rates (an effect of fluctuating inter-annual temperatures) may play a role in increasing outbreak frequency. If a stand experiences a string of years with temperatures unfavorable to MPB seasonality during an outbreak, growth rates could plummet and completely halt the outbreak. With the outbreak stopped short, the stand is left with a sizable number of susceptibles which could fuel another outbreak sooner than the expected natural return time. To investigate the possible effects of a stochastic beetle growth rate, we let R be a random variable from

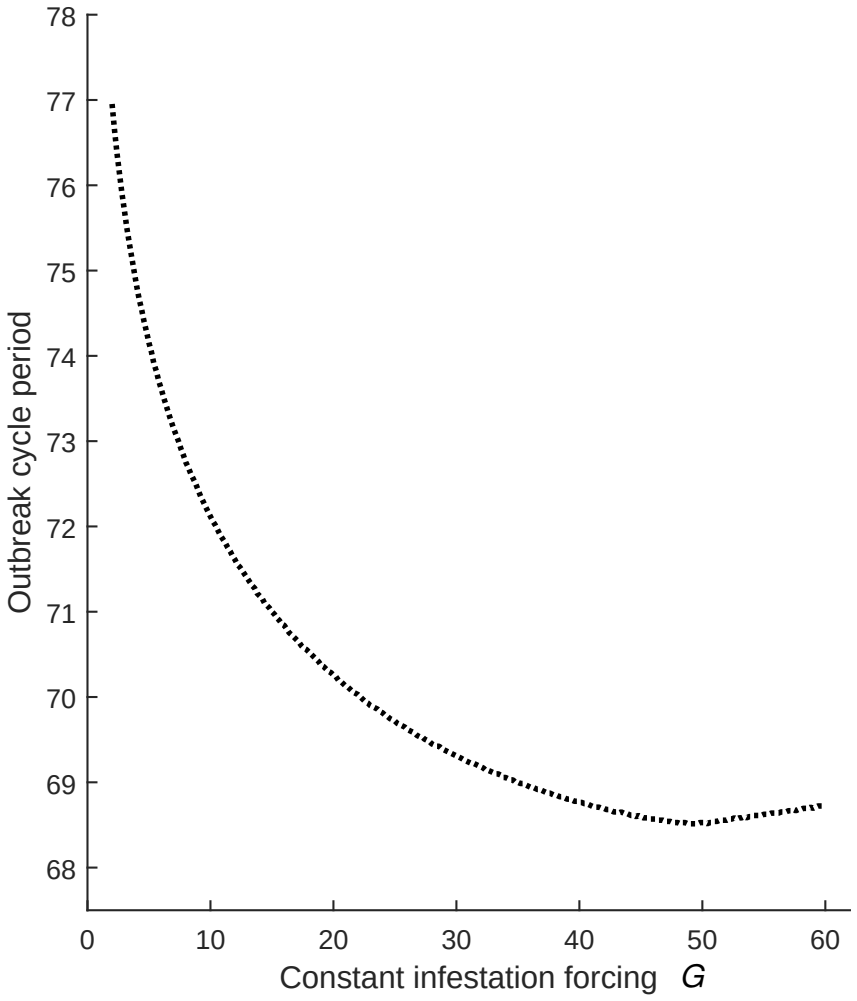

FIGURE 2.13: As the constant infestation forcing term G increases, the cycle period decreases and reaches a minimum value around 68 years for $G \approx 48$ infested trees.

a lognormal distribution. The lognormal distribution is chosen so that growth rates are nonnegative. The distribution mean and variance are left as control parameters in searching for lower period values.

We examine a variety of parameter combinations including the values obtained from the SNRA R-value projections (mean 2.2 and variance 1.0) only to find that the lognormality of growth rates causes an increase in the cycle period rather than a decrease. It appears that when outbreaks are shut down prematurely due to below average growth rates and more importantly $R < 1$, phase 4 recovery time RT is shortened and hence the return time for the next outbreak is also shortened. A series of large R values can cause I_n to increase dramatically and then rebound to a very low level. This results in an inordinately long time for infestation to build back up to an incipient outbreak

level (i.e. $I_n \approx I^*$). This is realized as an increase in RT and subsequently the time between outbreaks increases substantially. Since the lognormal distribution is skewed to the right, we expect high R values more often than low R values and thus the average period ultimately increases.

Growth Rate Parameter Forcing

While it is certainly true that there is random variation in growth rates, it may also be the case that high and low R values come in consecutive strings. It is suspected that El Niño/La Niña cycles may create roughly square-wave temperature signals with period of about 5 years (the average frequency of the El Niño/La Niña cycle). We model this with square wave forcing of the MPB growth rate in hopes of inducing oscillation at higher than natural frequency. A variety of R value square wave frequencies and amplitude ranges were tested in a search for a minimized cycle period. All combinations of forcing frequencies and amplitudes produced at most the natural outbreak recovery cycle with a superimposed low amplitude wave with the same frequency as the square wave function. The true outbreak return time is ultimately unaffected by growth rate parameter forcing.

2.6 Conclusion

We propose a set of equations for the dynamics of MPB population outbreaks in an age structured forest. Stability of two fixed points, one trivial and one corresponding to incipient epidemics, control epidemic behavior. As MPB population growth rates increase, the trivial fixed point loses stability to the incipient epidemic fixed point where the system exhibits damped oscillation. As growth rates increase further, the incipient epidemic fixed point becomes unstable through a Hopf bifurcation which creates periodic outbreaks.

From our mechanistic model we derive an approximation for predicting outbreak infestation. With this formula we predict the severity as well as the duration of an outbreak based on temperature-driven MPB growth rates. Additionally, we develop a formula for predicting the period of the outbreak-recovery cycle. These results indicate that higher MPB growth rates correspond to more severe outbreaks and, although counterintuitive, nearly constant outbreak return time. Earlier work done by Powell and Bentz (2009) shows that warmer temperatures lead to larger MPB emergence and subsequently higher growth rates. Thus we are able to see a connection between higher average temperatures and more intense MPB outbreaks in recent years.

To assess MPB impact on temperate and boreal forests, we calculate outbreak severities as a function of temperature-dependent MPB growth rates. Using historical temperature records and climate model projections of future daily temperatures as input for a distributional model of MPB phenology, we generate predicted yearly growth rates for the years 1950 to 2099 in the SNRA, ID. The MPB population used for phenology model parameterization came from this area. Using these growth rates, we predict potential severity of future outbreaks that reflects the effects of changing climate. Predicted MPB population growth rates increase as temperatures become more favorable to population growth. Warming during the last half of the twentieth century has likely created a temperature regime that supports MPB seasonality considerably more than in previous years at relatively low elevations. However, as temperatures continue to increase MPB at this elevation complete their life stages too quickly, hindering seasonality. Thus the optimal developmental window for MPB may be moving to higher elevations causing projected impacts at high elevation to increase while low elevation impacts diminish.

Our model overestimates the outbreak cycle period compared to observations. We explore possible mechanisms for lowering the model predicted cycle period and find that incorporating spatial variability and demographic heterogeneity can produce realistic outbreak frequencies in the range of observed values. Adding a constant endemic presence of MPB infestation also increases cycle frequency. Parametric heterogeneity, contrary to expectations, does not effectively shorten predicted outbreak cycle period.

The importance of spatial effects on periodicity and severity suggests that explicit spatial dispersal should be added into the age-structured model presented here. Recent work by Powell and Bentz (2014) indicates that spatially varying motility rates accurately describe observed patterns of MPB attack, and the earlier red-top model of Heavilin et al. (2007) showed that periodic outbreaks in time correspond to traveling waves of outbreak in space. Coupling an accurate dispersal model with a realistic model for forest age structure will likely endow our outbreak model with rich dynamics capable of producing realistic outbreak intensities and frequencies in space and time.

Chapter 3

ASSESSING FUTURE CLIMATE CHANGE IMPACTS ON NORTHERN U.S. ROCKY MOUNTAIN FORESTS: PHENOLOGY MODEL PREDICTED MOUNTAIN PINE BEETLE GROWTH RATES FROM CLIMATE MODEL TEMPERATURE PROJECTIONS

3.1 Introduction

Climate change has many effects on temperate forests including altered species composition, decreased water availability, increased wildfire intensity and frequency, transition of forests from carbon sink to carbon source, and larger pest outbreaks (Houghton et al.). Warmer annual minimum temperatures can increase some destructive outbreak insects overwintering survival and furthermore, allow for survival at higher than normal elevation (Weed et al., 2015). Temperature variation throughout the life history of the mountain pine beetle (*Dendroctonus ponderosae*) in particular, plays a major role in determining adult emergence numbers and generation time (voltinism) (Bentz et al., 2014). Higher adult MPB emergence translates to higher population growth rates which can have devastating effects on pine forest habitats.

The mountain pine beetle (MPB) is an aggressive, tree killing beetle whose hosts span the genus *Pinus*. Increasing ambient temperatures due to global climate change are a significant factor in explaining why outbreaks of MPB have been more severe and expansive in recent decades (Bentz et al., 2014). While MPB outbreak has historically been considered a natural disturbance regime for forests, these unprecedented intense outbreaks are responsible for elevated mortality in lodgepole pine tree (*Pinus contorta*) forests across the western United States and Canada (Meddens et al., 2012), generating a high volume of fuel and increased potential for forest fires. Furthermore, it is predicted that the current MPB outbreak in Canada will release 270 megatons of carbon dioxide into the atmosphere (Kurz et al., 2008). This is a substantial contribution to the greenhouse effect and subsequently warmer average temperatures, which triggered the outbreak to begin with.

MPB population growth rates have a direct effect on the severity of outbreaks in terms of total host tree mortality (Duncan et al., 2015). Thus, predicted growth rates in future climate scenarios can provide a good measure of the effects of climate change on bark beetle disturbances. Insect growth rates depend on the seasonal efficiency with which individuals develop and progress through the stages of their life history. Since MPB are poikilothermic, developmental rates in various life stages are dictated almost exclusively by temperature. Several thermally-driven phenological models have been constructed that predict development times for life stage emergence (Bentz et al., 1991; Logan and Bentz, 1999; Powell et al., 2000; Gilbert et al., 2004). Powell and Bentz (2009) used a distributional model of MPB phenology to generate adult emergence time distributions from hourly tree phloem temperatures. They connected the temperature-dependent phenology model to a mathematical description of criteria for successful infestation and colonization of a tree. Based on the number of trees successfully infested in a certain year and in the following year, they estimated the MPB population growth rate for that year. However, this mechanistic approach has not yet been applied in future climate scenarios to assess potential outbreak damage in forests at the landscape level across elevational gradients.

As ectotherms, MPB success at high elevation in colonizing valuable five-needle pines such as bristlecone and whitebark pine may be improved as a result of global warming. Elevations corresponding to temperature regimes favorable to MPB population growth are increasing with warming temperatures. Physiological adaptations of high elevation beetles to cool environments allow populations to more efficiently use available thermal energy and provide flexibility to shift from two year generation to one year generation life cycles in warm years (Bentz et al., 2014) thus increasing outbreak potential and severity. High elevation five-needle pines provide essential habitat for wildlife and are critical in the distribution of snow and therefore water (Logan and Powell, 2001); a vital resource in arid climates like the Rocky Mountain west. While low elevation lodgepole pine has co-evolved with MPB such that outbreaks are normative (Mattson, 1996), whitebark pine survival strategy, for example, would not be successful in the face of massive beetle outbreaks. Further investigation into the effects of warming on high-elevation beetle growth rates and subsequent consequences to pine species is needed.

Another means of assessing the effects of climate change on MPB populations is to monitor the number of generations completed per year (voltinism). At low and middle

elevations ($<$ 2300 m) in the northern U.S. Rocky Mountains, MPB life cycles are generally univoltine (one generation per year) whereas at higher elevations ($>$ 2300 m), beetle populations may be a mix of univoltine and semivoltine (one generation every two years) (Bentz et al., 2014). While fractional voltinism between one and two generations per year has been observed in warmer low latitudes (two generations in three years in southern California for example), life stage temperature thresholds in conjunction with seasonality requirements may serve to constrain a shift to two generations per year (bivoltinism) (Bentz et al. 2014). In historic and current climates, evolved adaptations to local climates have limited MPB capacity for true bivoltinism. Although completion of a generation over winter is constrained by evolved thresholds for development (Bentz et al., 2014), if adult emergence occurs early in the summer, a generation can be completed by fall and another completed by mid to late spring of the following year under an appropriate temperature regime.

Temperature-related increases in poikilotherm voltinism have been observed in, for example, fall webworm in Japan (Yamanaka et al., 2008) and predicted for other pests such as spruce bark beetle (Jönsson et al., 2008). With more generations per year, once benign insects can become major pest species (Tobin et al., 2008). A transition from univoltine to bivoltine life cycles for phytophagous MPB populations may have multiplicative effects on population growth rates and hence increase the capacity for mass attack resulting in significant increases in tree mortality.

Methods for predicting biological impacts of climate change have mostly been limited to statistical extrapolation from historical data. As there exist no data on MPB bivoltinism, these techniques would fail in predicting a transition from one to two generations per year under future warming assumptions. To date, there have been few mechanistic modeling approaches to predicting ecological ramifications of climate change using climate model temperature projections and thus no clear assessment of how MPB voltinism could be altered in future thermal regimes.

In this paper, we augment a model developed by Powell and Bentz (2009) for predicting yearly mountain pine beetle population growth rates for decades of climate model projected temperature signals over an area in the northern U.S. Rocky Mountains. Our temperature-dependent mechanistic R-model predicts growth rates using a distributional model of beetle phenology (Sharpe et al., 1977) with specific life stage developmental rate functions from Régnière et al. (2012) in conjunction with the criteria for successful infestation and colonization of trees outlined by Powell and Bentz

(2009). Daily minimum and maximum temperatures were obtained for the years 2006 to 2085 using Multivariate Adaptive Constructed Analogs (MACA) statistical downscaling method (Abatzoglou and Brown, 2013; Abatzoglou, 2013). Projected future temperatures were generated using three separate global climate models each with two different emissions scenario representative concentration pathways. We calculate MPB growth rates each year for an area defined by latitude range 42° N to 49° N and longitude range 108° W to 117° W on a Cartesian grid of approximately 4km mesh. Using these growth rates, we analyze how the optimal thermal window for MPB development is changing with respect to elevation as a result of climate change induced warming. We also use our combined model to evaluate if thermal regimes exist that would allow for bivoltine life cycles and discuss how yearly growth rates would change as a result. Our analysis of yearly MPB population growth rate, voltinism, and elevational range for optimal life stage development provides a good assessment of eruptive insect population behavior in response to changing climatic conditions.

3.2 Methods

3.2.1 Study area

The U.S. Forest Service is conducting an assessment of MPB impact under future climate scenarios to use for forest management planning (Bentz et al., 2016). To aid in this assessment, we predict yearly MPB population growth rates from temperature signals for parts of Forest Service regions 1, 2, and 4. Our study area contains the western two-thirds of Montana, the northwest corner of Wyoming, and all of Idaho (Fig. 3.1). This region contains Idaho Panhandle NF, Glacier NP, Beaverhead-Deerlodge NF, Gallatin NF, Bitterroot NF, Flathead NF, Bridger-Teton NF, Caribou-Targhee NF, and the Greater Yellowstone Area. The study area forms a rectangular area in the northern U.S. Rocky Mountains defined by latitude range 42° N to 49° N and longitude range 108° W to 117° W.

3.2.2 Temperature signals

The phenology component of our model is driven by temperature signals at various points in the study area. Daily minimum and maximum temperatures were obtained for the years 2006 to 2086 from the University of Idaho using Multivariate Adaptive Constructed Analogs (MACA) (Abatzoglou and Brown, 2013; Abatzoglou, 2013) statistical downscaling method
(http://maca.northwestknowledge.net). The MACA method is a statistical method for

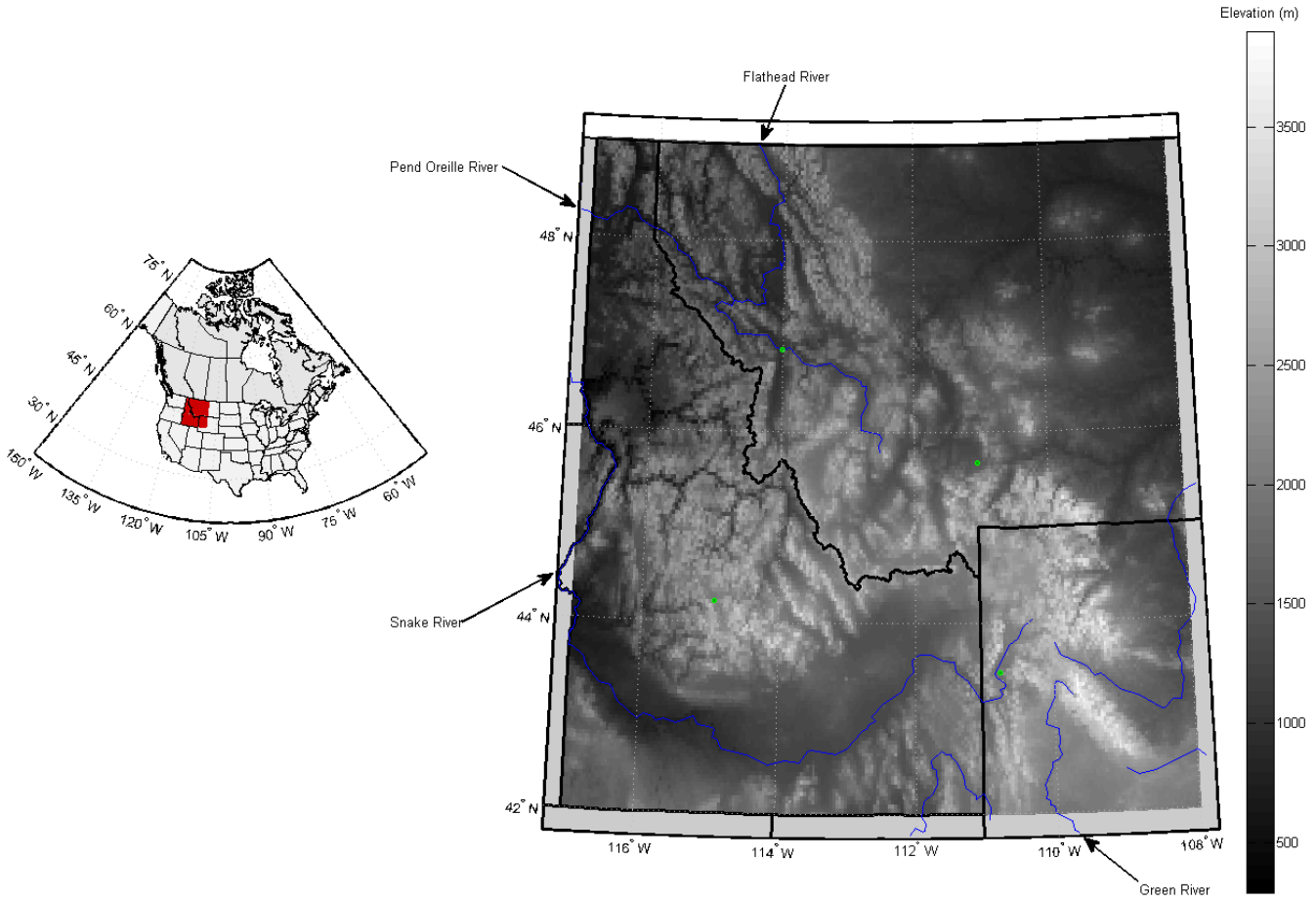

FIGURE 3.1: Study area geography and elevation. Cities, indicated by green points from left to right, are

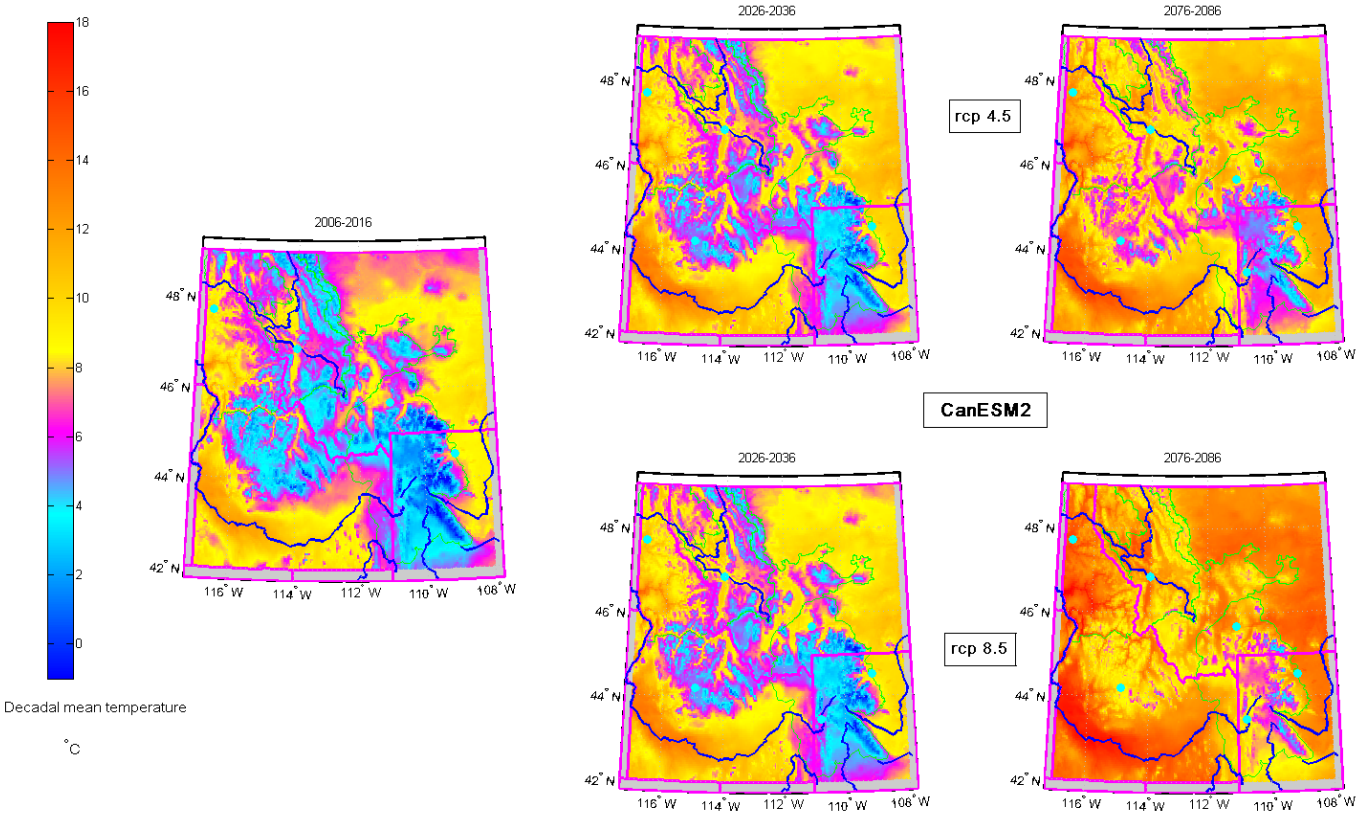

FIGURE 3.2: Study area mean temperatures generated by the CanESM2 climate model using both emissions scenarios RCP-4.5 (moderate climate mitigation) and RCP-8.5 (no climate mitigation).

downscaling Global Climate Model (GCM) outputs from their native coarse resolution to a higher spatial resolution. Projected temperatures were generated using three GCMs (CanESM2, CCSM4, and CNRM-CM5) chosen based on lowest error scores of performance metrics (Rupp et al., 2013).

For each GCM we use two different emissions scenario Representative Concentration Pathways (RCP-4.5 and RCP-8.5) (Vuuren et al., 2011; Thomson et al., 2011). RCP-4.5 is a future scenario of moderate climate action based on an experiment where an additional 4.5 W/m^2 is trapped in the earth-atmosphere system by 2100 compared to preindustrial conditions. RCP-8.5 refers to an experiment where an additional 8.5 W/m^2 is trapped by 2100, a future with no climate action and high emissions. Figure 3.2 shows current as well as projected temperatures for the area using the CanESM2 climate model for both emissions scenarios. Temperatures were available from MACA on a Cartesian grid with approximately 4km point spacing. We generated MPB growth rates for each point on the grid (a 170 by 218 matrix with 170 latitude points and 218 longitude points) for every year from 2025 to 2085.

3.2.3 MPB population growth rate model (R-model)

The mountain pine beetle is an aggressive bark beetle that attacks and lays its eggs in the phloem layer of pine trees. During the fall, winter, and spring, eggs hatch and the larvae feed on the phloem while developing into mature adults which eventually results in the death of the host tree (Amman and Schmitz, 1988). We use the R-model of Powell and Bentz (2009), that generates MPB population growth rates (R-values) using a distributional (cohort) model for MPB phenology (Sharpe et al., 1977) with life stage developmental rate curves parameterized by Régnière et al. (2012). The model takes as input a series of 408 daily high and low temperatures starting on July 19, the mean time when beetles begin attacking trees, to produce completion times for each life stage and ultimately a distribution of adult beetle emergence times during the attack season of the following year. From this distribution, net survivorship of eggs, and beetle fecundity, the R-model calculates the number of effective beetles in the distribution that exceed the daily attack threshold to achieve successful mass attack for an individual tree. The MPB population growth rate for the year is the product of the number of emerging effective beetles per infested tree and a parameter converting effective beetles to number of newly infested trees.

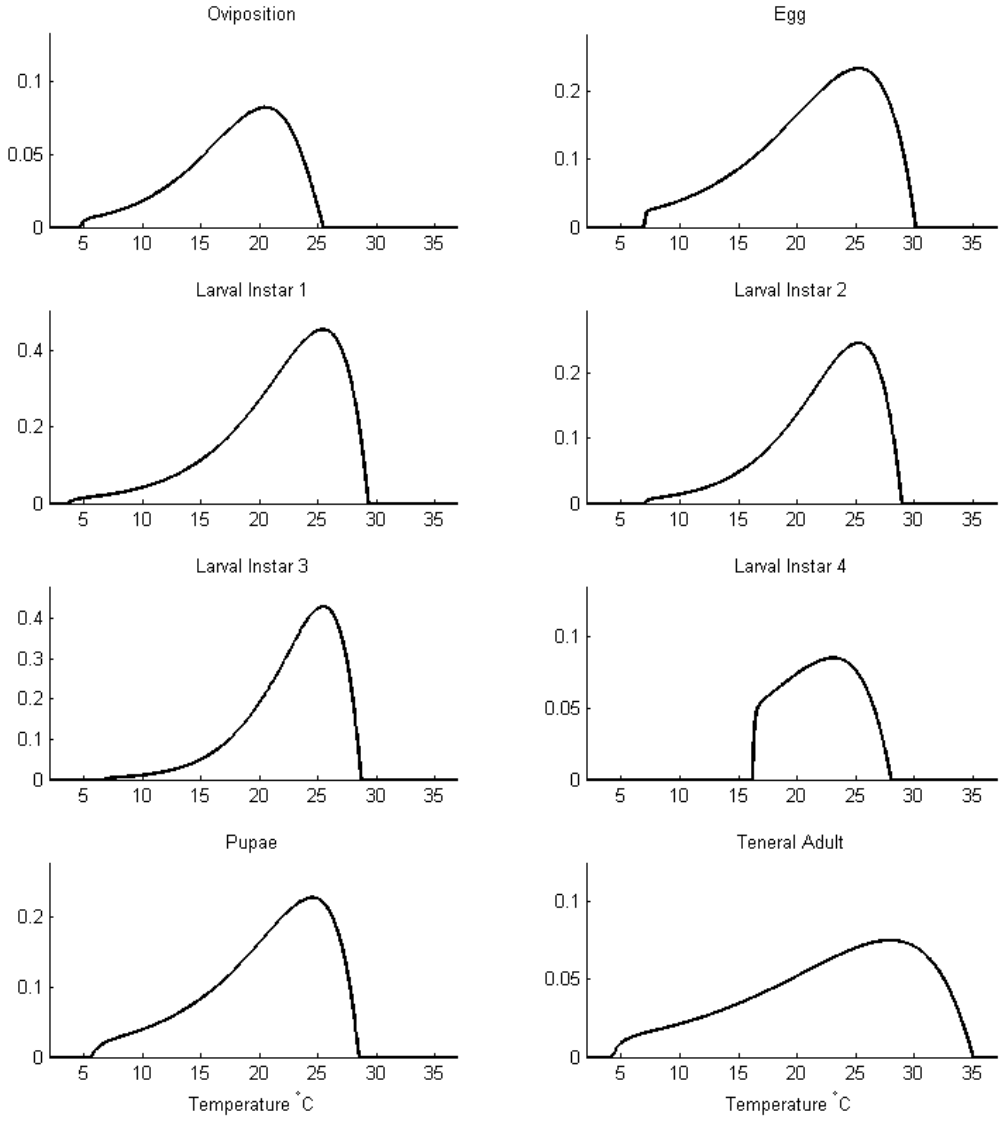

FIGURE 3.3: Developmental rate curves for the 8 mountain pine beetle life stages from Régnière et al. (2012). In all graphs, the vertical axis is measured in development/day.

Distributional model of MPB phenology

MPB develop through 8 life stages throughout the course of their life history: ovipositional adult, egg, 4 larval instars, pupae, and teneral adult. Each stage has a unique developmental rate function (rate curve) that depends on the temperature of the medium surrounding the beetle (tree phloem or ambient air). Rate curves in the *R*-model are taken from Régnière et al. (2012) (Fig. 3.3). While there is no true mechanistic basis underlying the derivation of the rate curves, they are an empirical mathematical description of the shape of developmental responses to temperature.

Not all individuals in a population of poikilothermic organisms progress through

particular life stages at the same rate. This is primarily due to intrinsic genetic variation at the individual level. We assume that developmental rates are randomly distributed across a population according to a lognormal distribution. The assumption of a distribution of rates is the core premise of a distributional model. We assume lognormality mainly for its positive skew which is a characteristic often observed in distributions of developmental rates of insects (Curry et al., 1978). Furthermore, a lognormal random variable cannot be negative and thus developmental rates are guaranteed to be nonnegative as in reality.

The lognormal distribution parameter which controls genetic variance in developmental rates as well as rate curve parameters were estimated by maximum likelihood using measured developmental times from samples of beetles for each life stage at various constant temperatures. See Régnière et al. (2012) for details of experiments, data collection methods, and parameterizations. Since it is believed that rate variability may be significantly different in the field, we introduce a variance multiplier υ to account for rate variability amplification due to natural exogenous forces such as daily variability in temperature and inherent differences among and within trees.

Distributional models (also called cohort models) keep track of numbers of individuals entering and exiting the life stages of an organism's life cycle (Sharpe et al., 1977). A cohort is a group of individuals that enter a certain life stage at the same time. A cohort model calculates the proportion of a cohort that completes the life stage during each time step given a distribution of developmental rates. In our R-model, the time step is one day and we use lognormally distributed developmental rates. Each life stage has an associated function that gives the sizes of all starting cohorts at every point in time. The cohort model uses this starting function (which comes from the previous life stage) to calculate the total number of beetles from all cohorts that complete life stage j at time t. The result is the life stage emergence function, denoted by $N_j(t)$, which is used as the input starting function for the next life stage. For example, the emergence function $N_8(t)$ gives the number of MPB completing the teneral adult life stage (emerging) on any given day between July 24 (the mean time when beetles begin attacking trees) of year $n-1$ and August 31 (the end of the attack season) of year n.

The starting function for the oviposition life stage, $N_0(t)$, is called the attack distribution and gives the probability of a beetle attacking the tree on a given day. We assume this distribution is normal with mean July 24, based on data in Bentz (2006),

and standard deviation 2 days. We denote the mean (potential fecundity) of a population of attacking beetles by f_0. Since a female beetle in the wild typically does not live up to its full potential fecundity and actually lay f_0 eggs, we introduce the parameter n_e to represent the true (mean) number of eggs laid by a female in the field. We note here that our version of the cohort model keeps track of all n_e individuals spawned by a single attacking female. We then multiply by the number of attacking females to get the total number of individuals in the tree. Details of our phenology model are in Appendix A.

MPB infestation effectiveness and population growth rate (R-value)

Some species of conifers including the primary MPB host, lodgepole pine, have adapted significant defense responses to bark beetle attacks such as the secretion of resin to impede a beetle's ability to bore into a tree (Amman and Cole, 1983). It is necessary for MPB to mass attack a tree to successfully outpace and overcome these defense mechanisms (Berryman et al., 1985). To model the requirement for mass attack, we define the number of effective beetles in the attack season (June 30 to August 31, i.e. JD 181 to JD 243) of year n, denoted E_n, as the number of emerging adult MPB that exceed an attack threshold A to successfully overcome host tree defenses. From the adult emergence function $N_8(t)$ associated with a tree in year n generated by the phenology model, we calculate the number of effective beetles,

$$E_n = \int_{181}^{243} \max(\beta N_8(t) - A, 0)dt,$$

where the parameter β is the product of the total number of attacking females per tree in a season and brood survivorship, and A is the number of MPB required on a daily basis to successfully infest a tree. (Fig. 3.4). The limits of integration correspond to reasonable limits on seasonality; development of eggs laid earlier than June 30 or later than August 31 will not be in the proper life stage (larvae or brood adult) to survive fall and winter cold temperatures (Bentz and Mullens, 1999; Régnière and Bentz, 2007).

The MPB population growth rate, R_n, for year n is the product of the number of emerging effective beetles per infested tree and the conversion factor α describing the number of potential new infestations per effective beetle,

$$R_n = \alpha E_n.$$

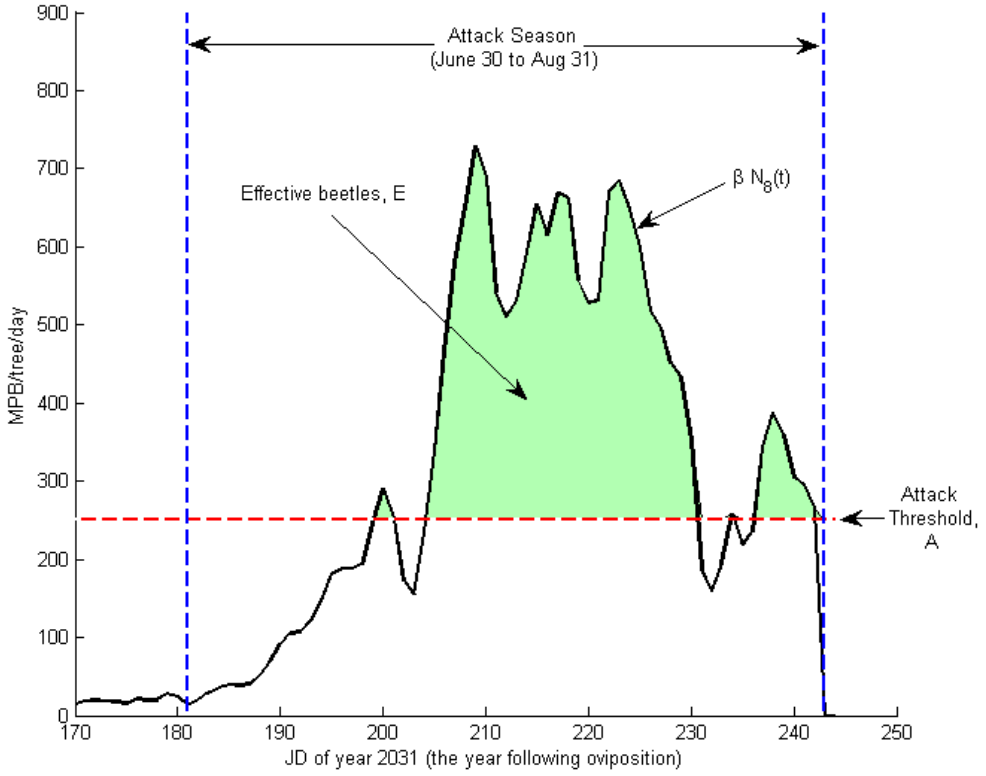

FIGURE 3.4: The number of effective beetles in the attack season (JD 181 to JD 243 of the year following oviposition) is the number of emerging adult MPB that exceed the attack threshold A to successfully overcome host tree defenses. Adult emergence function $N_8(t)$ was generated using the temperature signal from latitude 44°N and longitude 115°W for the years 2030 and 2031 projected by global climate model CCSM4 with emissions scenario RCP-4.5.

Numerical implementation

We use daily high and low temperatures generated by global climate models to drive the phenology model. Simpson's rule is used to integrate a life stage rate curve, which is a function of the temperature signal, over one day to get that day's amount of development. In order to apply Simpson's rule, we calculate mean temperatures between the day's (early morning) minimum and (mid-day) maximum as well as between the day's maximum and the next day's minimum. The result is a sequence of temperatures given every 6 hours for each day. These temperatures are input into the appropriate rate curve yielding five developmental rates for each day (overlapping at the minimum temperature) which partition the day into four subintervals (Simpson's rule step size 0.25 day).

Parameterization

Observed infestation data was derived from Aerial Detection Surveys (ADS) of the

TABLE 3.1: Model parameters and constants. Best fit parameter values for α, β, n_e, and υ are from maximum likelihood using ADS data on MPB impact in the SNRA. The per tree per day attack threshold of 250 is taken from Powell and Bentz (2009). Mean potential fecundity value is estimated in Régnière et al. (2012).

Model Parameters	**Description**	**Parameterized Values**
α	Number of potential new infestations per effective beetle	5.3882×10^{-4} trees/Effective MPB
β	Product of number of attacking females and egg survivorship	1139.2 MPB/tree
n_e	Mean MPB fecundity in the field	24.255 eggs/MPB
υ	Lognormal variance multiplier	1.4057 (dimensionless)
Constants	**Description**	**Estimated Values**
A	Attack threshold	250 MPB/tree/day
f_0	Mean potential fecundity	81.8 eggs/MPB

Sawtooth National Recreation Area (SNRA) in central Idaho conducted by USDA Forest Service, Forest Health Protection. Observers in fixed-wing aircraft measured the area impacted by MPB infestation each year. The MPB population growth rate is estimated as the ratio of the current year's area impacted to the previous year's area impacted. Predicted growth rates were generated by the R-model using hourly temperatures taken in the SNRA from 1992 to 2004. Best fit values of the parameters α, β, n_e, and υ were found by maximum likelihood (Table 3.1). Figure 3.5 shows the fit which has coefficient of determination $r^2 = 0.7$.

Validation

We test the R-model's accuracy by comparing predicted growth rates generated by input temperatures from a National Oceanic and Atmospheric Administration (NOAA) weather station in the Greater Yellowstone Area (GYA) with observed growth rates calculated from nearby ADS infestation data (Fig.3.6). Daily minimum and maximum temperatures were obtained from NOAA's Lick Creek weather station (45.5° N, 111.0° W, 2091 m elevation) in the Gallatin National Forest of Montana. ADS impact areas were obtained within a 16 km radius of the temperature station. The observed R-value is estimated as the ratio of the current year's area impacted to the previous year's area impacted. Years with available complete temperature signals and ADS data are 2000,

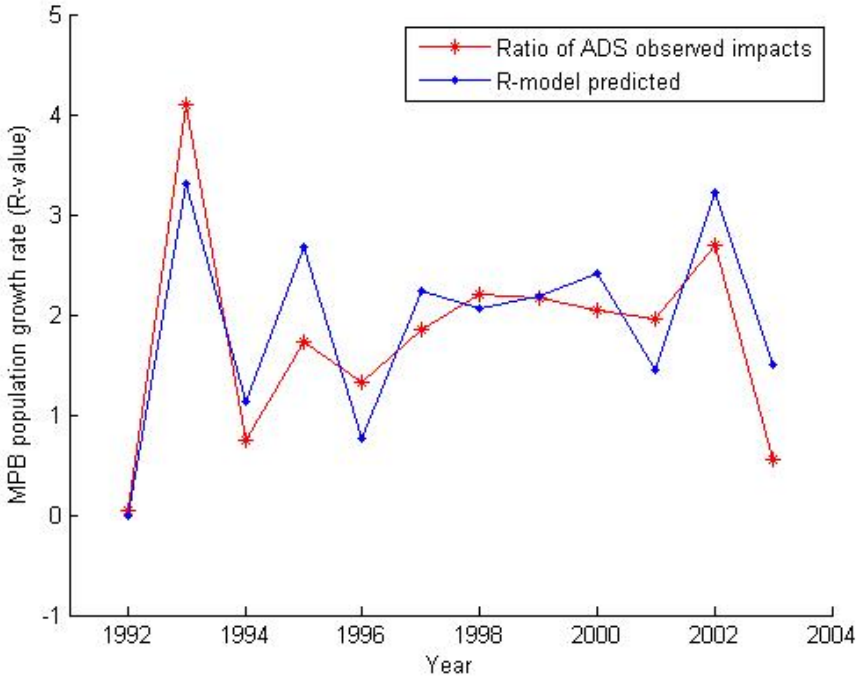

FIGURE 3.5: Parameterization best-fit: comparison of predicted MPB population growth rates with observed R-values used to parameterize the R-model. Predicted growth rates were generated by the R-model using hourly temperatures taken in the Sawtooth National Recreation Area (SNRA) from 1992 to 2004. Observed R-values were calculated by taking ratios of Aerial Detection Survey (ADS) infestation areas in the SNRA for neighboring years. Best fit values of the parameters were found by maximum likelihood and yields a coefficient of determination of 70% ($r^2 = 0.7$).

and 2003-2009. The R-model predictions match observations relatively well ($r^2 = 0.75$).

3.2.4 Bivoltinism

Under an appropriate temperature regime, MPB adult emergence could occur early enough in summer (i.e. June) for a generation to be completed by mid fall (i.e. September or October) (Reid, 1962; Bentz et al., 2014). With a warm enough winter, a subsequent generation may potentially complete by mid to late spring of the following year (i.e. June or early July). This would result in an unprecedented bivoltine MPB life cycle and consequently significantly higher population growth rate for that year. While summer generations are not unprecedented given the presence of adults that overwintered and were able to emerge in June, completion of an entire generation over winter (i.e. between September and June) has hitherto been constrained by lower developmental temperature thresholds (Bentz et al., 2014). In particular, the fourth larval instar requires temperatures above at least 15°C to molt into pupae. We developed a test to

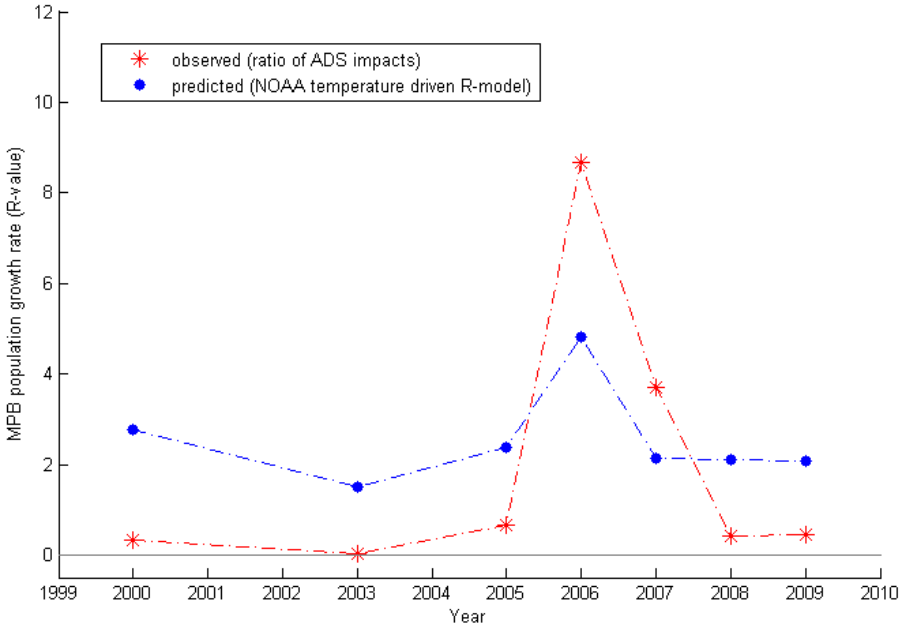

FIGURE 3.6: Model validation: comparison of observed and predicted MPB population growth rates. Predicted R-values were generated by the R-model using daily minimum and maximum temperatures measured by NOAA's Lick Creek weather station. Observed R-values were calculated by taking ratios of ADS infestation areas within a 16 km radius of the temperature station. The coefficient of determination is $r^2 = 0.75$.

check if bivoltinism is possible given a particular (projected) temperature signal based upon appropriate timing windows and thermal limits for overwintering. If the test indicates the potential for bivoltinism, we consider the combined effects of adult emergence for both generations on yearly population growth rates.

Test for bivoltine life cycle potential

Given a temperature signal and an attack beginning sometime between May 31st and June 30th (when parent adults typically emerge), we use the phenology model to calculate the mean adult emergence date. For bivoltinism to be possible, emergence must occur early enough in fall for successful oviposition and egg survival. The emergence date is used as the starting attack date for the second generation. If the adult emergence date of the second generation is within 10 days of the original (first generation) starting date, we conclude that a bivoltine life cycle is possible. However, we must check that temperatures were not too cold during specific life stages. Temperatures below $-18°$C will kill any eggs or pupae (Reid and Gates, 1970). Thus, if any day during the first or second generation egg or pupae stage had a low temperature of $-18°$C or below, we conclude that bivoltinism is not possible for that temperature signal even if the phenology

model predicts that the second generation would complete within a year (plus 10 day grace period).

Bivoltine population growth rate

Where our test for bivoltinism is positive, we calculate the yearly population growth rate based on adult emergence of both generations. The attack (normal) distribution of the first generation is centered about the first starting day between May 31st and June 30th that leads to a positive test result for bivoltine potential. The cohort model generates the corresponding adult emergence function which we use to calculate the number of effective beetles and subsequently the first generation R-value denoted by R_1. The bottom of the adult emergence function is truncated by the attack threshold A and then normalized (by dividing by the number of effective beetles) into a probability distribution which we use as the attack distribution for the second generation. The cohort model generates the second generation adult emergence function from which we calculate the R-value for the second generation denoted by R_2.

The effect of bivoltinism on a yearly population growth rate is multiplicative. That is, if the temperature signal permits the emergence (from a singe tree infested in June) of enough first generation effective adults in the fall to infest R_1 more trees, and if R_2 trees are then infested by each of those R_1 trees by the end of next June, the total number of trees newly infested by the original tree is $R_1 \cdot R_2$. Thus, we take the population growth rate for the year to be the product of the first and second generation R-values,

$$R_{BV} = R_1 R_2,$$

where we use R_{BV} to denote the yearly growth rate of a bivoltine population of beetles.

3.3 Results

In providing an assessment of climate change impact on bark beetle disturbances, we predict and analyze yearly univoltine MPB population growth rates, the potential for bivoltine life cycles, and where the potential exists, yearly bivoltine growth rates.

3.3.1 Univoltine population growth rates

Figures 3.7-3.10 show decadal geometric means of predicted univoltine R-values across the study area between 2025 and 2085. Included in each plot is a forest cover map (green areas) indicating the presence of MPB host trees. Positive mean R-values inside forested areas are plotted using the colormap on the left side of the figure while

values not in forested areas are plotted in grayscale.

Between 2025 and 2035, our model predicts non-zero growth rates in areas where MPB is currently known to have a presence. For example, we see sizable R-values in middle-elevation areas such as the Sawtooth National Forest, Greater Yellowstone area, and Flathead National Forest. With the exception of CanESM2 RCP-4.5 and CNRM-CM5 RCP-4.5, overall R-values generally decrease with time contradicting the intuitive notion that global warming should create conditions favorable to MPB life stage development and therefore population growth. Furthermore, elevations with significant growth rates increase as temperatures across the entire region increase.

3.3.2 Potential for bivoltine life cycles

In figures 3.13-3.16, we have plotted the number of years in a particular decade in which thermal signals permitted bivoltinism. Included in each plot is a forest cover map (green areas) indicating the presence of MPB host trees. Bivoltine potential inside forested areas are plotted using the colormap on the left side of figure while values not in forested areas are plotted in grayscale.

In general, bivoltine potential increases with time presumably as thermal conditions producing two generations per year set in with warming temperatures. Initially, bivoltinism is predicted for low elevations (for example, the snake River Plane and Montana grasslands) where temperatures are generally warmer. These areas are mostly unforested and therefore not relevant in our analysis as they have no MPB presence. However, with warming temperatures, bivoltine life cycles become possible at middle elevations and in particular, in MPB host tree areas. We first see host area potential for bivoltinism in the Clearwater River valley of Idaho which eventually extends well into Clearwater National Forest, Nez Perce National Forest, and Coeur D'Alene National Forest. Bivoltinism also begins to encroach on Boise and Sawtooth National Forests of Idaho as well as on Lewis and Clark and Helena National Forests of Montana in future thermal regimes.

3.3.3 Bivoltine population growth rates

The climate model CanESM2 RCP-8.5 yielded the largest area with MPB bivoltinism potential by the 2080s. As a worst case scenario, we have plotted in Fig. 3.19 geometric means of bivoltine population growth rates (R_{BV}-values) over the decade 2075-2085 generated by CanESM2 RCP-8.5 for the study area. Note that the range of R_{BV}-values is much larger than that of univoltine R-values due to the multiplicative nature of yearly population growth with two generations per year. Furthermore, bivoltine

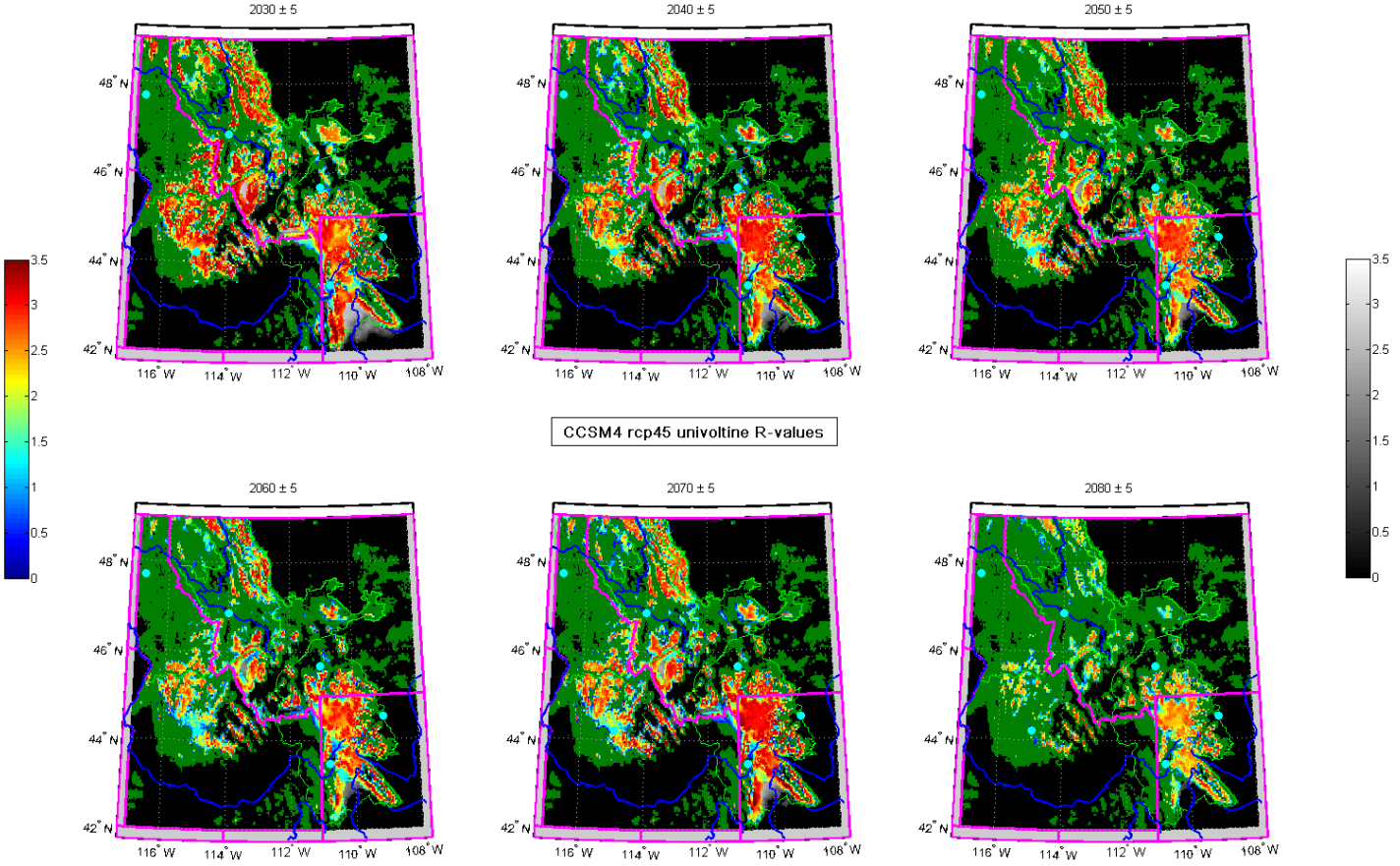

FIGURE 3.7: Decadal geometric means of MPB population growth rates (R-values) for climate model CCSM4 with RCP-4.5 emissions scenario (moderate climate mitigation). Positive R-values inside MPB host tree areas are plotted using the colormap on the left side of the figure while values not in host areas are plotted in grayscale. In time, R-values tend to diminish (beginning at low elevations) as temperatures increase and thermal regimes become unfavorable to univoltine MPB population success.

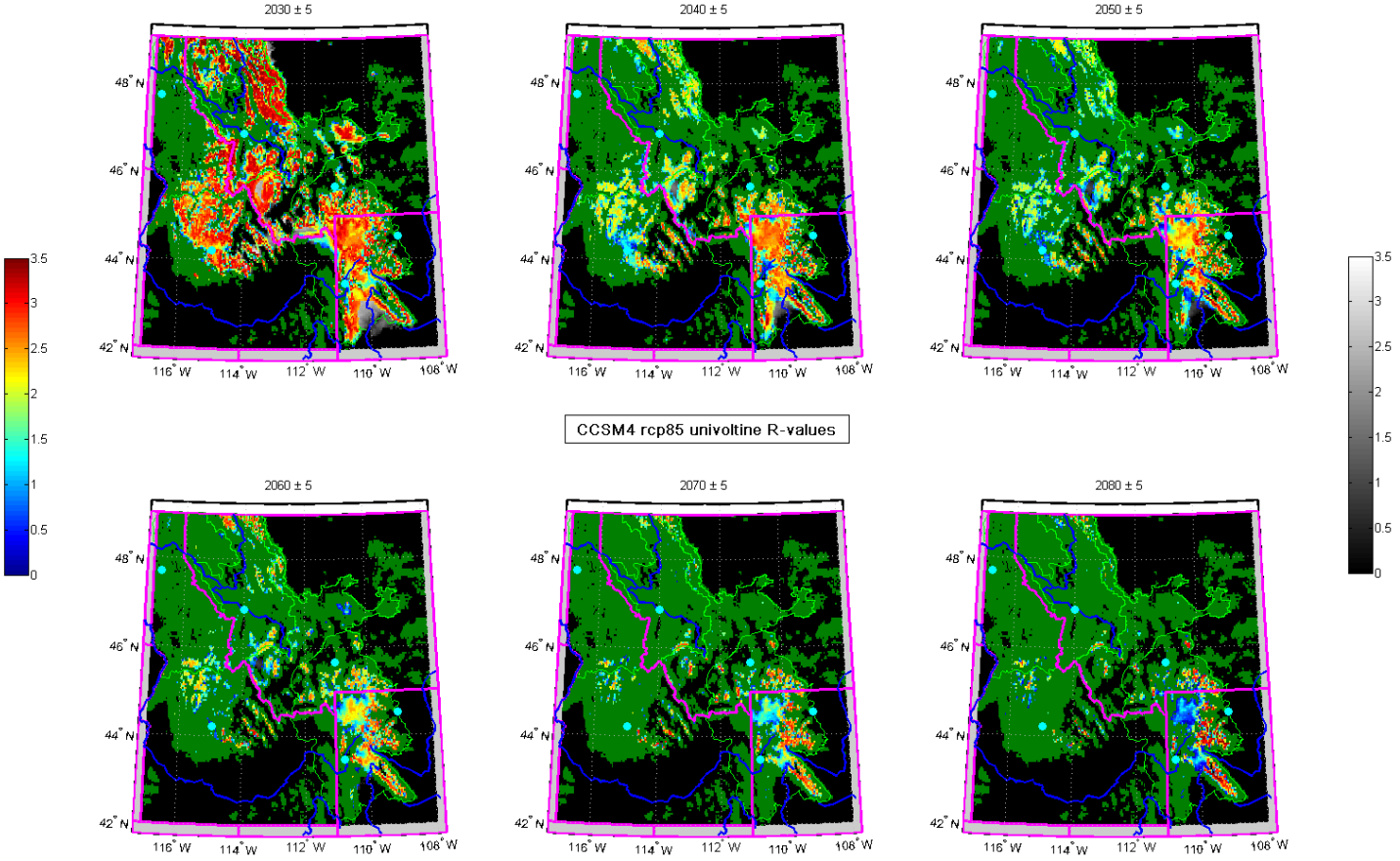

FIGURE 3.8: Decadal geometric means of MPB population growth rates (R-values) for climate model CCSM4 with RCP-8.5 emissions scenario (no climate mitigation). Positive R-values inside MPB host tree areas are plotted using the colormap on the left side of the figure while values not in host areas are plotted in grayscale. Significant warming creates conditions detrimental to univoltine MPB life cycles and hence, R-values diminish more rapidly than with RCP-4.5.

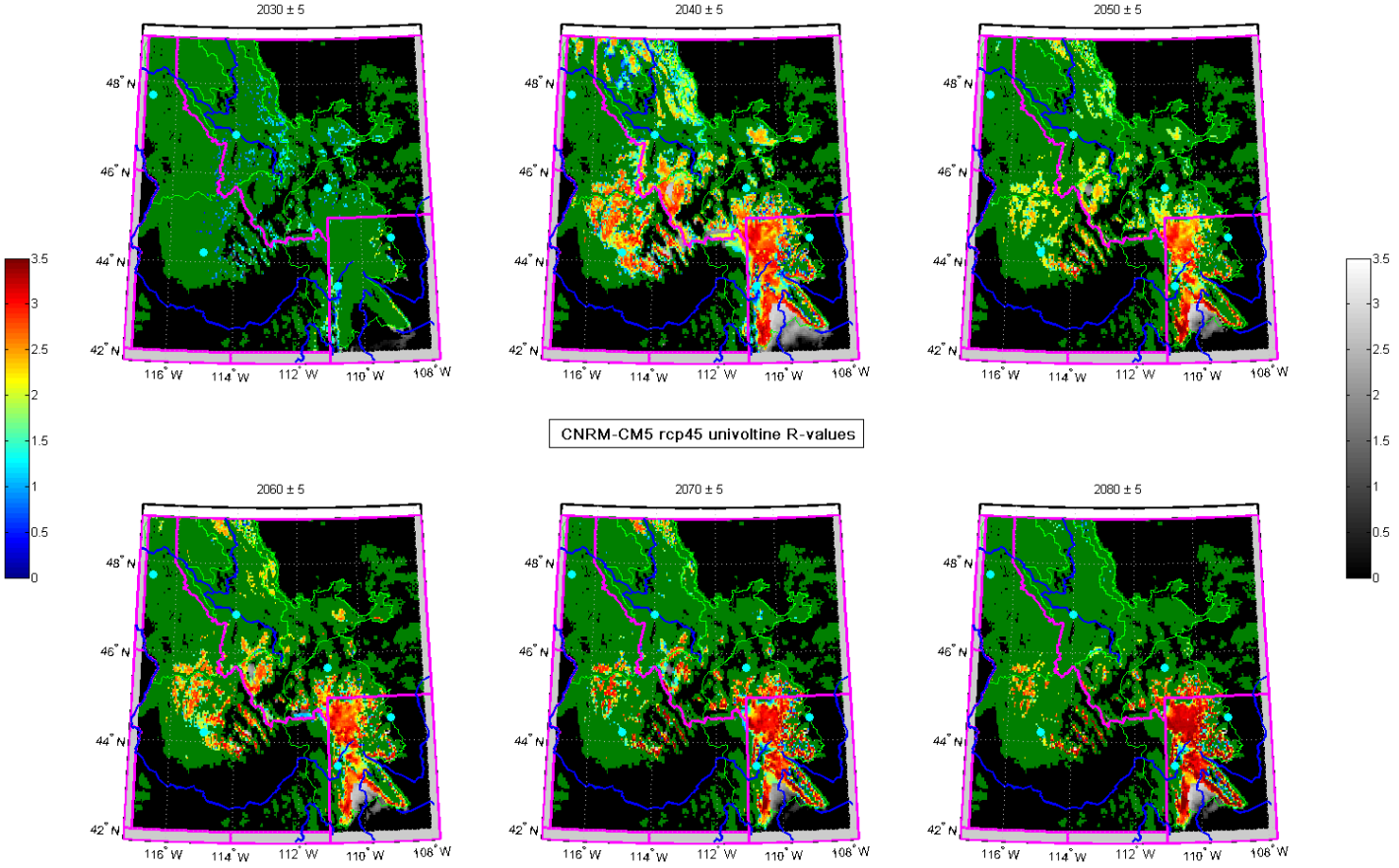

FIGURE 3.9: Decadal geometric means of MPB population growth rates (R-values) for climate model CNRM-CM5 with RCP-4.5 emissions scenario (moderate climate mitigation). Positive R-values inside MPB host tree areas are plotted using the colormap on the left side of the figure while values not in host areas are plotted in grayscale. Beginning around 2040, R-values at middle elevations diminish with time as temperatures increase and thermal regimes become unfavorable to univoltine MPB population success.

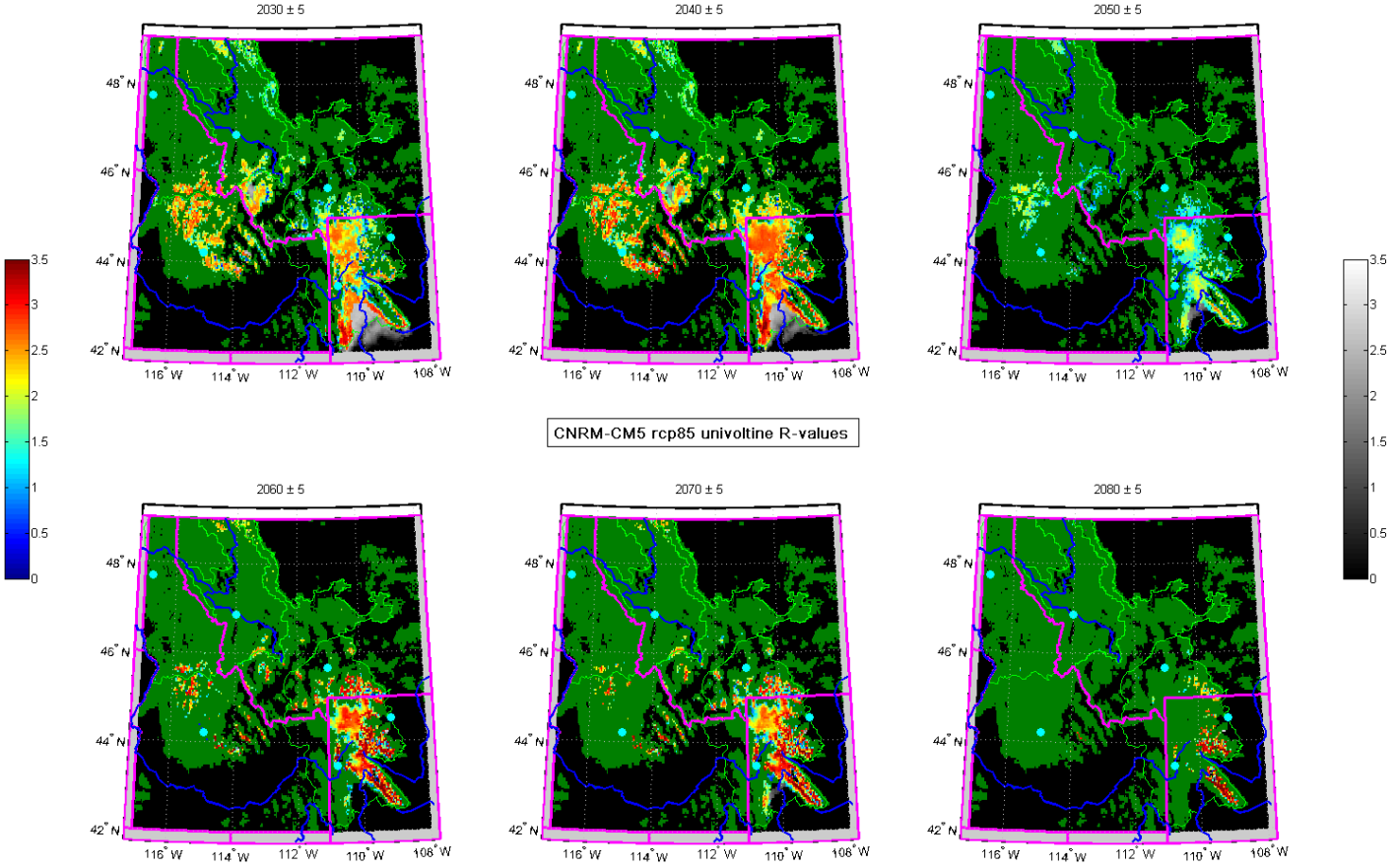

FIGURE 3.10: Decadal geometric means of MPB population growth rates (R-values) climate model CNRM-CM5 with RCP-8.5 emissions scenario (no climate mitigation). Positive R-values inside MPB host tree areas are plotted using the colormap on the left side of the figure while values not in host areas are plotted in grayscale. By 2080, significant warming creates conditions detrimental to univoltine MPB life cycles and hence, R-values diminish considerably across the study area.

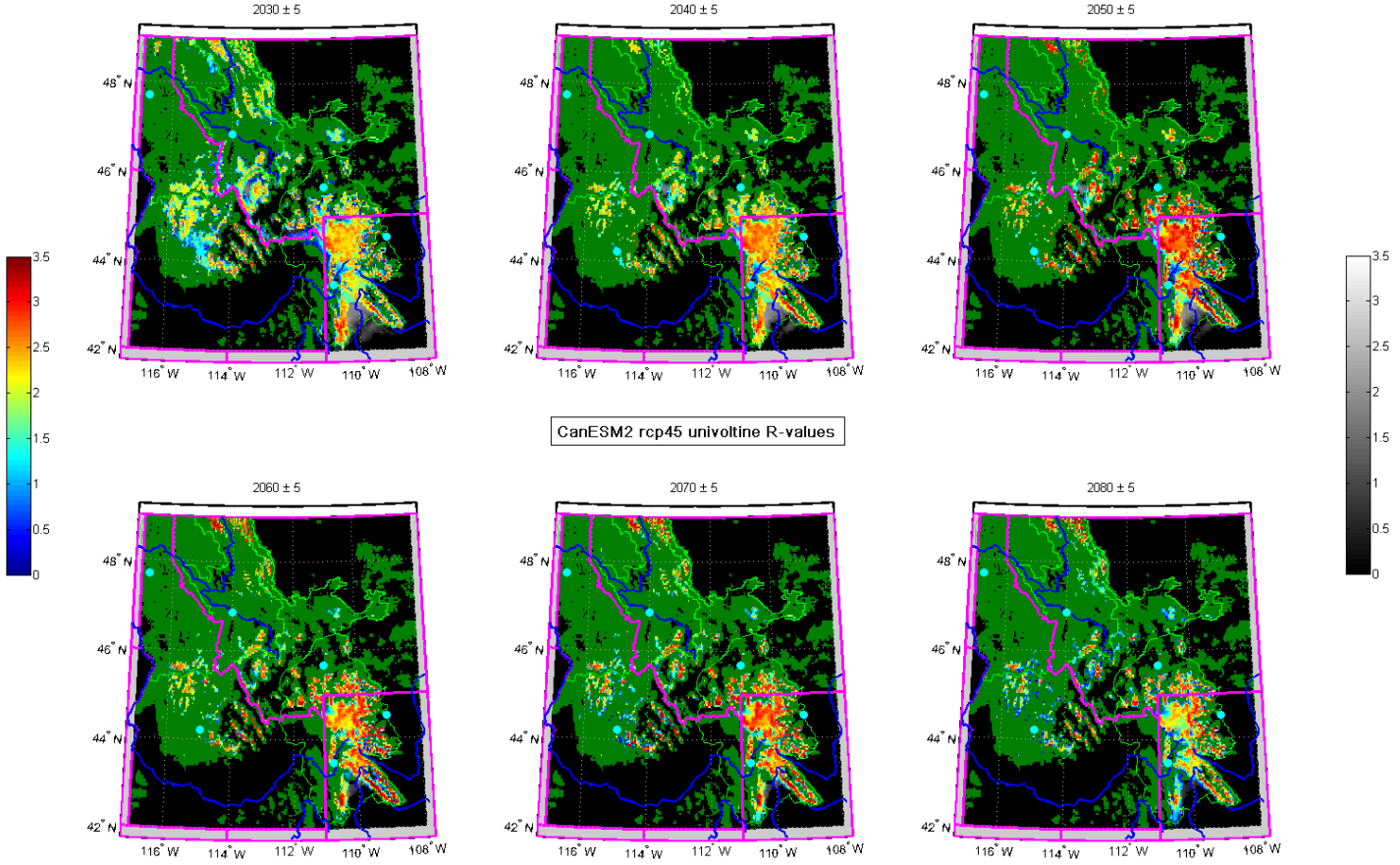

FIGURE 3.11: Decadal geometric means of MPB population growth rates (R-values) for climate model CanESM2 with RCP-4.5 emissions scenario (moderate climate mitigation). Positive R-values inside MPB host tree areas are plotted using the colormap on the left side of the figure while values not in host areas are plotted in grayscale. Growth rates initially increase and peak during the 2050s before slowly decreasing as thermal regimes become unfavorable to univoltine MPB population success.

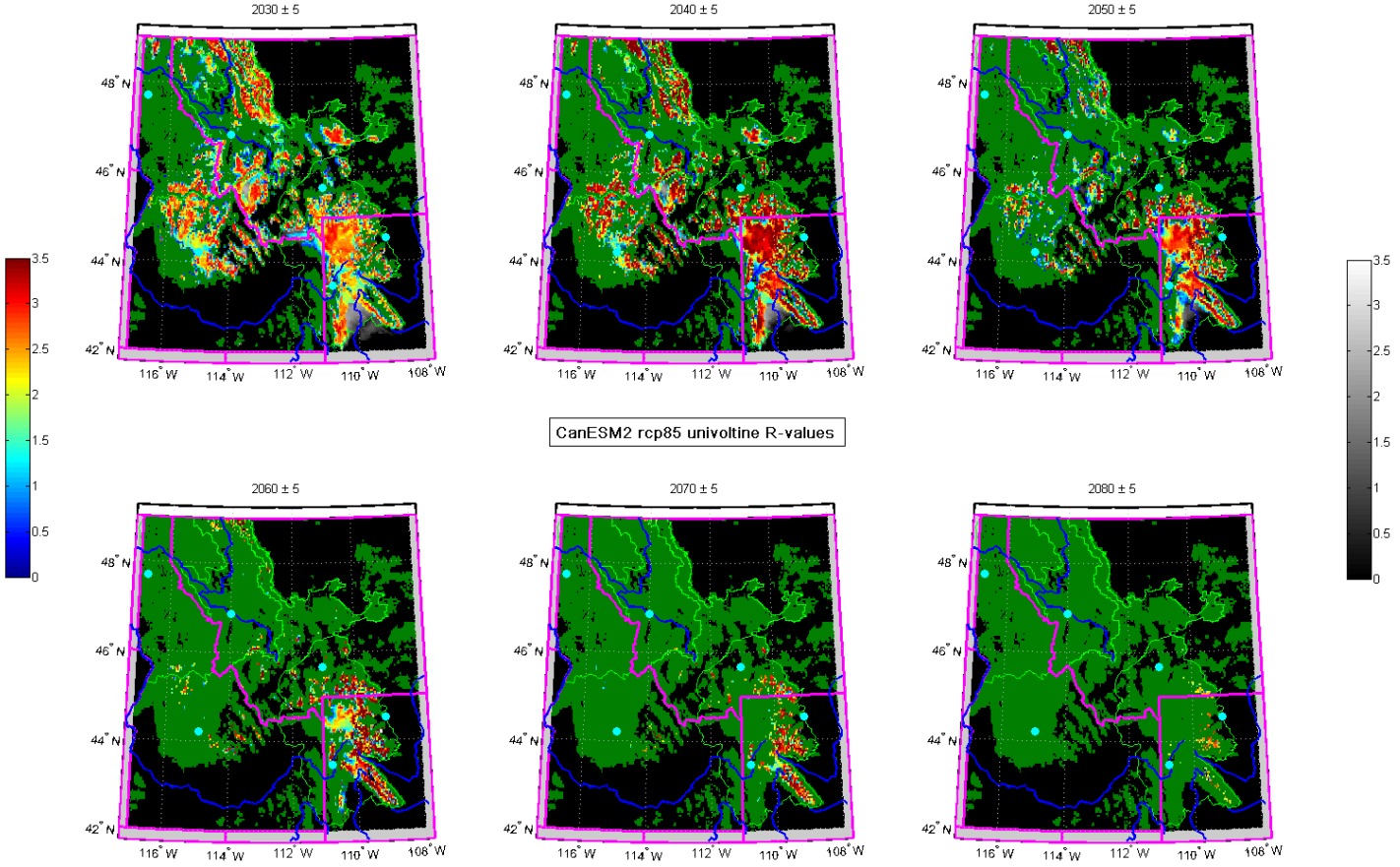

FIGURE 3.12: Decadal geometric means of MPB population growth rates (R-values) for climate model CanESM2 with RCP-8.5 emissions scenario (no climate mitigation). Positive R-values inside MPB host tree areas are plotted using the colormap on the left side of the figure while values not in host areas are plotted in grayscale. Significant warming creates conditions detrimental to univoltine MPB life cycles and hence, R-values diminish more rapidly than with RCP-4.5.

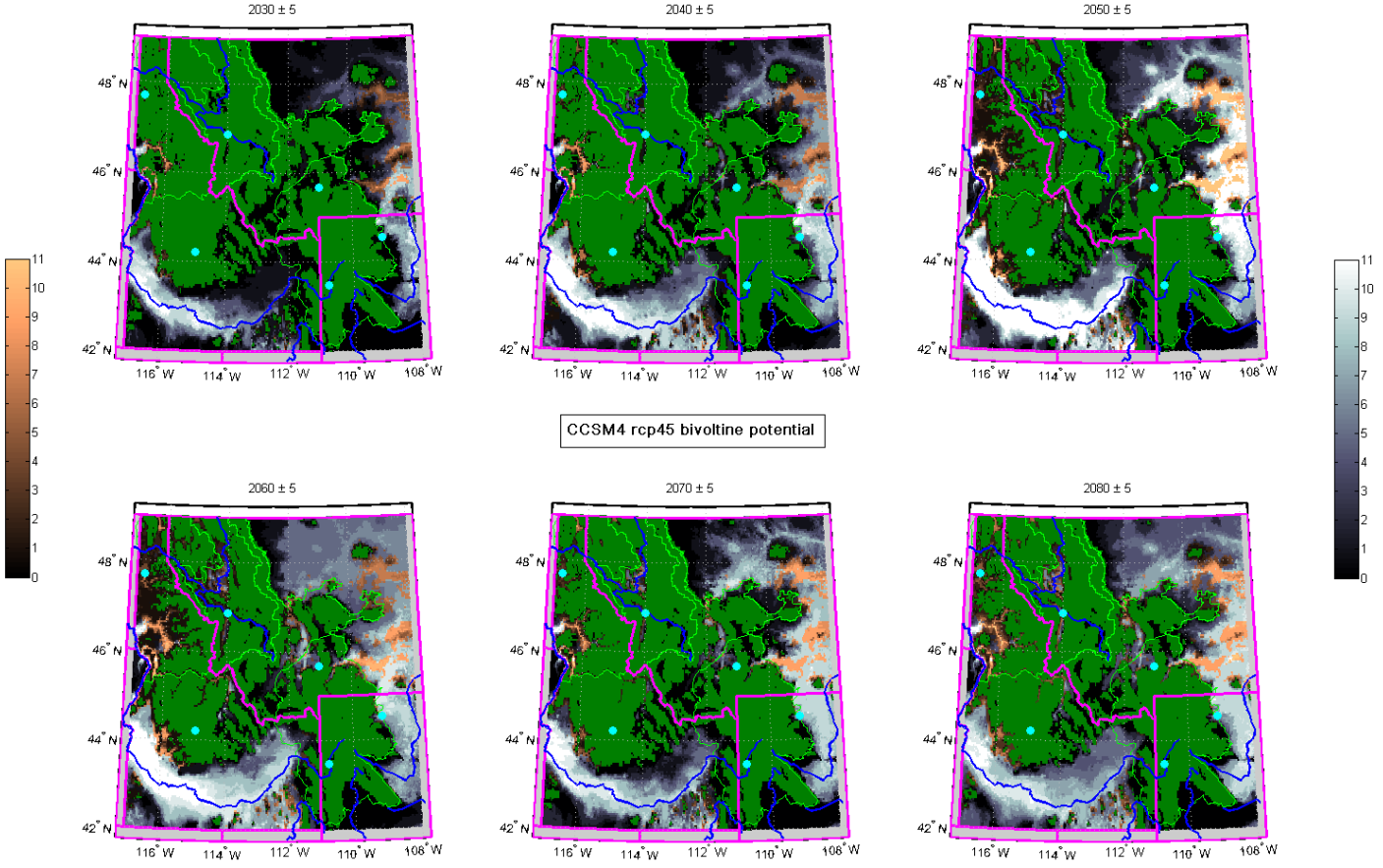

FIGURE 3.13: Number of years in a particular decade in which temperatures will permit bivoltinism for climate model CCSM4 with RCP-4.5 emissions scenario (moderate climate mitigation). Number of years with predicted bivoltine life cycles inside MPB host tree areas are plotted using the colormap on the left side of the figure while values not in host areas are plotted in grayscale. Initially, bivoltinism potential exists at low elevation areas primarily without forest cover (for example, the Snake River Plane and Montana grasslands) where temperatures are generally warmer. With warming temperatures, bivoltine life cycles become possible at middle elevations and in particular, in MPB host areas.

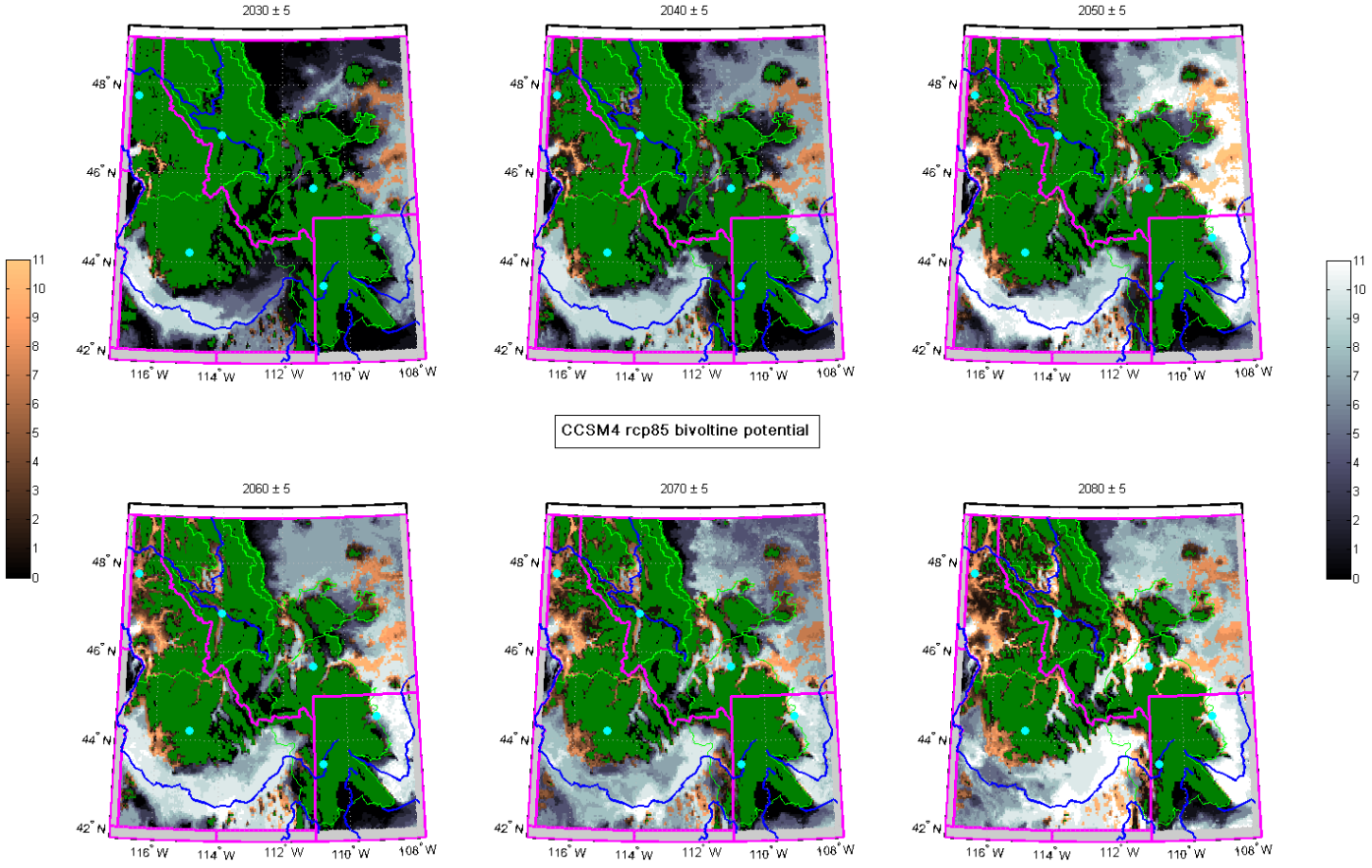

FIGURE 3.14: Number of years in a particular decade in which temperatures will permit bivoltinism for climate model CCSM4 with RCP-8.5 emissions scenario (no climate mitigation). Number of years with predicted bivoltine life cycles inside MPB host tree areas are plotted using the colormap on the left side of the figure while number of bivoltine years not in host areas are plotted in grayscale. Initially, bivoltinism potential exists at low elevations (for example, the Snake River Plane and Montana grasslands) where temperatures are generally warmer. In time, as temperatures are projected to increase significantly more than with RCP-4.5, potential for bivoltinism increases substantially across the study area and in particular, in MPB host areas.

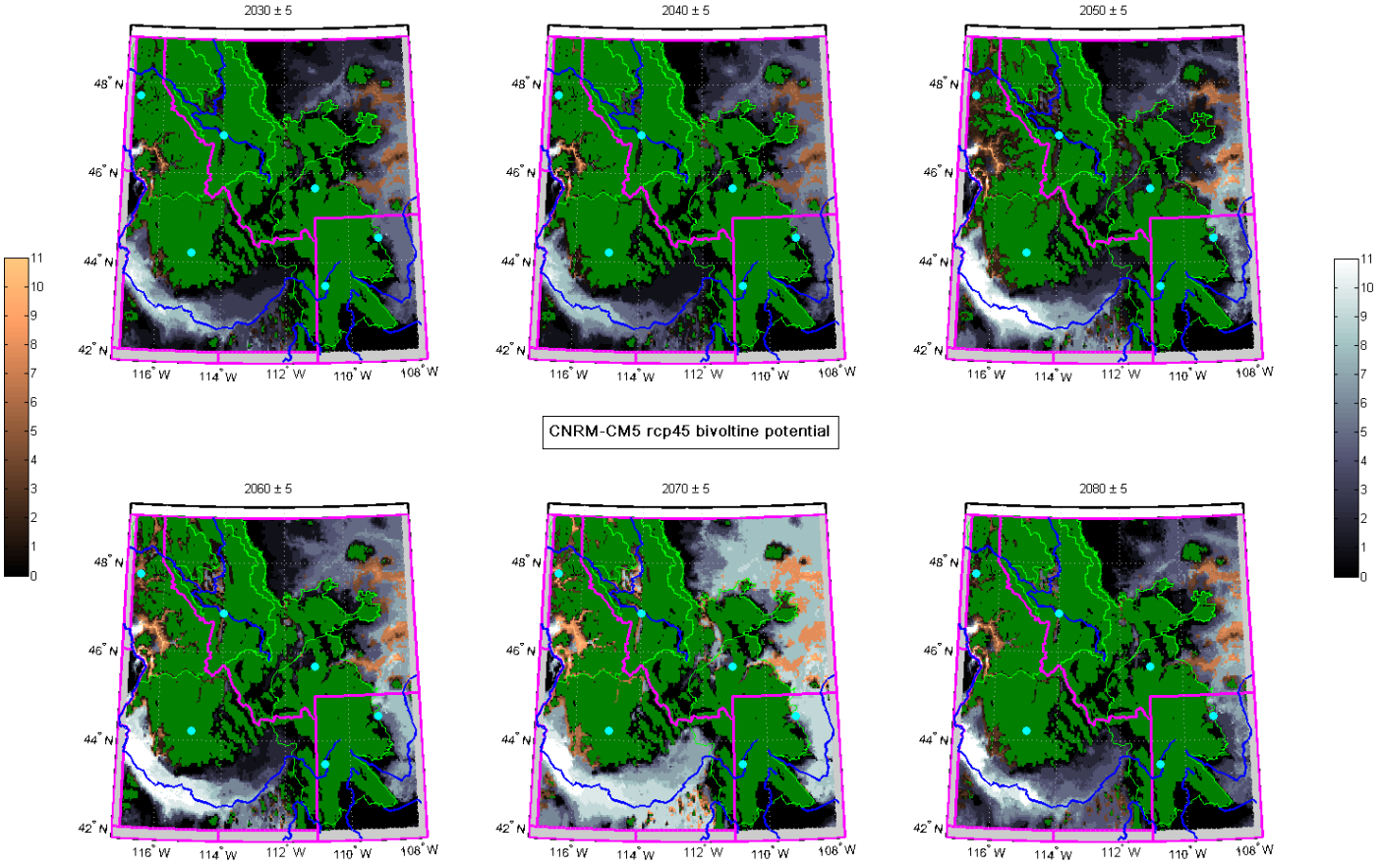

FIGURE 3.15: Number of years in a particular decade in which temperatures will permit bivoltinism for climate model CNRM-CM5 with RCP-4.5 emissions scenario (moderate climate mitigation). Number of years with predicted bivoltine life cycles inside MPB host tree areas are plotted using the colormap on the left side of the figure while number of bivoltine years not in host areas are plotted in grayscale. Initially, bivoltinism potential exists at low elevation areas primarily without forest cover (for example, the Snake River Plane and Montana grasslands) where temperatures are generally warmer. With moderately warmer temperatures projected by CNRM-CM5 RCP-4.5, bivoltinism expands only slightly into middle elevations and MPB host areas.

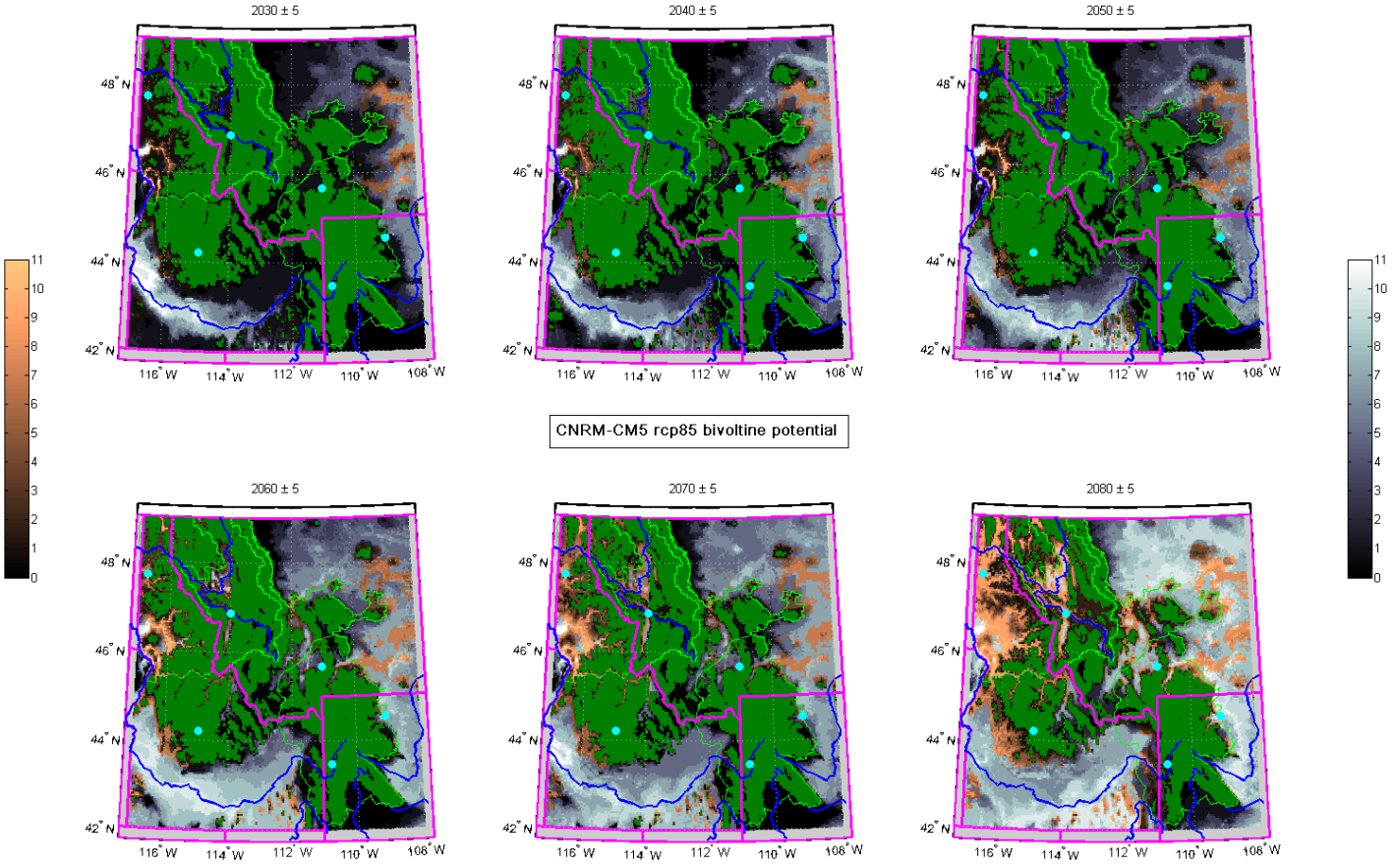

FIGURE 3.16: Number of years in a particular decade in which temperatures will permit bivoltinism for climate model CNRM-CM5 with RCP-8.5 emissions scenario (no climate mitigation). Number of years with predicted bivoltine life cycles inside MPB host tree areas are plotted using the colormap on the left side of the figure while number of bivoltine years not in host areas are plotted in grayscale. Initially, bivoltinism potential exists at low elevations (for example, the Snake River Plane and Montana grasslands) where temperatures are generally warmer. In time, as temperatures are projected to increase significantly more than with RCP-4.5, potential for bivoltinism increases substantially across the study area and in particular, in MPB host areas.

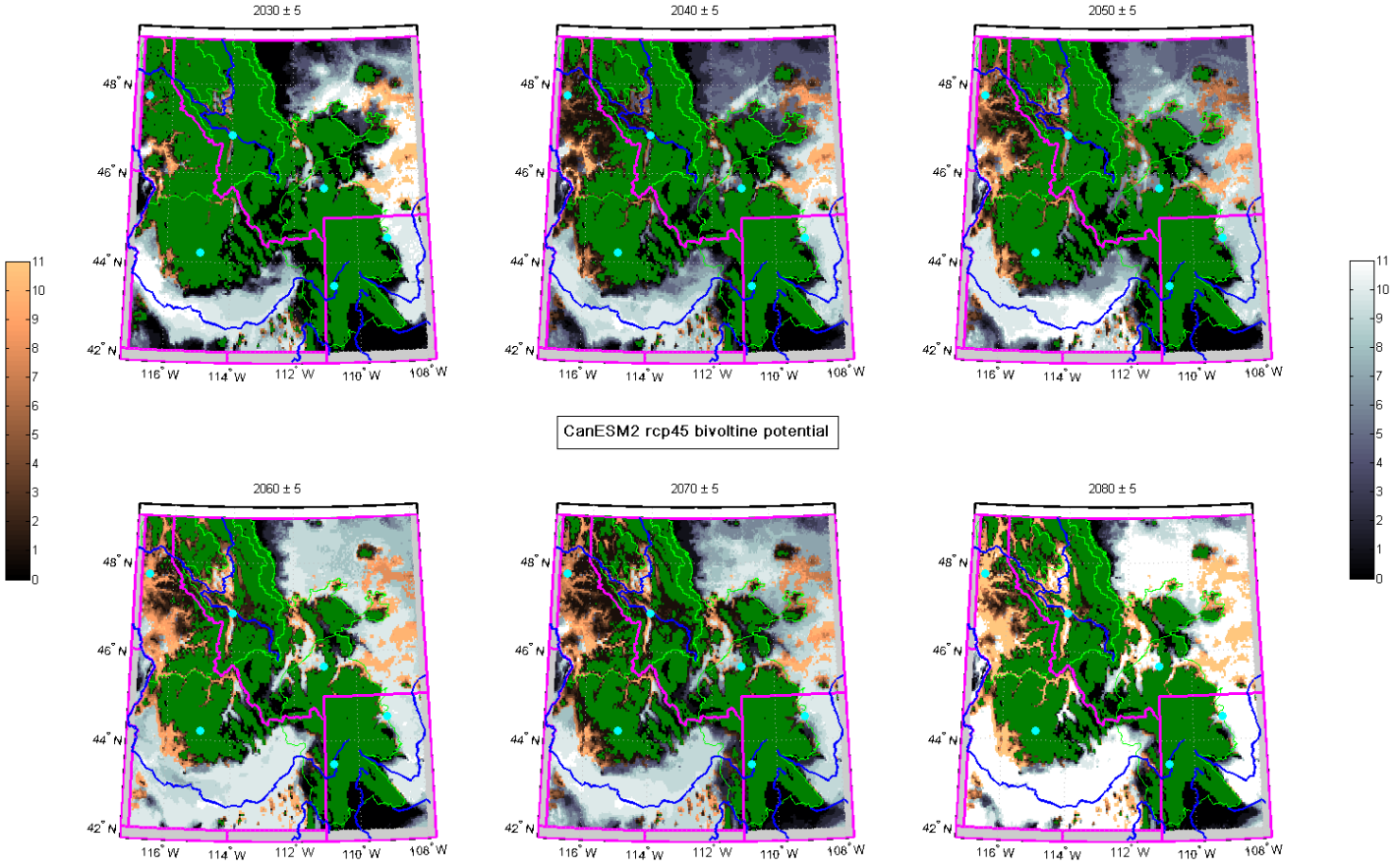

FIGURE 3.17: Number of years in a particular decade in which temperatures will permit bivoltinism for climate model CanESM2 with RCP-4.5 emissions scenario (moderate climate mitigation). Number of years with predicted bivoltine life cycles inside MPB host tree areas are plotted using the colormap on the left side of the figure while number of bivoltine years not in host areas are plotted in grayscale. Initially, bivoltinism potential exists at low elevation areas primarily without forest cover (for example, the Snake River Plane and Montana grasslands) where temperatures are generally warmer. With more warming projected by CanESM2 RCP-4.5 than with CCSM4 RCP-4.5 and CNRM-CM5 RCP-4.5, bivoltine life cycle potential becomes more expansive at middle elevations in MPB host areas than with the other two GCMs.

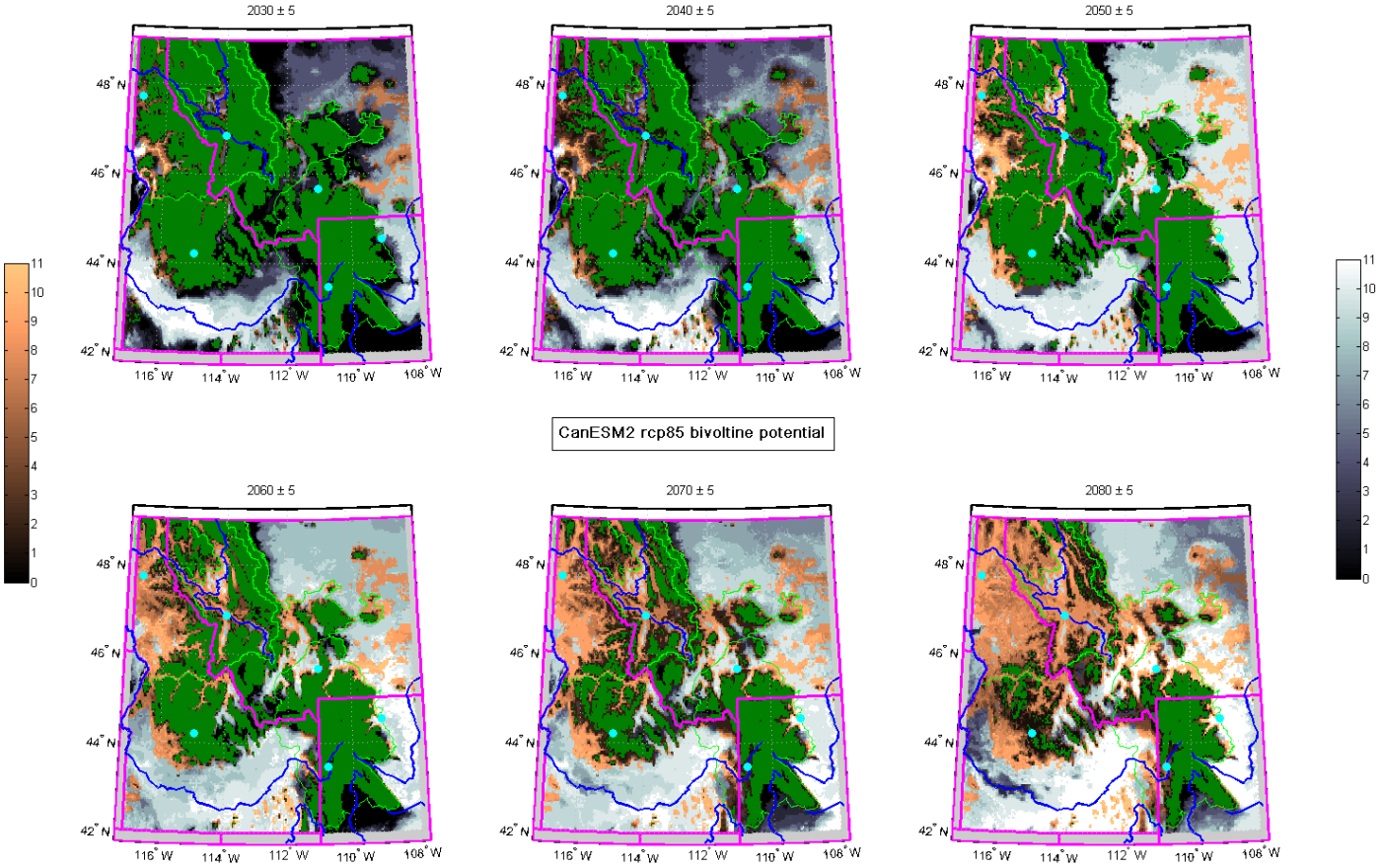

FIGURE 3.18: Number of years in a particular decade in which temperatures will permit bivoltinism for climate model CanESM2 with RCP-8.5 emissions scenario (no climate mitigation). Number of years with predicted bivoltine life cycles inside MPB host tree areas are plotted using the colormap on the left side of the figure while number of bivoltine years not in host areas are plotted in grayscale. Initially, bivoltinism potential exists at low and slightly at middle elevations (for example, the Snake River Plane, Montana grasslands, and the Clearwater River valley of Idaho) where temperatures are generally warmer. With the most significant temperature increases projected by any of the GCMs, CanESM2 RCP-8.5 epitomizes a worst case scenario. As temperatures increase, potential for bivoltinism nearly envelopes the entire host tree area in the northeast quadrant of the study area.

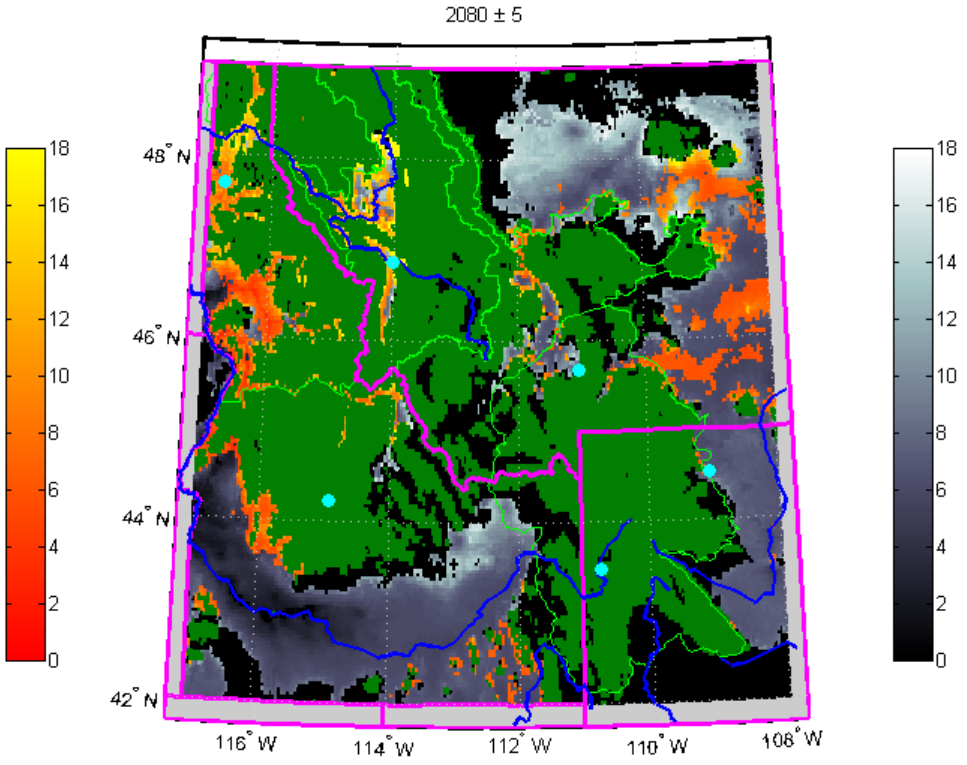

FIGURE 3.19: Geometric means of predicted bivoltine population growth rates (R_{BV}-values) over the decade 2075-2085 generated by CanESM2 RCP-8.5. Note that the range of bivoltine R_{BV}-values is much larger than that of univoltine R-values due to the multiplicative nature of yearly population growth with two generations per year.

potential must exist in all years of the decade in order to have non-zero geometric mean of R_{BV}-values. Areas with significant R_{BV}-values include the Coeur D'Alene region, Clearwater River valley, Boise National Forest, and small patches in Flathead National Forest and around Missoula, MT and Helena, MT.

3.4 Discussion and Conclusion

At low to middle elevations (< 2000m), univoltine population growth rates decrease on average across the study area (Fig. 3.20). As temperatures increase with time due to global warming, the R-model predicts lower adult emergence and correspondingly smaller univoltine R-values. It is likely that significantly high temperatures actually disrupt MPB seasonality and produce unsynchronized adult emergence (Bentz et al. 2014). This is reflected in the R-model by the seasonal window for successful attack. If adult emergence is outside this window or spread out enough so the attack threshold is never exceeded, effective beetles E_n and hence R will be zero. Furthermore, because warmer temperatures generally translate to faster life stage development, beetles may

end up in non-cold-hardened life stages over winter and experience high overwintering mortality. Since RCP-8.5 assumes no climate action and hence higher mean surface temperatures, MPB population growth rates decline more rapidly with RCP-8.5 than with RCP-4.5.

At middle elevations (2000m to 3000m), decline in population growth rates is (relatively) less dramatic. Thermal conditions for optimal MPB development and hence high population growth are already present in this elevational range. Higher than some critical elevation in this range where growth rates are roughly constant, R-values transition from decreasing to increasing.

At high elevations ($>$ 3000m), beetle populations may initially be semivoltine but temperatures are too low for univoltinism. In time, univoltine R-values increase as warming creates developmentally favorable conditions. The higher the elevation, the longer beetles must wait for univoltine-optimal temperature signals.

As temperatures increase across all elevational ranges, some beetles may acquire the phenological potential to complete two generations in a single year while avoiding overwintering mortality. This results in zero univoltine population growth ($R = 0$) while the potential for bivoltinism increases (Fig. 3.20). Since RCP-8.5 projects worst case scenario warming, area with predicted bivoltinism is greater with RCP-8.5 than with RCP-4.5. Low elevations ($<$ 1000m) experience the greatest bivoltine potential regardless of emissions scenario. However, when limited to areas with pine tree coverage, total area with bivoltine potential is significantly reduced since there are few pines at very low elevations.

Host areas with greatest bivoltine potential are between 1000m and 2000m where there is ample thermal energy to allow for bivoltinism. At elevations between 2000m and 3000m, area with potential for bivoltine life cycles increases with time but overall is substantially smaller than at lower elevations as thermal energy is less available. Finally, at high elevations, temperatures are too cold for bivoltinism.

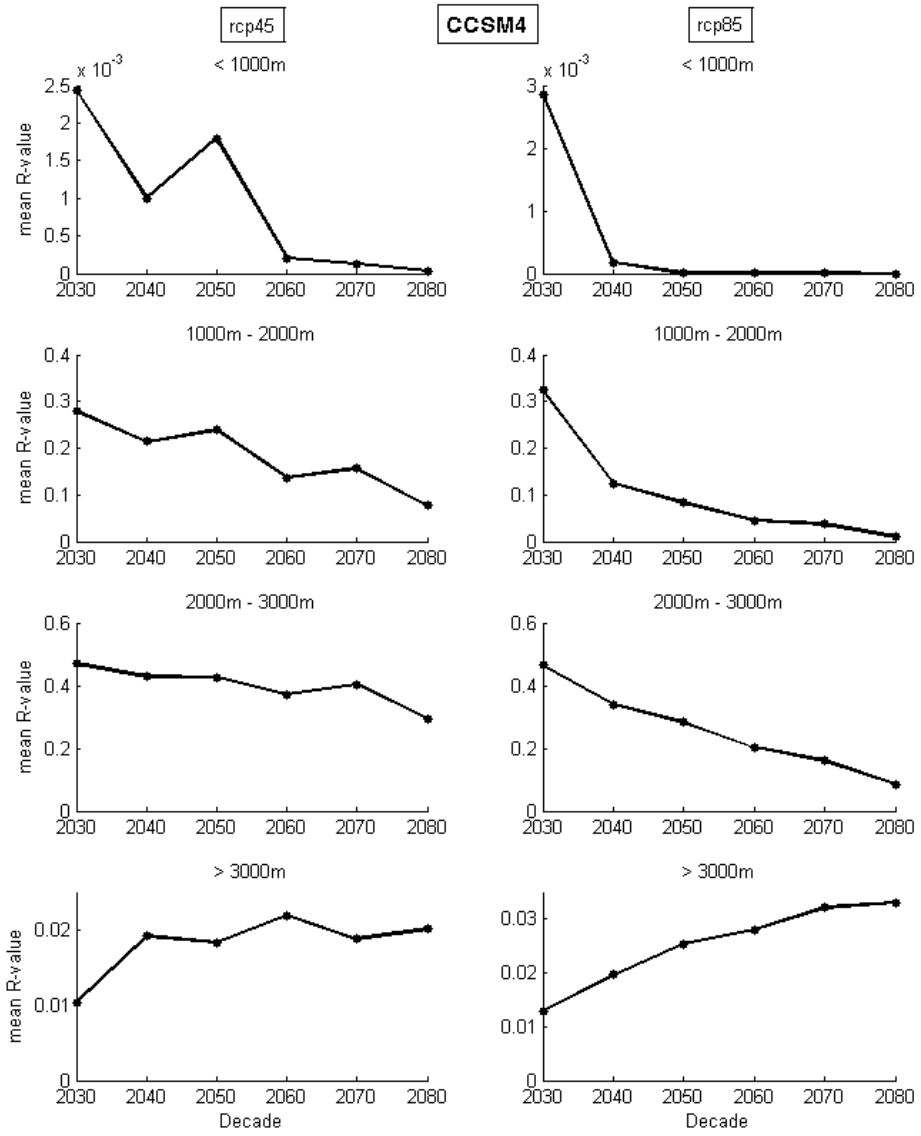

FIGURE 3.20: Decadal mean univoltine population growth rates (R-values) across forested regions of the study area. At low to middle elevations (< 2000m), univoltine population growth rates decrease on average across the study area as high temperatures disrupt MPB seasonality and produce unsynchronized adult emergence. Since RCP-8.5 assumes no climate action and hence higher mean surface temperatures, MPB growth rates decline more rapidly with RCP-8.5 than with RCP-4.5. At high elevations (> 3000m), R-values increase as warming creates developmentally favorable conditions. Because RCP-8.5 projects more warming than RCP-4.5, MPB growth rates increase more rapidly with RCP-8.5 than with RCP-4.5.

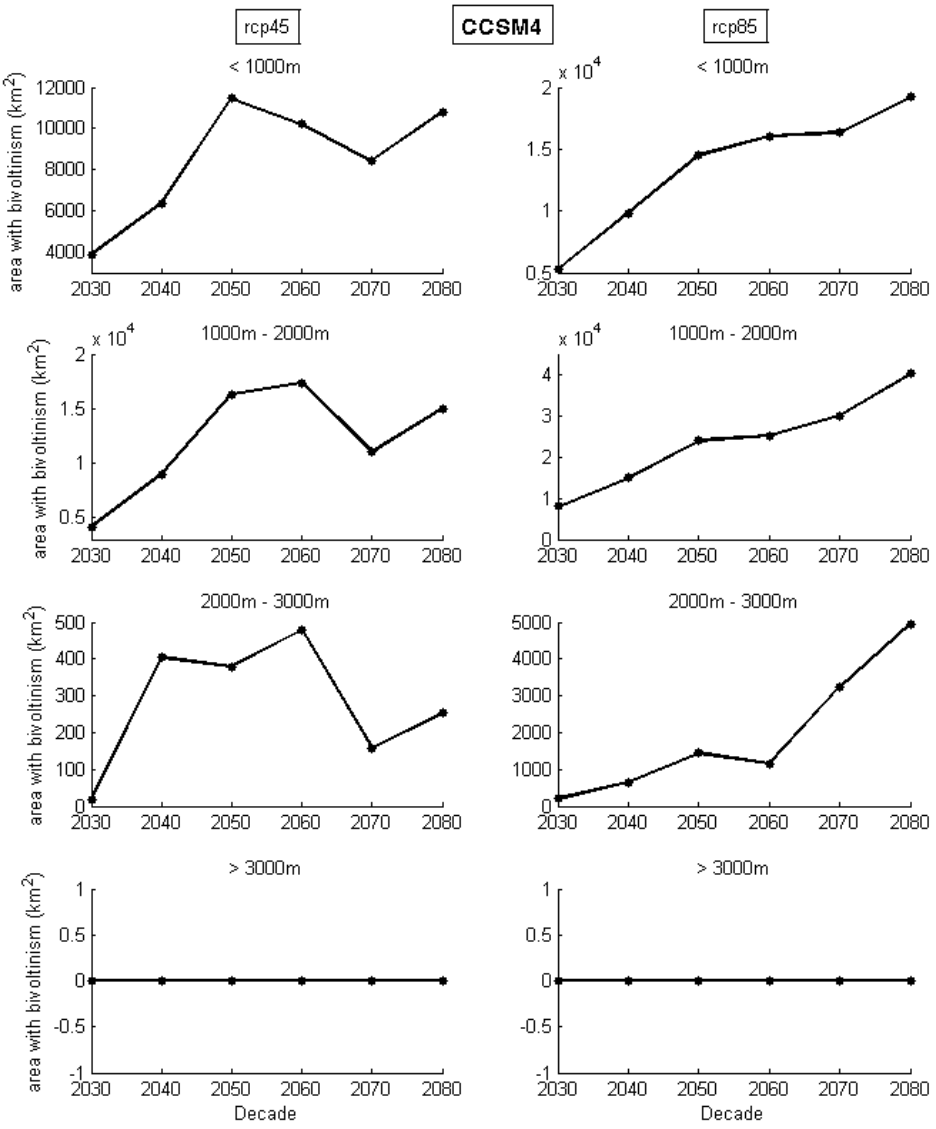

FIGURE 3.21: Decadal mean area with bivoltine potential across forested regions of study area. Host areas with greatest bivoltine potential are between 1000m and 2000m where there is ample thermal energy to allow for bivoltinism. At elevations between 2000m and 3000m, area with potential for bivoltine life cycles increases with time but overall is substantially smaller than at lower elevations as thermal energy is less available. At high elevations, temperatures are too cold for bivoltinism. Since RCP-8.5 projects worst case scenario warming, area with predicted bivoltinism is greater with RCP-8.5 than with RCP-4.5.

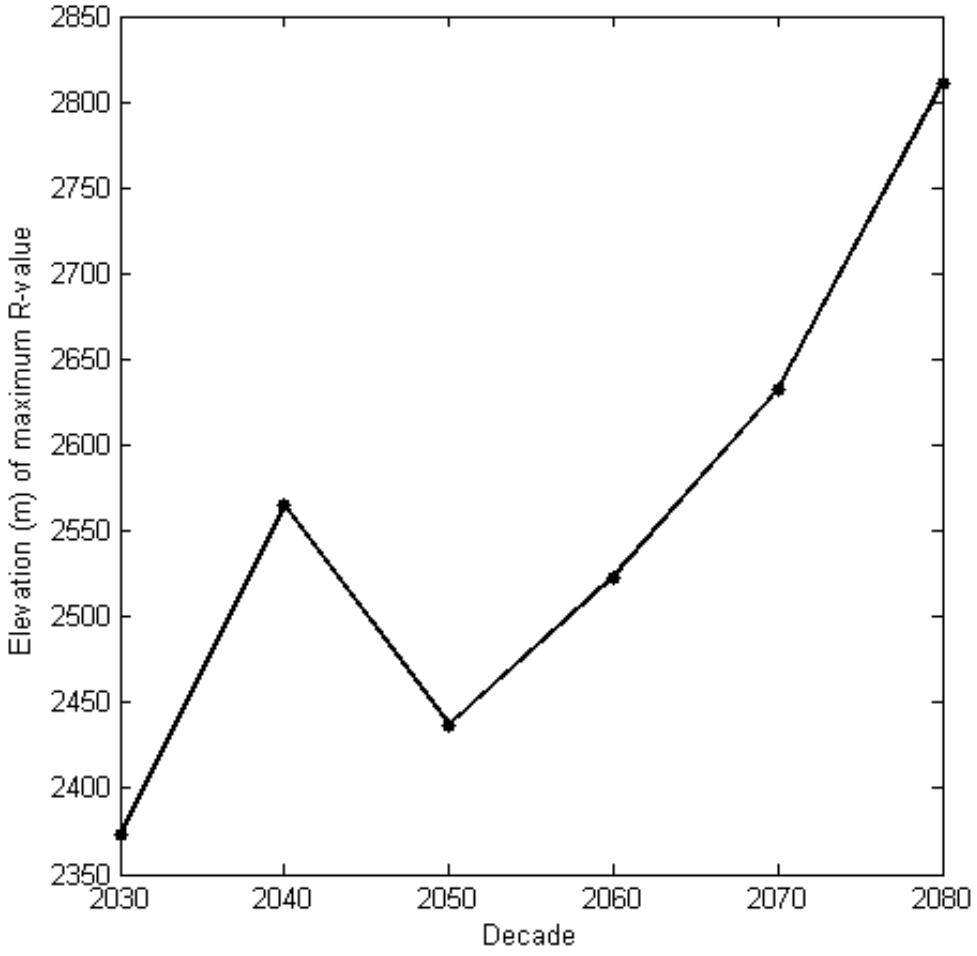

FIGURE 3.22: Elevation with optimal thermal conditions for univoltine MPB development increases with time (using mean R-values across GCMs).

Chapter 4
INVASION WAVE SPEED AND SEVERITY OF MOUNTAIN PINE BEETLE OUTBREAKS

4.1 Introduction

The mountain pine beetle (*Dendroctonus ponderosae*) is one of the most aggressive phytophagous predators in western North American forests. Some species of conifers have evolved significant defensive responses to bark beetle attacks such as the secretion of resin to impede a beetle's ability to bore into a host tree (Amman and Cole, 1983). It is necessary for mountain pine beetle (MPB) to mass attack a tree to successfully overcome these anti-predator adaptations (Berryman et al., 1985). Attacking adults lay eggs in the phloem layer, then larvae hatch and consume the phloem, killing the host tree. The summer following an effective attack, pine needles will have turned red, while MPB emerge en masse from "red-tops" and take flight in search of new hosts to colonize (Reid, 1962).

Although outbreaks of MPB have historically been normative (Mattson, 1996) in lodgepole pine (*Pinus contorta*) forests, recent outbreaks have been far more severe and expansive than in previous decades due in part to warming climate (Bentz et al., 2010). Aside from temperature-dependent phenology, two of the main drivers of the irruptive nature of MPB population dynamics are host tree stand demographic structure and spatial effects of beetle dispersal (Bjornstad et al., 2002; Aukema et al., 2008).

There is a clear analogy between waves of disease in human and animal populations (Anderson and May, 1979a,b) and waves of MPB infestation in pine forests; an extensive literature on infectious disease models with demographic structure also exists (Hethcote, 1994, 2000; Keeling, 1999; Riley, 2007). Heavilin et al. (2007); Heavilin and Powell (2008) built several red-top models in the spirit of the classic SIR (Susceptible-Infected-Recovered) infectious disease model (Kermack and McKendrick, 1927). These models elucidated that the severity of an outbreak wave depends on the number of available susceptible individuals, infectivity of the disease, and removal/recovery rate of infected

individuals.

However, Heavilin's red-top and other epidemiological models, though class structured, fall short of capturing the long recovery period of a forest affected by a MPB outbreak. A stand of pines is considered recovering when most trees are juvenile and do not have a large enough phloem layer to facilitate successful MPB colonization. It takes 50 to 100 years for a lodgepole pine to reach sufficient size to be susceptible to MPB attack. In order to model the dynamics of an outbreak cycle with an extended recovery period and make realistic predictions of severity, it is necessary to incorporate several latency classes.

While the red-top models of Heavilin and Powell (2008) are successful in capturing the advance of infestation through a forest of healthy trees by addressing MPB dispersal, their model-generated waves of infected trees do not persist indefinitely as in realistic forests. Abramson et al. (2003), who modeled the spread of the hantavirus infection in deer mice using a continuous SIR type epidemiological model coupled with a diffusion term for spatial dispersal of infectives, showed that travelling waves of infection can persist indefinitely. However, a continuous (e.g. differential equation) model is not appropriate for insect infestations on account of the discrete nature of insect life cycles. In particular, MPB typically completes one generation per year which necessitates discrete time modelling constructs such as difference equations. There is a substantial amount of literature proving the existence of travelling waves generated by disease outbreak models (for example, (Ruan and Xiao, 2004). However, methods for predicting the impact of a propagating wave on hosts are few. Furthermore, there exist no analytic approximations of outbreak severity to date.

The speed of an invading wave of infestation plays a critical role in determining the intensity of an outbreak. Kot et al. (1996) as well as Neubert and Caswell (1996) have discussed methods for calculating invasion speeds for unstructured and structured invasive populations respectively. Outbreak wave profiles in time (at a fixed position in space) due to travelling waves are known to be asymmetrical with different peak values than the symmetrical waves of disease generated by standard (non-spatial) SIR models. Duncan et al. (2015) developed analytic methods for approximating the severity of an outbreak generated by an age-structured forest demographic model which did not account for spatial structure created by MPB dispersal. However, methods for predicting the intensity of travelling periodic invasion waves arising from structured demographic models conjoined with dispersal components have not yet been developed.

In this paper, we construct a system of integrodifference equations (IDE) that model the densities of pine trees infested by MPB, healthy uninfested trees, and age classes of juvenile trees which are not susceptible to mass MPB attack. The structured demographic model is coupled with a Gaussian redistribution kernel to emulate MPB dispersal each summer in their search for new susceptible host trees. Redistributing MPB across a landscape in which previously infested trees may not be reinfested for 50 - 100 years (via mortality and seedling regrowth to susceptible size) generates a train of sustained solitary waves of infestation that move through a forest with constant speed. At a stationary point in the forest, a passing wave manifests temporally as an outbreak at the stand level.

We use a WKB approximation in conjunction with the method of steepest descent to evaluate the convolution integral in the IDE for infested trees. This enables a transition to a continuous setting by converting the resulting difference equation to a second order nonlinear partial differential equation (PDE). A search for travelling wave solutions of the PDE results in predictions of the shape of an outbreak wave profile and of its peak (maximum infestation) as functions of the speed of the wave. By linearizing the IDE, we calculate an estimate of the rate of invasion that depends solely on model parameters. We are left with an explicit formula for predicting the severity of an outbreak based on MPB population growth rate and host searching efficiency. This prediction compares favorably with peak impact observations taken during a recent outbreak in the Sawtooth National Recreation Area (SNRA) of central Idaho.

4.2 Model Development

MPB spend their first 7 life stages (egg through pupae) beneath the bark of a host pine tree (Reid, 1962). Upon molting into mature adults, they emerge from the tree and disperse by flight in search of new hosts. Adult MPB attack live trees and lay eggs in the phloem layer typically during mid to late summer. Eggs hatch and the larvae feed on the phloem while developing into mature MPB, which eventually results in the death of the host tree (Amman and Schmitz, 1988). As the tree dies, needles turn red (these trees are called “red tops” or “red snags”) by the following summer when MPB once again emerge and begin searching for new hosts. Two to three years later, needles turn gray (“gray snags”) and begin to fall off the tree. Lodgepole pine trees are shade intolerant and therefore need light to regenerate. The death of trees opens up the forest floor to sunlight and frees up resources previously unavailable to

seedlings (Schmidt and Alexander, 1985). Below we present a structured model for forest infestation, including susceptibles, snags, and nonsusceptible juveniles, with birth rates proportional to space freed up for seedlings as snags lose their needles and juveniles succumb to natural mortality.

4.2.1 Host Tree Life Cycle and Demographics

Juvenile Age Classes

MPB cannot successfully infest trees smaller than 25 cm in diameter at breast height (DBH) since the phloem layer is too thin to support beetle development. Furthermore, beetles developing in small trees have lower population growth rates and brood production increases with DBH (Safranyik, 2003). We assume a lower DBH threshold of 25 cm for infestations that lead to significant mass adult emergence. Thus, trees below a given age will be considered nonsusceptible and this age, NJ, is the number of juvenile age classes. For example, if trees have fixed radial growth rate of 1.5 mm/year (Reid and Gates, 1990), juvenile trees age 80 or younger are not susceptible to MPB attacks, and we take $NJ = 80$. The population density of juvenile trees in the k^{th} age class in year n at spatial location x is denoted by $j_{k,n}(x)$ while the total density of juveniles from all NJ age classes is represented by $J_n(x)$ measured in stems per hectare (ha). Figure 4.1 diagrams the evolution of host tree demographics over the course of one MPB generation (1 year) as well as the entire life history of a host.

In the spring, juvenile trees in an age class either survive with (constant) probability s and graduate to the next age class, or die with probability $d = 1 - s$. Total juvenile mortality in year n is dJ_n and

$$j_{k+1,n+1} = sj_{k,n}, \ k = 1, .., NJ - 1. \tag{4.1}$$

The total density of trees in the juvenile latency class is given by

$$J_n = \sum_{k=1}^{NJ} j_{k,n}. \tag{4.2}$$

Successful infestation kills the host tree and lodgepole pines lose nearly all their needles two years after infestation. Since lodgepole pine trees are not shade tolerant, seeds only germinate in gaps in the forest floor left by MPB infestation or other mortality. Hence, the snag classes, I_{n-1} and I_{n-2}, must be included in the model because they still shade the forest floor, delaying initiation of juvenile recruitment. Assuming there is

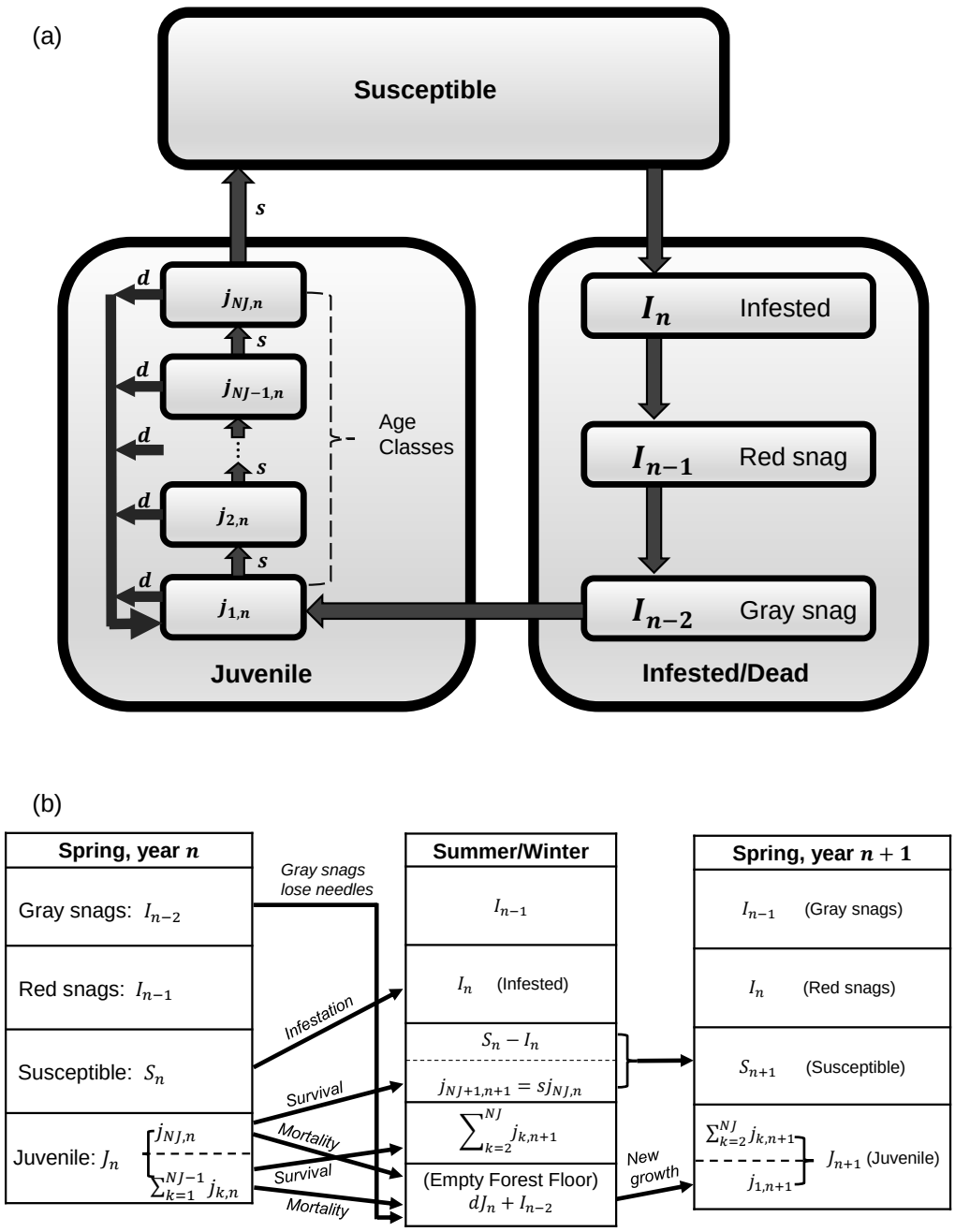

FIGURE 4.1: **(a)** Host tree life-cycle diagram. Natural juvenile mortality, d, opens up forest floor space to new seedling growth. Likewise, infestation mortality translates to seedling growth (after a once infested tree spends two years as a snag). Juvenile age class survivorship $s = 1-d$ is constant. Trees that survive to age $NJ+1$ years graduate (mature) into the class of susceptibles. **(b)** In spring, juvenile trees either die and leave empty spaces on the forest floor, or survive and graduate to the next age class. In summer, a susceptible tree either becomes infested or avoids infestation and remains in the class of susceptible trees. Over the winter, two-year-old snags lose all their needles creating a gap in the forest floor. In spring, seedlings sprout in any open forest floor space created by natural juvenile mortality or infestation mortality.

always an ample supply of seeds on the ground, seedlings sprout in the unshaded areas of the forest and we have

$$j_{1,n+1} = dJ_n + I_{n-2}. \tag{4.3}$$

Infested Class

In mid to late summer, beetles emerge from infested trees, search for new hosts, and attack. We let $I_n(x)$ denote the population density of infested trees and use a Ricker-type model (Ricker, 1958) for newly infested trees (following Powell and Bentz (2009)),

$$I_{n+1} = RI_n e^{-\beta(J_{n+1}+I_n+I_{n-1})},$$

where $J_{n+1} + I_n + I_{n-1}$ comprises the population of nonsusceptible trees. Here R is the number of trees that will become infested next year for each infested tree this year. The exponential factor represents the probability of infesting beetles encountering new susceptible trees in a Poisson search process with failure rate β, i.e., host searching inefficiency. When the density of nonsusceptible trees is greater than $\frac{\ln R}{\beta}$, a MPB epidemic cannot propagate.

To estimate the value of β, Powell and Bentz (2009) used observed infestation data derived from Aerial Detection Surveys (ADS) of the Sawtooth National Recreation Area (SNRA) in central Idaho conducted by USDA Forest Service, Forest Health Protection. Observers in fixed-wing aircraft measured the area impacted by MPB infestation each year with 30 m resolution. (Powell and Bentz, 2009) estimated the failure rate β at 10.8×10^{-6} per hectare of trees impacted using infestation (ADS) data taken during an outbreak that occurred in the SNRA between 1995 and 2005. From Crabb et al. (2012), the mean impact in the SNRA during the outbreak was estimated at 8.12 infested stems per hectare of all trees impacted (regardless of tree species). Furthermore, Crabb et al. (2012) estimated the total area of host trees (lodgepole pine) in the SNRA prior to the outbreak to be around 8410 ha. Thus we take

$$\beta = \left(10.8 \times 10^{-6} \frac{1}{\text{ha impacted}}\right)\left(\frac{1 \text{ ha impacted}}{8.12 \text{ infested stems}}\right)(8410 \text{ ha of hosts})$$

$$= 0.011 \frac{\text{ha}}{\text{infested stem}}.$$

Susceptible Class

In spring the density of susceptible trees, denoted $S_n(x)$, will be its previous value,

minus the number of trees that became infested last summer, plus the number of NJ year old juveniles that survived and matured into adult susceptible trees,

$$S_{n+1} = S_n - I_n + sj_{NJ,n}. \tag{4.4}$$

The total number of trees per hectare T is conserved from year to year reflecting finite floor space and therefore stand carrying capacity,

$$T = J_{n+1} + S_{n+1} + I_n + I_{n-1}, \tag{4.5}$$

which allows for a more convenient form of the infestation equation,

$$I_{n+1} = RI_n e^{-\beta(T - S_n + I_n - sj_{NJ,n})}. \tag{4.6}$$

We estimate T based on the mean host tree density, 390 stems/ha, in the SNRA prior to the outbreak that began there in the mid-1990s (Crabb et al., 2012). See Table 4.1 for a summary of variables, parameters, units and estimated nominal values. Detailed analysis of this demographic model, including fixed point stability analysis and estimated outbreak cycle period and severity, appear in Duncan et al. (2015).

4.2.2 MPB Dispersal

Beetles disperse in late summer in search of new hosts after emerging from previously infested trees. In a relatively large and homogeneous host area, the spread of infested trees can be viewed as a one-dimensional process. Furthermore, large two-dimensional travelling waves are approximately one-dimensional at the stand level. Therefore, we model beetle dispersal on a continuous one-dimensional habitat using the ecological diffusion equation (Turchin, 1998),

$$\begin{aligned} \frac{\partial P}{\partial t} &= \frac{\partial^2}{\partial x^2}(DP), \quad -\infty < x < \infty, \ t > 0, \\ P(x,0) &= \alpha I_n(x), \end{aligned} \tag{4.7}$$

where $P(x,t)$ represents the density of MPB at location x (hundred meters from the origin) at time t days, D is the rate at which beetles disperse (motility), and α is the mean number of MPB that emerge from an infested tree. Powell and Bentz (2014) estimate mean MPB emergence at $\alpha = 2043$ MPB/stem using infestation (ADS) data taken from the SNRA during the recent outbreak.

To estimate the value of D, we employ the motility function of Powell and Bentz (2014) which adjusts MPB dispersal rates according to variable landscape type, i.e. host density. MPB motility D as a function of host density S is given by

$$D = D_0 e^{-(D_1 + \ln D_0)\frac{S}{1000}}, \tag{4.8}$$

where D_0 gives the maximum dispersal rate when host density is zero. Motility decays exponentially to e^{-D_1} as host density increases to a saturated stand capacity of 1000 stems/ha. The exponential decrease in motility with susceptible host density reflects increasing residence time in denser stands as MPB search for new susceptible hosts or trees already under attack. Values of $D_0 = 3.79$ km^2/day and $D_1 = 10.9$ were estimated from ADS data taken from the SNRA outbreak over the years 1995-2003 (Powell and Bentz, 2014). Assuming susceptible host tree density in the absence of MPB is a constant 390 stems/ha, we use the motility function (4.8) to calculate our estimate of MPB dispersal rate $D = 3.21$ ha/day. Since individual beetles fly for only one day per season (year), we obtain the per year dispersal rate $D = 3.21$ ha/year.

To incorporate beetle dispersal in the demographic model, we rewrite (4.6) as

$$I_{n+1}(x) = \gamma C_n(x) e^{-\beta(T - S_n(x) + I_n(x) - s j_{NJ,n}(x))}. \tag{4.9}$$

where $C_n(x)$ denotes the density of colonizing MPB at the end of the previous summer and γ represents the number of trees that can be colonized per attacking beetle. An estimated 250 attacking beetles per tree are required to successfully overcome a host's defensive mechanisms, and subsequent attacks fill up trees at a rate of 698 MPB/host (Powell and Bentz, 2014). Since we are constructing an outbreak model wherein beetle populations are generally well above the attack threshold (250 MPB/stem), we can combine the beetle-to-infested tree conversion rate (1/698 stems/MPB) with the attack threshold to get an estimate of $\gamma = 1/948$, where $948 = 250 + 698$.

When susceptible host density is high, the number of new infestations is simply proportional to the number of attacking beetles which we compute by the convolution,

$$C_n(x) = \int_{-\infty}^{\infty} k(x - y)\alpha I_n(y) dy,$$

where k is the fundamental solution of (4.7) (with $t = 1$), called the Gaussian diffusion kernel,

$$k(x) = \frac{1}{\sqrt{2\pi}\sigma} e^{\frac{-x^2}{2\sigma^2}}.$$

Here we have the relation between MPB dispersal rate and the variance of the Gaussian distribution, $\sigma^2 = 2Dt$, where $t = 1$ year since individual MPB only disperse 1 day/year. With the estimated dispersal rate $D = 3.21$ ha/year, we have $\sigma = 253.5$ m. Combining the sedentary (population growth) and dispersal stages we can write (4.9) as the integrodifference equation

$$I_{n+1}(x) = Re^{-\beta(T-S_n(x)+I_n(x)-sj_{NJ,n}(x))} \int_{-\infty}^{\infty} k(x-y)I_n(y)dy. \tag{4.10}$$

where $R = \gamma\alpha$ represents the number of new infestations per infested tree, which can be viewed as the net reproductive rate of MPB. The full model is

$$\begin{aligned}
j_{1,n+1}(x) &= dJ_n(x) + I_{n-2}(x), \\
j_{k+1,n+1}(x) &= sj_{k,n}(x), \ k = 1, .., NJ-1, \\
S_{n+1}(x) &= S_n(x) - I_n(x) + sj_{NJ,n}(x), \\
I_{n+1}(x) &= Re^{-\beta(T-S_n(x)+I_n(x)-sj_{NJ,n}(x))} \int_{-\infty}^{\infty} k(x-y)I_n(y)dy.
\end{aligned}$$

When initialized with a few hectares of low density infestation near the origin, the model generates a train of solitary waves of MPB infestation that propagate through a medium of host trees (Fig. 4.2). These traveling waves in space correspond to outbreaks in time for a particular point on the landscape. The speed of the leading right-travelling wave, i.e., invasion speed, is approximately 312 m/year and peak infestation is around 30 stems/ha with nominal parameters estimated from the SNRA outbreak. The subsequent train of periodic waves have smaller peaks and less steep edges since they are moving into a landscape with less than ideal conditions, i.e., with sizable densities of nonsusceptible trees whereas the initial wave invades area saturated with susceptible hosts. In what follows, we estimate the speed of the leading wave which we will use to construct an approximation of outbreak severity as measured by peak infestation.

TABLE 4.1: Model variables and parameters. Estimates for NJ and d were determined using reference values consistent with field observation. Powell and Bentz (2009, 2014) estimated β, R, and σ from data taken during a recent outbreak of MPB in the Sawtooth National Recreation Area (SNRA), Idaho. Total host density T is estimated for the SNRA in (Crabb et al., 2012).

Variables	**Description**	**Units**
$S_n(x)$	Susceptible tree density in year n at location x	stems/ha
$I_n(x)$	Infested tree density in year n at location x	stems/ha
$j_{k,n}(x)$	Juvenile tree density of the k^{th} age class in year n at location x	stems/ha
$J_n(x)$	Total juvenile tree density	stems/ha
$C_n(x)$	Density of beetles colonizing trees at the end of the dispersal season in year n	MPB/ha
Parameters	**Description**	**Estimated Values/Units**
T	Total number of trees per hectare	$T = 390$ stems/ha
NJ	Number of juvenile age classes	$NJ = 80$ age classes
d	Natural mortality rate for juveniles	$d = 0.01$ per year
$s = 1 - d$	Natural juvenile survivorship	$s = 0.99$ per year
β	Failure rate in MPB search process	$\beta = 0.011$ ha/stem
$R = \gamma\alpha$	Net reproductive rate of MPB	$R = 2.16$ per year
σ	Standard deviation of Gaussian dispersal kernel	$\sigma = 253.5$ m
Values to approximate	**Description**	**Units**
c^*	Speed of an invading infestation wavefront	m/year
τ^*	Shape parameter of an invading wavefront	1/m
I_{max}	Maximum MPB impact in a single year throughout an outbreak	stems/ha

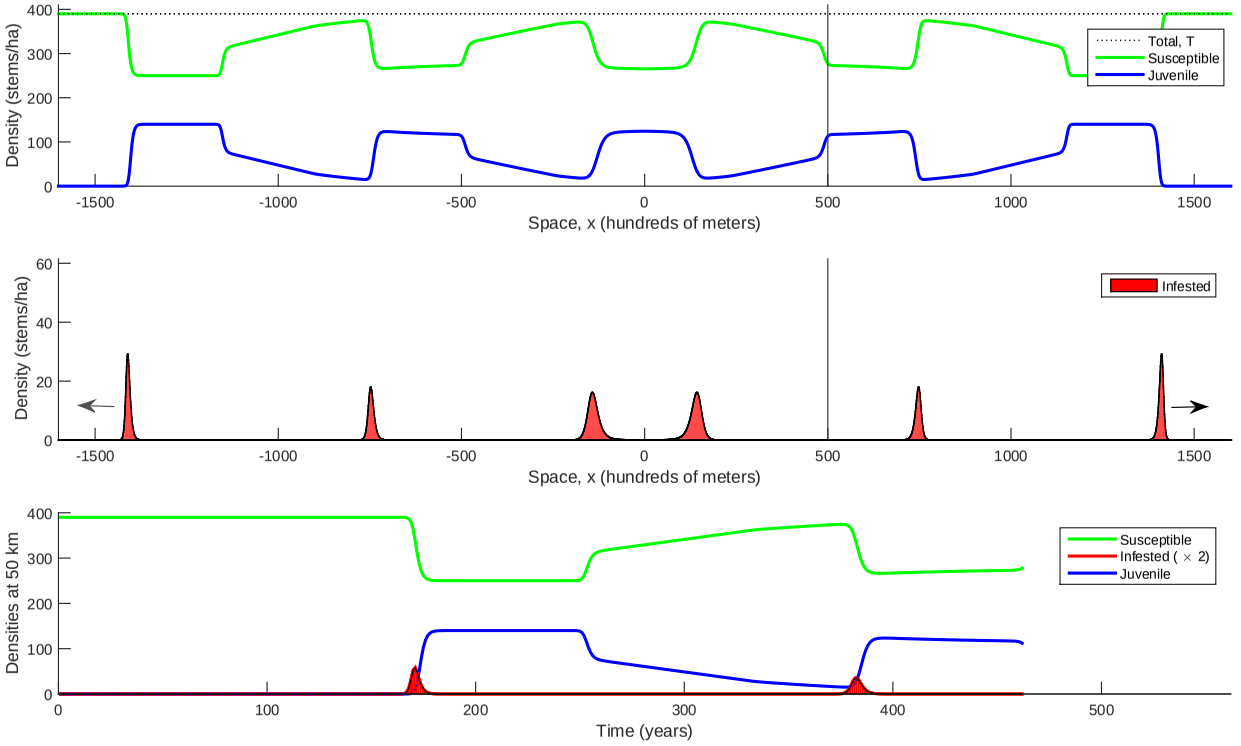

FIGURE 4.2: Simulation of the model with small initial infestation source with compact support centered about the origin. We focus our analysis on the initial right-traveling wave of infestation ($x \approx 1410$ hectometers in middle graph). The speed of invasion is approximately 312 m/year and peak infestation is around 30 stems per hectare. The bottom graph shows population densities in time for a fixed point in the forest at $x = 500$ hectometers.

4.3 Predicting the Speed of a MPB Invasion

4.3.1 Asymptotic Travelling Wave Speed

Our model can be written in matrix form as

$$\mathbf{Y}_{n+1}(x) = \int_{-\infty}^{\infty} \mathbf{B}_{\mathbf{Y}}(x,y)\mathbf{Y}_n(y)dy \tag{4.11}$$

where,

$$\mathbf{Y}_n = \begin{bmatrix} j_{1,n} & j_{2,n} & \dots & j_{NJ,n} & S_n & I_n & I_{n-1} & I_{n-2} \end{bmatrix}^{\mathrm{T}}$$

denotes the population densities of all classes of trees and the matrix

$$\mathbf{B}_{\mathbf{Y}}(x,y) = \left[\begin{array}{ccccc|ccc} d\delta & d\delta & d\delta & \cdots & d\delta & 0 & 0 & 0 & \delta \\ s\delta & 0 & 0 & \dots & 0 & \vdots & \vdots & \vdots & 0 \\ 0 & s\delta & 0 & \ddots & \vdots & & & & \vdots \\ \vdots & \ddots & \ddots & \ddots & & & & & \\ & & & & 0 & & & & \\ 0 & \dots & & 0 & s\delta \quad 0 & 0 & 0 & 0 & 0 \\ \hline 0 & \dots & & & 0 \quad s\delta & \delta & -\delta & 0 & 0 \\ 0 & \dots & & & 0 & 0 & Re^{-\beta(T-S_n+I_n-sj_{NJ,n})}k & 0 & 0 \\ 0 & \dots & & & 0 & 0 & \delta & 0 & 0 \\ 0 & \dots & & & 0 & 0 & 0 & \delta & 0 \end{array}\right] \tag{4.12}$$

encapsulates density dependent tree population growth and MPB dispersal. We use the Dirac delta function $\delta = \delta(x-y)$ to model the absence of dispersal in transitions between any two stages other than from I_n to I_{n+1} (see Neubert and Caswell (1996) for details). In transitioning from I_n to I_{n+1}, infested trees beget more infested trees through beetle dispersal (via the Gaussian kernel $k = k(x-y)$) and colonization. Matrix $\mathbf{B}$ is partitioned to show the upper-left $NJ \times NJ$ block corresponding to the juvenile age classes. In an effort to approximate the speed of travelling waves generated by the model, we linearize around the trivial steady state (given below) and calculate the speed of waves generated by the linearized model.

We linearize about the state

$$\tilde{\mathbf{Y}} = \begin{bmatrix} 0 & \dots & 0 & T & 0 & 0 & 0 \end{bmatrix}^{\mathrm{T}} \tag{4.13}$$

and let $\mathbf{A} = \mathbf{B}_{\tilde{\mathbf{Y}}}$ be the Fréchet derivative of $\mathbf{B}$ at $\tilde{\mathbf{Y}}$. Here we have assumed that before a MPB invasion moves in, the forest consists of mostly susceptible trees and negligible densities of juvenile and infested trees. By the linear conjecture of van den Bosch et al. (1990), the speed of an invasion wave generated by a nonlinear model can be approximated by its linearization at low invasive population densities. The linearized model takes the form of a convolution which can be written as

$$\mathbf{Y}_{n+1}(x) = \int_{-\infty}^{\infty} \mathbf{A}(y)\mathbf{Y}_n(x-y)dy. \tag{4.14}$$

In a moving frame of reference with unknown speed $c > 0$ near the invasion front,

$$\mathbf{Y}_{n+1}(x) = \mathbf{Y}_n(x-c)e^{\varepsilon},$$

where ε is an unknown wave growth rate parameter that depends on c. That is, we imagine that the wave is translating to the right with speed c and growing vertically by a factor of e^{ε} each year with respect to our frame of reference (Fig. 4.3 (a)).

We assume that the edge of the wavefront is of the form

$$\mathbf{Y}_n(x) = e^{-\tau x}\mathbf{v}, \tag{4.15}$$

where $\mathbf{v}$ gives the (constant) relative abundance of each tree class in the travelling wave and τ determines the shape of the advancing edge of the wave. Then the linearized model (4.14) becomes

$$e^{\tau c+\varepsilon}\mathbf{v} = \mathbf{H}(\tau)\mathbf{v},$$

where $\mathbf{H}(\tau) \equiv \int_{-\infty}^{\infty} \mathbf{A}(y)e^{\tau y}dy$.

Since the behavior of $e^{\tau c+\varepsilon}\mathbf{v}$ is dictated by the dominant eigenvalue of $\mathbf{H}(\tau)$, denoted $\rho(\tau)$, we have

$$e^{\tau c+\varepsilon}\mathbf{v} \sim \rho(\tau)\mathbf{v},$$

and thus,

$$\varepsilon = -\tau c + \ln \rho(\tau). \tag{4.16}$$

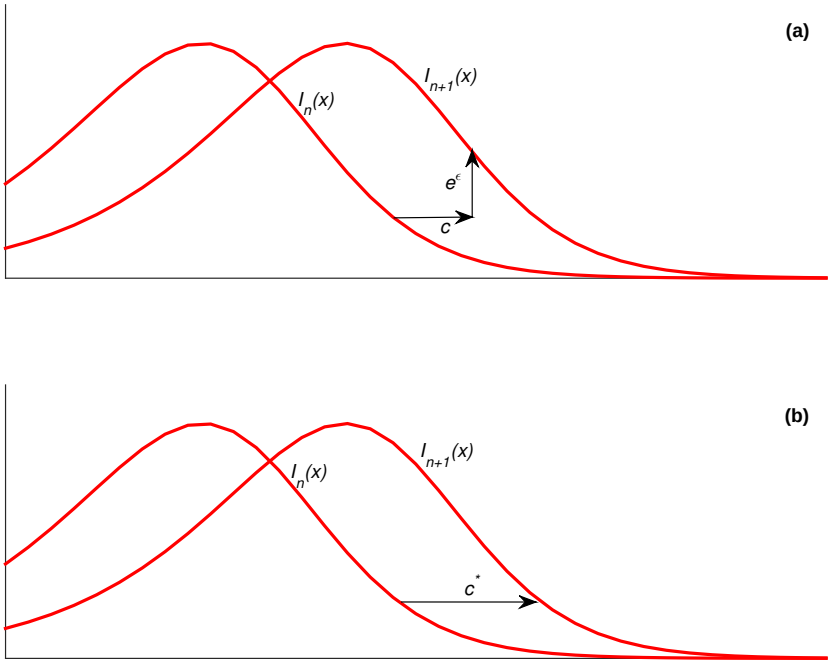

FIGURE 4.3: (a) In a moving frame of reference with speed c near the front of the invasion, a point on the next generation's front is a horizontal translation and a vertical multiple of some point on the current front. (b) We predict the speed on the invasion by choosing the frame of reference speed that corresponds to a vertical multiple of unity ($\varepsilon = 0$).

Furthermore, since the long-term behavior of wave growth is controlled by the maximum value of ε, setting $\frac{d\varepsilon}{d\tau} = 0$ using (4.16) gives

$$c = \frac{\rho'(\tau)}{\rho(\tau)}. \tag{4.17}$$

Since $\varepsilon = 0$ in a frame of reference moving with the wave of invasion, Eq. 4.16 becomes

$$c = \frac{1}{\tau} \ln \rho(\tau) \tag{4.18}$$

(Fig. 4.3 (b)). From (4.17) and (4.18), we have

$$\frac{\rho'(\tau)}{\rho(\tau)} = \frac{1}{\tau} \ln \rho(\tau)$$

which is the condition that arises when minimizing $\frac{1}{\tau} \ln \rho(\tau)$. It is necessary to minimize c in order to maximize ε according to (4.16). Therefore, the predicted wave speed is

given by

$$c^* = \min_{0<\tau} \left(\frac{1}{\tau} \ln \rho(\tau) \right) \tag{4.19}$$

as derived in Neubert and Caswell (1996) for a simpler, related system.

4.3.2 Speed of Model-Generated Invasion Wave

To predict the speed of a wave of infestation moving across a landscape generated by our model, we require the spectral radius of

$$\mathbf{H}(\tau) = \left[\begin{array}{ccccccc|ccc} d & d & d & \cdots & & d & 0 & 0 & 0 & 1 \\ s & 0 & 0 & \ldots & & 0 & \vdots & \vdots & \vdots & 0 \\ 0 & s & 0 & \ddots & & \vdots & & & & \vdots \\ \vdots & \ddots & \ddots & \ddots & & & & & & \\ & & & & & 0 & & & & \\ 0 & \ldots & & 0 & s & 0 & 0 & 0 & 0 & 0 \\ 0 & \ldots & & & 0 & s & 1 & -1 & 0 & 0 \\ \hline 0 & \ldots & & & & 0 & 0 & Re^{\frac{\sigma^2}{2}\tau^2} & 0 & 0 \\ 0 & \ldots & & & & 0 & 0 & 1 & 0 & 0 \\ 0 & \ldots & & & & 0 & 0 & 0 & 1 & 0 \end{array}\right],$$

which is block-upper triangular and hence its spectrum is the union of the spectra of the diagonal blocks. Let $\mathbf{H}_1$ and $\mathbf{H}_2$ denote the upper-left and lower-right blocks respectively. By the Gershgorin circle theorem with respect to the columns of $\mathbf{H}_1$, the spectral radius of $\mathbf{H}_1$ is no more than 1. Since the spectral radius of $\mathbf{H}_2(\tau)$ is clearly $Re^{\frac{\sigma^2}{2}\tau^2}$, the largest eigenvalue of $\mathbf{H}(\tau)$ is

$$\rho(\tau) = Re^{\frac{\sigma^2}{2}\tau^2},$$

provided $R > 1$; which is required for the propagation of an outbreak anyway.

Applying (4.19), we have an approximation of the speed of the invading wavefront,

$$c^* = \sigma\sqrt{2 \ln R}, \tag{4.20}$$

where the minimizing value of the wave shape parameter is

$$\tau^* = \frac{\sqrt{2 \ln R}}{\sigma}. \tag{4.21}$$

Thus, we have closed-form approximations of the speed and shape of the right tail of the (right-traveling) invading wavefront in terms of model parameters alone. Note the relation between wave speed and shape,

$$c^* = \sigma^2 \tau^*.$$

Equations 4.20 and 4.21 are also derived in Kot et al. (1996) for an unstructured model of an invasive population that disperses according to a normal distribution.

4.4 Invasion Wave Amplitude Approximation

4.4.1 Converting the IDE into a PDE

Our goal here is to derive analytic predictions of the shapes of the right and left tails of an invading wavefront and to numerically reconstruct the entire wave profile. These predictions will enable the development of an approximation of outbreak severity based on MPB population growth rate. To facilitate the construction of such approximations, we derive a partial differential equation (PDE) from the integrodifference equation (IDE) model for infested trees (4.10). The first step in this derivation is to approximate to the convolution integral in Eq. 4.10.

We start with a WKB approximation and assume the solution of the integral equation (4.10) is of the form

$$I_n(x) = e^{u_n(x)} \tag{4.22}$$

for some function $u_n(x)$. Then the convolution $(k * I_n)(x)$ becomes

$$k * e^{u_n} = \int_{-\infty}^{\infty} \frac{1}{\sqrt{2\pi}\sigma} e^{h(y)} dy,$$

where

$$h(y) = u_n(x-y) - \frac{y^2}{2\sigma^2}.$$

We approximate this integral using the method of steepest descent. Expanding u_n in its Taylor series, we have

$$h(y) = u_n(x) - u_n'(x)y + \frac{u_n''(x)}{2!}y^2 - \ldots - \frac{y^2}{2\sigma^2}.$$

Ignoring higher order terms, the critical point of h (denoted y^*) satisfies

$$h'(y^*) = -u_n'(x) + u_n''(x)y^* - \frac{y^*}{\sigma^2} = 0,$$

which implies

$$y^* = -\sigma^2 u_n' \frac{1}{1 - \sigma^2 u_n''}.$$

Expanding as a power series in σ^2, we have

$$y^* = -\sigma^2 u_n'(1 + \sigma^2 u_n'' + \sigma^4 (u_n'')^2 + \ldots). \tag{4.23}$$

Now

$$h(y^*) = u_n + (u_n')^2 + \mathcal{O}(\sigma^4),$$

and at leading order,

$$h''(y^*) = u_n'' - \frac{1}{\sigma^2} \approx -\frac{1}{\sigma^2},$$

provided $\sigma^2 << 1$. Thus, by the method of steepest descent,

$$k * I_n \approx \frac{1}{\sqrt{2\pi}\sigma} \sqrt{\frac{2\pi}{|h''(y^*)|}} e^{h(y^*)} = e^{u_n + \frac{1}{2}\sigma^2 (u_n')^2 + \mathcal{O}(\sigma^4)}. \tag{4.24}$$

We now move to a continuous setting by transforming (4.10) to an (approximately) equivalent partial differential equation (PDE). Neglecting higher order terms in (4.24), we can rewrite (4.10) as

$$e^{u_{n+1}} = Re^{-\beta(T - S_{n+1})} e^{u_n + \frac{1}{2}\sigma^2 (u_n')^2}, \tag{4.25}$$

or equivalently,

$$e^{u_n} = Re^{-\beta(T - S_n)} e^{u_{n-1} + \frac{1}{2}\sigma^2 (u_{n-1}')^2}. \tag{4.26}$$

Dividing (4.25) by (4.26) yields

$$e^{u_{n+1} - u_n} = e^{u_n - u_{n-1} + \frac{1}{2}\sigma^2 [(u_n')^2 - (u_{n-1}')^2]} e^{\beta(S_{n+1} - S_n)}.$$

Since $j_{NJ,n}$ is small just before the invasion wave hits,

$$S_{n+1} - S_n = -I_n + s j_{NJ,n} \approx -e^{u_n}$$

and hence, after equating exponents and rearranging, we have

$$u_{n+1} - 2u_n + u_{n-1} = \frac{1}{2}\sigma^2[(u'_n)^2 - (u'_{n-1})^2] - \beta e^{u_n}. \tag{4.27}$$

Suppose

$$u_n(x) = w(t = n\Delta t, x)$$

for some twice continuously differentiable function w and time step size $\Delta t = 1$. Then (4.27) becomes the second order nonlinear PDE,

$$w_{tt} = \sigma^2 w_x w_{xt} - \beta e^w, \tag{4.28}$$

upon Taylor expanding $u'_{n-1}(x) = w_x\big((n-1)\Delta t, x\big)$.

4.4.2 Travelling Wave Profile

We look for travelling wave solutions of (4.28) by assuming $w = f(z)$ for some function $f(z)$ where $z = x - ct$ with wave speed $c > 0$. Substituting into (4.28) we have

$$c^2 f'' = -c\sigma^2 f' f'' - \beta e^f$$

which, after multiplying by f', integrates to

$$\frac{1}{2}c^2(f')^2 + \frac{1}{3}c\sigma^2(f')^3 + \beta e^f = C \tag{4.29}$$

for some constant C which can be viewed as the "energy" along trajectories. Let

$$E_1(f') = \frac{1}{2}c^2(f')^2 + \frac{1}{3}c\sigma^2(f')^3$$

represent the "energy" of motion and

$$E_2(f) = \beta e^f$$

be the "energy" of position. Solutions of (4.29) are isoclines of the potential $E_1 + E_2$. Assuming $I_n(x)$ attains a maximum value, I_{max}, at $x = 0$ when $n = t = 0$, we find $C = \beta I_{max}$. Peak infestation, I_{max}, is the measure of outbreak severity we seek to estimate. At this point, E_1 is at a local minimum, $(E_1(0) = 0)$ and $E_2(\ln I_{max}) = \beta I_{max}$

(Fig. 4.4). The maximum stable value of E_1 is $\frac{c^4}{6\sigma^4}$ and if

$$\frac{-c}{\sigma^2} \leq f' \leq \frac{c}{2\sigma^2},$$

then $0 \leq E_1 \leq \frac{c^4}{6\sigma^4}$.

We require $I_n(x) \to 0$ as $x \to \pm\infty$ which forces $f(z) \to -\infty$ since $z \to \pm\infty$ as $x \to \pm\infty$ (for fixed t) and $f = \ln I$. As $f \to -\infty$, (4.29) becomes

$$\frac{1}{2}c^2(f')^2 + \frac{1}{3}c\sigma^2(f')^3 = \beta I_{max}. \tag{4.30}$$

We choose the maximum stable energy state of E_1, when $f' = \frac{-c}{\sigma^2}$ or $f' = \frac{c}{2\sigma^2}$, in order to obtain a worst case scenario (i.e., largest possible peak) approximation of I_{max}. From (4.30) we have

$$I_{max} = \frac{c^4}{6\beta\sigma^4}. \tag{4.31}$$

Figure 4.5 shows a phase diagram of (4.29) with the trajectory corresponding to the maximum stable energy state.

The horizontal asymptotes, $\frac{-c}{\sigma^2}$ and $\frac{c}{2\sigma^2}$ of the trajectory in Figure 4.5 represent the slopes of f as $z \to \pm\infty$, respectively. For fixed n, $\ln(I_n(x)) = \ln(I(x)) \approx f(x-ct) = f(z)$ for some fixed t and therefore

$$f'(z) = \frac{I'(x)}{I(x)} \to \frac{-c}{\sigma^2} \text{ as } z \to +\infty.$$

Hence, for $x >> \frac{\sigma^2}{c}$, we have

$$I(x) \sim I_{max} e^{\frac{-c}{\sigma^2}x}. \tag{4.32}$$

Similarly, for $x << -\frac{\sigma^2}{c}$, we have

$$I(x) \sim I_{max} e^{\frac{c}{2\sigma^2}x}. \tag{4.33}$$

The accuracy of the analytic approximations of the shape of an invading wave, Eqs. 4.31, 4.32, and 4.33, is illustrated in Figure 4.6. To construct an approximation of the entire wave profile, we numerically integrate (4.29) using Euler's method with wave speed c estimated by Eq. 4.20 (Fig. 4.6). The slopes of the right tails of $\ln I$ from simulation and approximation approach the same value as $x \to \infty$ indicating that Eq. 4.32 is a good approximation of the shape of the invading wave tail.

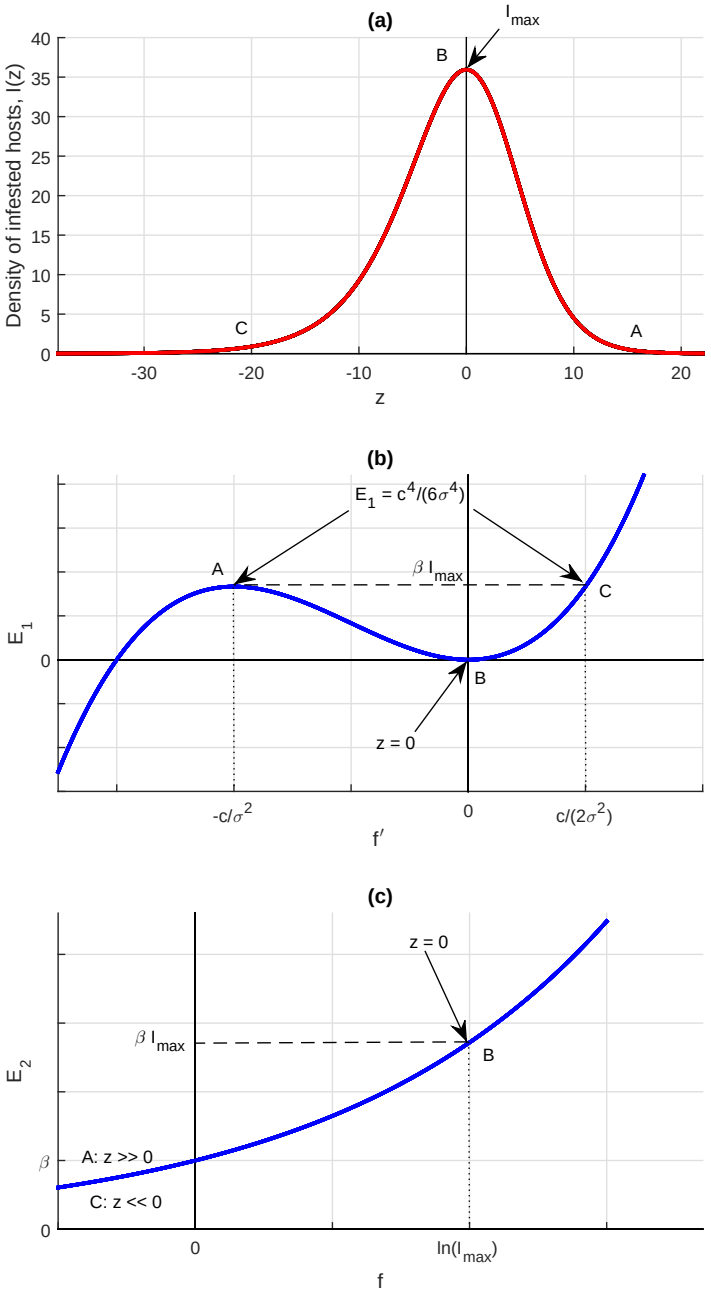

FIGURE 4.4: The left-hand side of the traveling wave equation (4.29) contains the kinetic and potential energy functions E_1 and E_2 respectively. The maximum possible peak value of E_1 produces our approximation of wave amplitude, Eq. 4.31, after noting that $E_2(\ln I_{max}) = \beta I_{max}$ when $z = 0$. We envision a particle moving in the positive f direction (z decreasing from $+\infty$) along E_2 in (c) starting at point A. When the particle reaches point B, the outbreak peaks and the particle reverses direction, heading back toward point C. Corresponding points are labelled on the invasion wave profile in (a) and on E_1 in (b) .

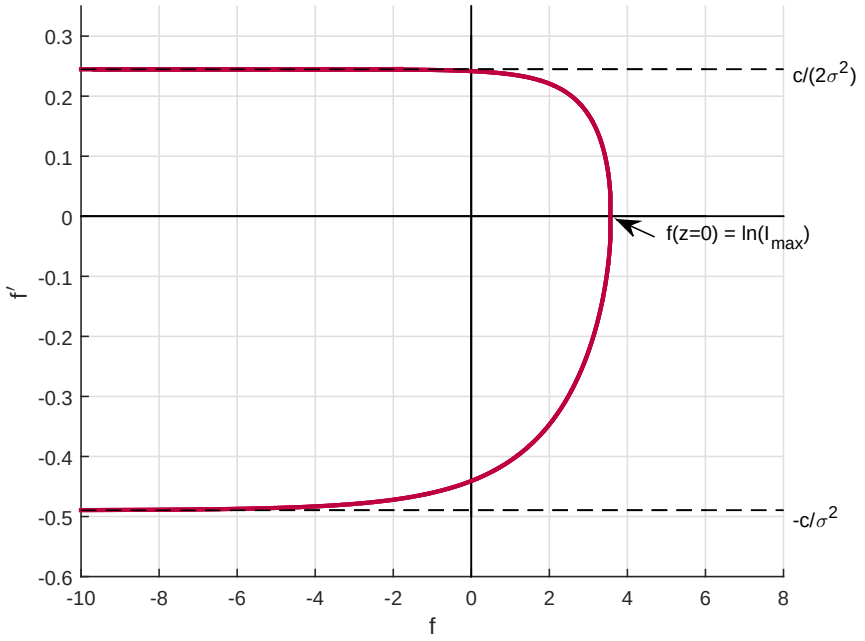

FIGURE 4.5: Phase plane of (4.29) generated using parameter values from Table 4.1 with maximum value of E_1 for stable solutions of (4.29) and estimated wave speed c^* from Eq. 4.20. Asymptotes of the trajectory correspond to exponential shape parameter values that describe the left and right tails of the invasion wave. We derive an approximation of peak outbreak infestation (maximum MPB impact, Eq. 4.31) using the value of f when $f' = 0$.

Using the approximation of invasion speed c from Eq. 4.20 in (4.31), we obtain a prediction of outbreak severity in terms of the net reproductive rate of MPB R and MPB host searching parameter β,

$$I_{max} = \frac{2(\ln R)^2}{3\beta}. \tag{4.34}$$

The approximation of the exponential decay rate of the advancing wave's leading edge in (4.32) agrees exactly with the wave shape parameter prediction (4.21). This is no surprise since (4.32) is based on the the maximum energy state of E_1, and the method employed in the derivation of (4.21) provides a maximum wave speed using dominant eigenvalues and wave growth rates.

4.5 Results

Figure 4.7 compares predicted wave speeds for varying MPB population growth rate R using (4.20) with speeds from simulation. With nominal parameter values (Table 4.1), we predict an invasion speed of 315 m/yr. There is a less than 1% error between this prediction and the estimated speed from simulation (312 m/yr). Figure 4.8 compares

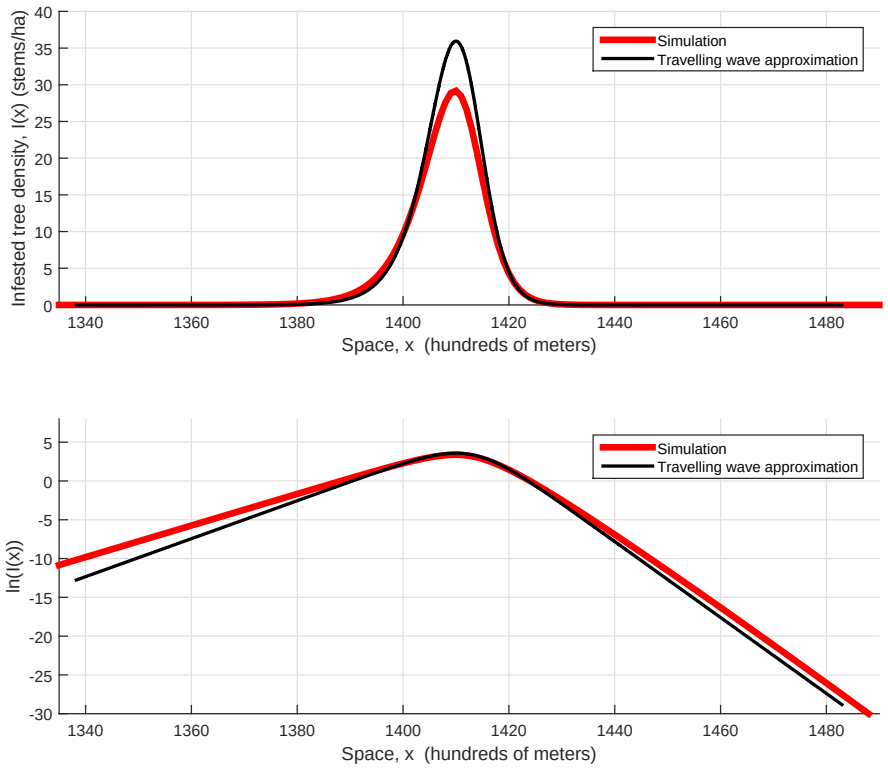

FIGURE 4.6: Comparison of the numerical solution of (4.29) with the actual wave profile generated by model simulation. The slopes of the right tails of $\ln I$ from simulation and approximation approach the same value as $x \to \infty$ meaning Eq. 4.32 is a good approximation of the shape of the invading wave tail. There is only a small error in comparing the slopes of the left tails of $\ln I$ from simulation and approximation Eq. 4.33.

the shape of the initial advancing wavefront generated by simulation with the predicted wave shape from (4.15) (equivalently, Eq. 4.32) using $\tau = 0.490$ from approximation (4.21).

Figure 4.9 compares our prediction of outbreak severity (4.34) with peak impacts from model simulation for varying MPB reproductive rate R. With nominal parameter values, maximum infestation from simulation is 29.2 stems/ha. Approximation (4.34) predicts peak infestation at 35.9 stems/ha. The 23% relative error is due to truncating terms that may not be negligible in the series expansion (4.23) since σ^2 is not necessarily small. In fact, since σ and x are the only variables with spatial units, nondimensionalization results in $\sigma = 1$. We also assume σ^2 is small in using the method of steepest descent, introducing some error. Even so, the approximation does a relatively good job tracking the general trend of positive association between outbreak intensity and MPB population growth rate. Furthermore, there is only a 14.8% mean relative error over all

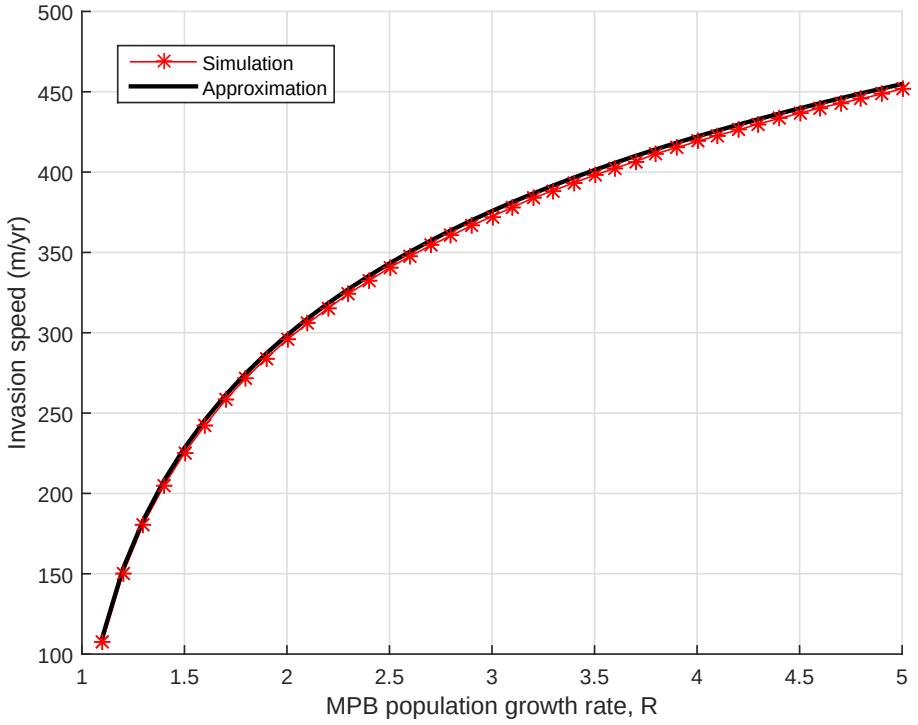

FIGURE 4.7: Comparison of predicted wave speeds for varying R using (4.20) with speeds from simulation. With the parameter values given in Table 4.1, we predict 315 m/year for the invasion speed which is very close to the estimated speed from simulation, 312 m/year.

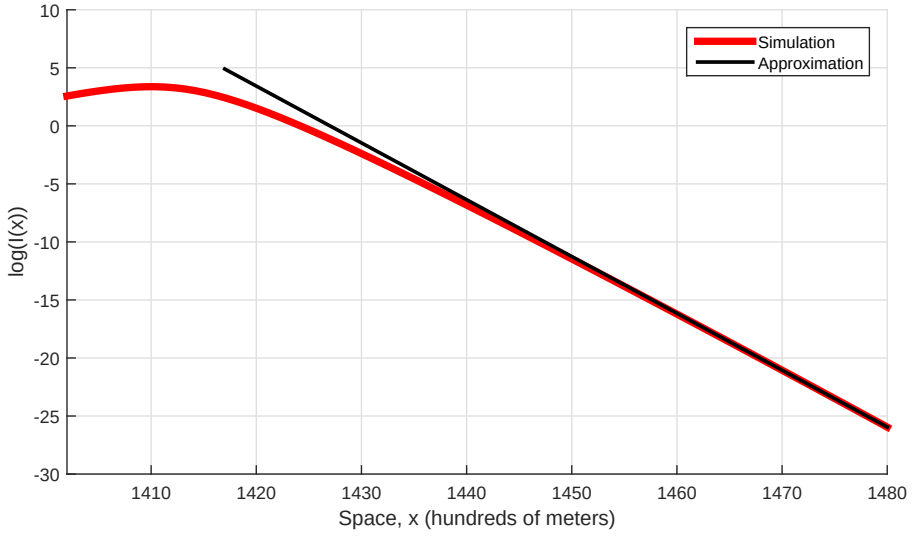

FIGURE 4.8: Comparison of the initial advancing waveform with positive speed from simulation and the predicted shape of the leading edge. The wave shape parameter approximated from Eq. 4.21 (used in Eqs. 4.15 and 4.32) is $\tau = 0.490$. The slope of the right tail of $\ln I$ from simulation is approaching $-\tau^*$ as $x \to \infty$ meaning Eq. 4.21 is a good approximation of the shape of the invading wave tail.

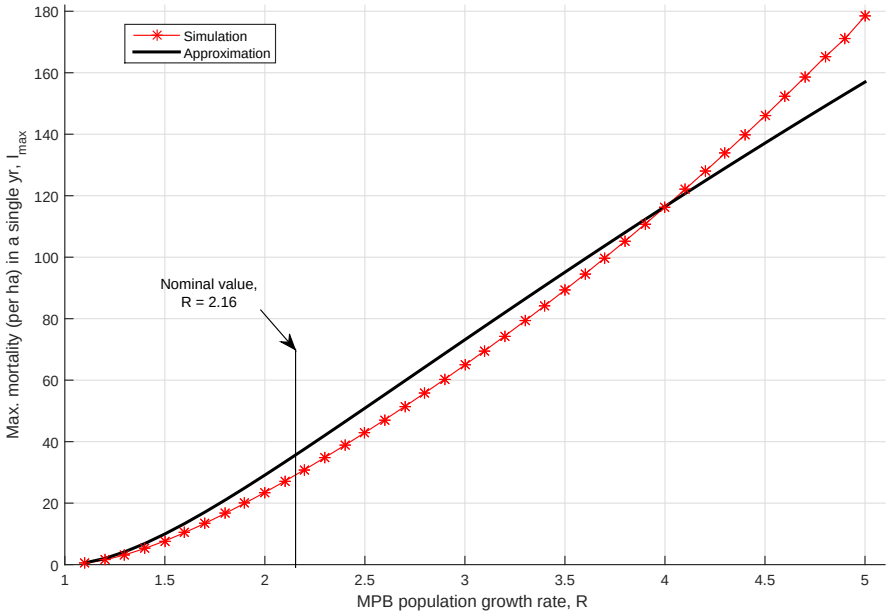

FIGURE 4.9: Comparison of predicted peak infestation using Eq. 4.34 with actual peak infestation, I_{max}, from simulation. There is only a 14.8% mean relative error over all R values between 1.1 and 5.0.

R values between 1.1 and 5.0.

Figure 4.10 compares our prediction of outbreak severity (4.34) with peak impacts from model simulation for varying MPB host searching failure rate β. Approximated peak values follow simulation peaks closely and it is clear that outbreak intensity diminishes as search inefficiency, β, increases.

4.6 Discussion

4.6.1 SNRA Impact Data

Because of host heterogeneity on a realistic 2-dimensional landscape, it is difficult to find 1-dimensional travelling waves of infestation during MPB outbreaks. However, ADS data from the SNRA outbreak reveals a solitary wave of infestation travelling south down a narrow valley at the southern end of the Stanley basin over the years 2002-2003 (Fig. 4.11). The average of the two peaks is 36 stems/ha which is close to the I_{max} value predicted by model simulation and even closer to the value predicted by approximation (4.34) as seen in Figs. 4.6, 4.9, and 4.10.

While host density was otherwise a fairly constant 377 stems/ha throughout the valley at the time, divots in each profile between approximately -18 km and -17 km correspond to a large meadow in the valley floor sparsely populated by host trees. During

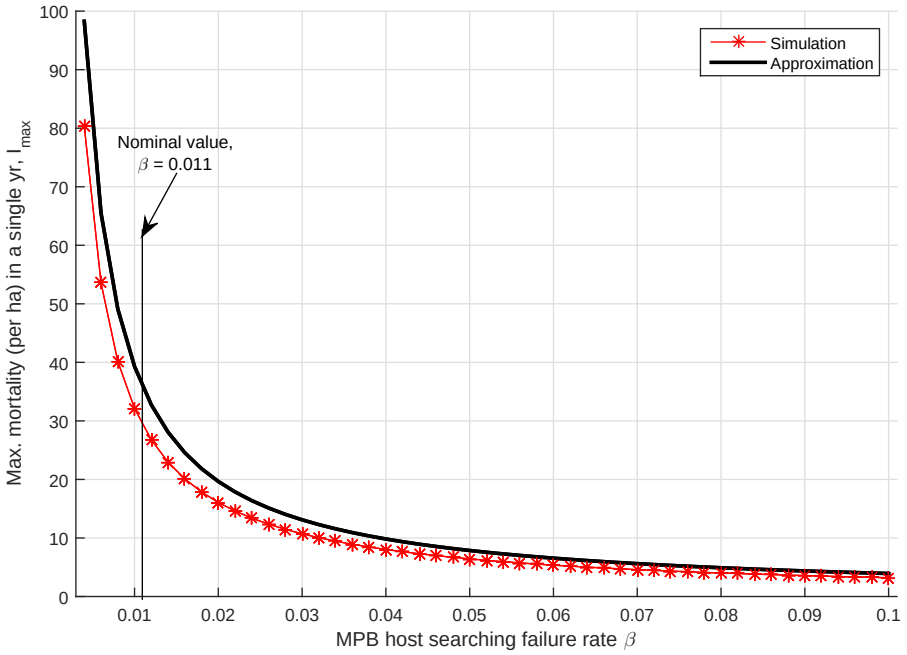

FIGURE 4.10: Comparison of predicted peak infestation using Eq. 4.34 with actual peak infestation, I_{max}, from simulation. Approximated peak values follow simulation peaks closely as outbreak intensity diminishes with increasing search inefficiency β.

the two years, the wave is travelling around 644 m/year which is more than twice the speed predicted by the model with nominal parameter estimates. However, average host density in the valley was actually 377 stems/ha, less than the mean density across the entire SNRA (390 stems/ha). Since beetles disperse faster through habitats with lower host density, we should expect this invasion wave to move slightly faster overall due to reduced mean host density. Moreover, there is a 1 km long meadow along the length of the valley that spans its width. Beetles likely skipped over the meadow completely causing the wave to jump ahead dramatically which subsequently caused the speed of the entire wave profile to move considerably faster than predicted.

To test this hypothesis, we utilize the motility function of Powell and Bentz (2014) (Eq. 4.8) to generate MPB dispersal rates for the varying host densities in the valley. In the 1 km meadow, host density is estimated to be around 10 stems/ha. With a mean of 377 stems/ha hosts throughout the valley (assuming constant host density outside the meadow) we calculate the non-meadow host density to be 438 stems/ha. Using the motility function, we calculate the dispersal rates for the meadow and non-meadow areas which are in turn used to calculate the corresponding Gaussian dispersal kernel standard deviations via $\sigma = \sqrt{2D}$. We then calculate the rate of invasion for each landscape type

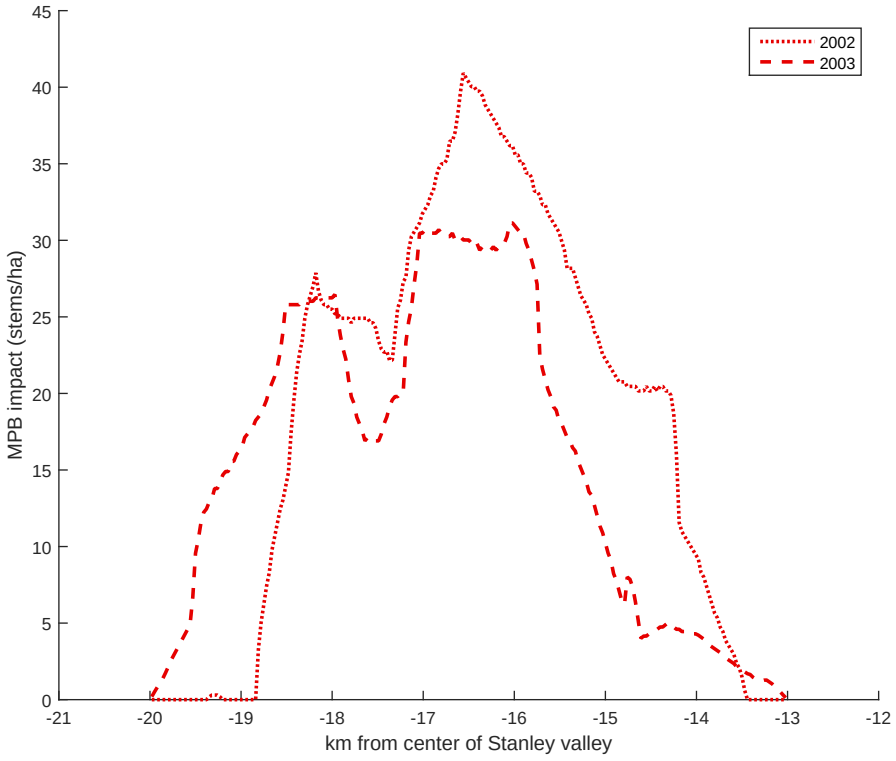

FIGURE 4.11: A solitary wave of infestation travels west down a narrow valley at the southern end of the Stanley basin (SNRA) over the years 2002-2003 at a speed near 644 m/year. Average peak infestation of 36 stems/ha agrees well with the I_{max} value from simulation as well as with the predicted value from approximation (4.34). MPB dispersal rate is considerably higher through the large meadow with low host density between approximately -18 km and -17 km (north) from the center of the Stanley Basin.

using Eq. 4.20. Finally, averaging the speed through the 1 km meadow with the speeds through each of the remaining 6 kilometers of non-meadow (constant 438 stems/ha host density), we have a modified invasion speed prediction of 660 m/year which is reasonably close to the actual 644 m/year invasion speed inferred from ADS data.

4.6.2 Simulation in 2-Dimensions

To illustrate the relevance of our 1-dimensional analysis, we simulate the model on a realistic landscape using the 2-dimensional ecological diffusion equation,

$$\frac{\partial P}{\partial t} = \left(\frac{\partial^2}{\partial x^2} + \frac{\partial^2}{\partial y^2} \right) [DP],$$

with constant MPB dispersal rate $D = 3.21$ ha/year. When initialized with variable density of susceptible trees (to mimic realistic demographic heterogeneity) across the

2-dimensional habitat, the model generates periodic closed loop waves of infestation that propagate outward from the initial infestation source at the origin (Fig. 4.12). Infestation moves in the direction of nearby high density stands of susceptible trees. After enough time, infestation builds up to detectable levels (incipient epidemic state) as small local outbreaks develop and coalesce to form a full scale outbreak (center-) wave. Near the temporal end of this first outbreak-recovery cycle, small spots of infestation appear near the origin again and merge to form another closed loop wave emanating outward. Long-term simulations show that these periodic waves eventually resolve into concentric circular waves with constant speed, amplitude, and period.

Peak infestation of the initial invasion wave is approximately 18 stems/ha whereas in the 1-dimensional model, we saw peak impacts near 29 stems/ha. This difference can be attributed to intrinsic effects of 2-dimensional dispersal. E.g., MPB are dispersing in infinitely many directions (360°) with the 2-dimensional model as opposed to just two directions (left and right) on a 1-dimensional habitat. The essentials of the spatiotemporal dynamics, however, are the same and we may still infer a great deal from the 1-dimensional model about the nature of realistic invasion waves and make relatively accurate predictions of outbreak intensity. Indeed, a radial cross-section of a circular wave generated by the 2-dimensional model yields a waveform pattern which is nearly indistinguishable from a 1-dimensional simulation. Furthermore, 2-dimensional invasion wave speed is exactly the same as that of the 1-dimensional analog.

4.6.3 Local Temporal vs. Spatiotemporal Outbreak Dynamics

We have seen that our model generates a train of invasion waves that move across a forest landscape with constant speed. At a stationary point in the forest, a passing wave appears as a local outbreak in time. Duncan et al. (2015) provide a detailed temporal analysis of stand-level outbreaks generated by a similar tree demographic model sans explicit MPB dispersal. In fact, were there no dispersal component in our model, i.e. $\sigma^2 = 0$, then the PDE in Eq. 4.28 would reduce to the ordinary differential equation (ODE),

$$w_{tt} = -\beta e^w,$$

whose solution after noting that $I = e^w$ is

$$I(t) = I_{max}\text{sech}^2\left(\sqrt{\frac{\beta I_{max}}{2}}t\right),$$

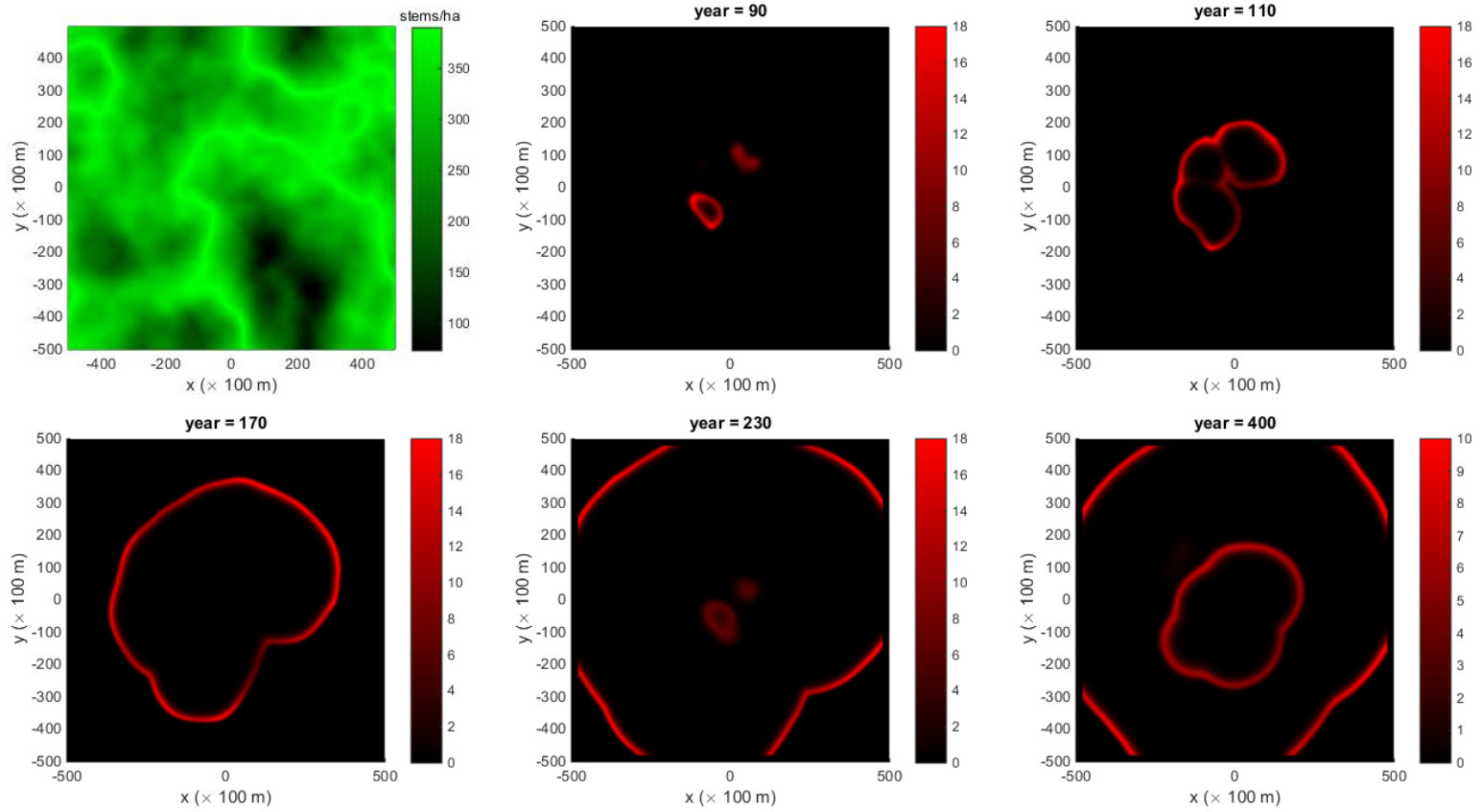

FIGURE 4.12: Simulation of the model in 2-dimensional space with small initial infestation source centered about the origin. The simulation is initialized with variable density of susceptible hosts, $S_0(x, y)$ (top left), to mimic realistic forest heterogeneity. The model generates periodic closed loop (asymptotically, circular) waves of infestation that propagate outward at a rate of approximately 312 m/year. Peak infestation of the initial wave is around 18 stems per hectare.

TABLE 4.2: Comparison of outbreak severity predicted by our model with peak impacts predicted by the non-spatial forest demographic model of Duncan et al. (2015) and with mean yearly impacts across the SNRA during the recent outbreak. Our predictions of outbreak intensity (I_{max}) and duration are in close agreement with the corresponding approximations made by Duncan et al. (2015). However, our approximations of peak infestation and outbreak duration are closer to the respective observed values from the SNRA outbreak.

	SNRA	Present Paper		Duncan et al. (2015)	
		Simulation	Approx.	Simulation	Approx.
Peak (stems/ha)	39.6	29.2	35.9	19.0	27.5
Outbreak duration (years)	≈ 10	12.4	8.1	15.4	13.6

which is the explicit approximation of the outbreak curve in time derived in Duncan et al. (2015) under the assumption that I attains its maximum value, I_{max}, when $t = 0$.

Using our model, tracking infestation at a single point leads to a skewed outbreak wave profile with respect to time while the sech-squared function of Duncan et al. (2015) is symmetric (Fig. 4.13). However, approximations of outbreak severity and duration from our model are relatively close to those derived by Duncan et al. (2015) (using our nominal parameter estimates) as well as to actual mean yearly impacts from the SNRA (Table 4.2). We also point out that Eq. 4.34 is structurally similar to the approximation of maximum MPB impact derived in Duncan et al. (2015), $I_{max} = I^* + \frac{(\ln R)^2}{2\beta}$, where I^* is the (relatively small) fixed point for the population of infested trees.

To assess the accuracy of our I_{max} prediction and wave shape parameter estimates, we compare the temporal length of an invasion wave as it passes over a particular point with the prediction of outbreak duration made by Duncan et al. (2015) and with SNRA impact data (Table 4.2). The system is in outbreak phase when $I > I^*$ (Duncan et al., 2015); so to get a rudimentary estimate of the spatial width of a traveling wave profile, we set the right sides of (4.32) and (4.33) equal to I^* separately and solve for x. Adding the resulting x values gives us the desired width. Dividing the wave width by the wave speed (approximated by Eq. 4.20) gives a predicted outbreak duration of 8.1 years. While this outbreak duration prediction matches SNRA data fairly well, it is ultimately an underestimate since we used the wave tail approximations without taking into account how they are connected (i.e., the shape of the wave when the outbreak is in full swing). In reality, the concave down nature of the outbreak curve near the center surely adds to the outbreak duration. It is yet an open question whether or not it is

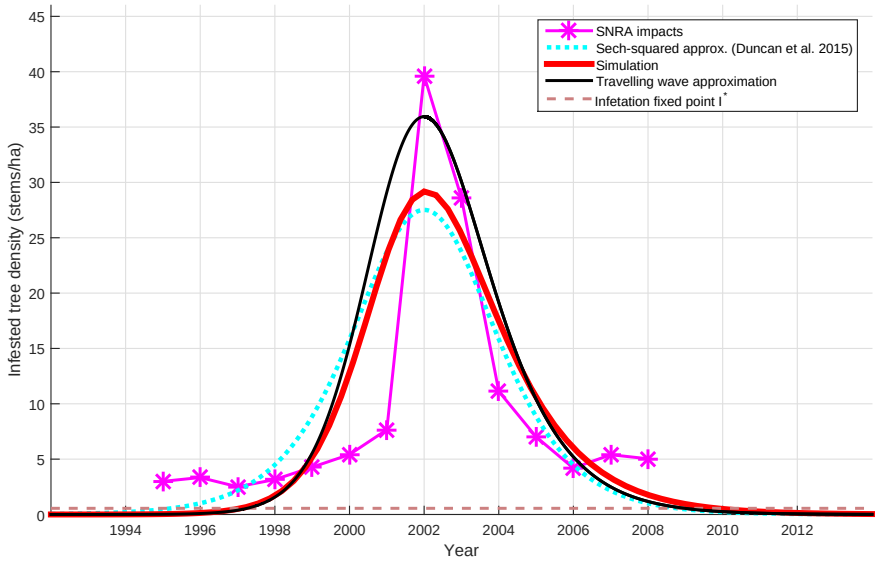

FIGURE 4.13: Comparison of the temporal dynamics of the invasion wave as it passes over a particular point with the sech-squared approximation of Duncan et al. (2015) and with SNRA impact data. The system is in outbreak phase when $I > I^*$ (Duncan et al., 2015).

possible to construct an analytic approximation of the invasion wave profile (such as the sech-squared function of Duncan et al. (2015) for the non-spatial model).

4.7 Conclusion

In this paper we have developed a MPB outbreak model that accurately emulates infested tree population dynamics exhibited in realistic epidemics. The model captures the temporal dynamics of an outbreak-recovery cycle by incorporating juvenile latency classes to account for size requirements for attack-susceptible trees. Beetle dispersal is modeled by convolution of the Gaussian diffusion kernel with the previous year's population density function.

Initializing the model with a small infestation near the origin generates a train of solitary waves of MPB infestation that propagate through a medium of host trees in space. The rate at which beetles disperse, as well as their net reproductive rate, determines the speed of these periodic waves which we predict using a method similar to that of Neubert and Caswell (1996). The resulting speed and wave shape approximations agree with formulas derived in Kot et al. (1996) for predicting invasion rates of organisms that disperse according to a normal distribution.

In an effort to predict outbreak severity based on MPB population growth rates, we approximate the convolution integral in the IDE model for infested trees using the

method of steepest descent and a WKB approximation for infested tree density. Upon substituting the difference equation for susceptible trees, we derive a PDE that models (the log of) infestation. Travelling wave solutions of the PDE satisfy an ODE whose trajectories correspond to invasion wave profiles. Using conservation of energy along trajectories, we deduce exponential growth and decay rates for the left and right tails (resp.) of a wave of MPB infestation. Viewing the ODE as a potential function, we use the maximum stable energy state to obtain an approximation of peak infestation in terms of wave speed. Combining this approximation with our estimation of invasion speed yields an accurate prediction of outbreak severity in terms of net reproductive rate of MPB and host searching efficiency.

Our invasion speed prediction is nearly 100% accurate with only minor deviations from simulation wave speeds for (unrealistically) large MPB population growth rates. The speed prediction also compares well to actual (ADS) infestation data taken from an outbreak in the SNRA after accounting for variable host density through the MPB motility function of Powell and Bentz (2014). A numerical reconstruction of the travelling invasion wave profile illuminates the accuracy of our wave tail shape approximations derived from the PDE (4.28). With a mean relative error of less than 15% across a range of reasonable MPB population growth rates, our approximation of peak infestation enables us to make relatively good predictions of outbreak severity. Simulations of the model in 2-dimensions confirm the assertion that we can gain much insight about the nature of realistic invasion waves and make relatively accurate predictions of outbreak intensity from our analysis of the 1-dimensional model.

Finally, we saw that the model-generated train of infestation waves correspond to periodic outbreaks with respect to time from the standpoint of a stationary point on the landscape (Fig. 4.2. This outbreak-recovery cycle mirrors that which is generated by the similar demographic model devised by Duncan et al. (2015). Our predictions of outbreak intensity (I_{max}) and duration are in close agreement with the corresponding approximations made by Duncan et al. (2015). However, our approximations of peak infestation and outbreak duration are closer to the respective observed values from the SNRA outbreak.

Chapter 5
CONCLUSION

The overall intent of this work was to predict the severity, duration, frequency, and invasion speed of outbreaks of phytophagous forest pests in terms of their sedentary hosts. The main results provide relatively simple analytic approximations of these characteristics for a variety of outbreak insects, based explicitly on measurable biological parameters - pest net reproduction rate, mean dispersal distance, and host search efficiency. Since many insect species' life history developmental rates depend heavily on thermal inputs, understanding the effects of temperature signals on various life stages is critical in predicting population growth rates and subsequently, outbreak intensity, timing, and invasion rate.

Throughout the course of this dissertation, we constructed and analyzed a sedentary host demographic model with outbreak insect dispersal motivated by the lodgepole pine tree-MPB interaction. The model is appropriate for a spectrum of pests attacking the later age classes of long lived hosts, including MPB, spruce budworm, and spruce beetle. We also examined the explicit dependence of MPB reproductive rates on thermal regimes. The effect of temperature on insect populations is an important variable to analyze in understanding outbreak dynamics, especially in light of recent climate change phenomena.

In chapter two we developed the mechanistic SIJ host demographic model which included a parameter representing temperature-dependent MPB population growth rate. The model captures the temporal dynamics of an outbreak-recovery cycle by incorporating age classes of nonsusceptible juveniles to account for size requirements for attack susceptible hosts. We found that the stability of two fixed points, one trivial and one corresponding to incipient epidemics, control general outbreak behavior. As the MPB growth rate parameter increases, both fixed points become unstable through a Hopf bifurcation which creates periodic outbreaks consistent with periodic irruptive population behavior exhibited by realistic MPB populations.

From the SIJ model we derived an approximating function for the outbreak curve in time (the sech-squared function). With this formula we predicted the severity as well as the duration of an outbreak based on temperature-driven MPB growth rates. Additionally, we developed a formula for predicting the period of the outbreak-recovery cycle. These results indicate that higher growth rates significantly increase the severity of outbreaks but have little effect on outbreak frequency.

Chapter three contained a detailed assessment of MPB impact on temperate and boreal forests by examining population growth rates across northern U.S. Rocky Mountain pine forests under future climate scenarios. We developed the thermally-driven mechanistic R-model to predict growth rates using a distributional model of beetle phenology in conjunction with criteria for successful host colonization. Using projected daily minimum and maximum temperatures for the years 2025 to 2085 generated by three separate global climate models each with two different emissions scenarios, we calculated growth rates each year for the study area at 4km resolution.

At low to middle elevations, univoltine MPB population growth rates decrease on average across the study area. As temperatures increase with time due to global warming, the R-model predicts lower adult emergence and correspondingly smaller R-values for this elevational range as optimal thermal regimes move up in elevation. At high elevations, R-values increase as warming creates developmentally favorable conditions. Consequently, the higher the elevation, the longer semivoltine beetles must wait for univoltine-optimal temperature signals.

As temperatures increase across all elevational ranges, some beetles acquire the phenological potential to complete two generations in a single year (bivoltinism) while avoiding overwintering mortality. We predicted that low (warmer climate) elevations would experience the greatest bivoltine potential. However, when restricted to areas with pine tree coverage, total area with bivoltine potential is significantly reduced since host density is limited at very low elevations. Nevertheless, our mechanistic model does predict the potential for an unprecedented switch from univoltine to bivoltine MPB life cycles in host (lodgepole pine) areas. This could have multiplicative effects on yearly population growth rates and subsequently, catastrophic effects on North American pine forest ecosystems.

Finally, in the fourth chapter we returned to our study of MPB outbreak dynamics and equipped the SIJ model with a Gaussian kernel for MPB dispersal, thus transforming the model into a spatially-dependent system of integrodifference equations. Simulation

of the model showed a train of periodic invasion waves of infestation moving through space. In deriving an approximating PDE from the IDE for infested hosts and searching for travelling wave solutions, we obtained explicit formulas of invasion wave amplitude and speed in terms of biological parameters (pests reproductive rate, mean dispersal distance, and host search efficiency). These predictions compared favorably with peak impact observations taken during the recent outbreak in the SNRA.

We saw that the model-generated train of infestation waves correspond to periodic outbreaks with respect to time from the standpoint of a stationary point on the landscape. This outbreak-recovery cycle closely mirrors that which is generated by the (non-spatial) SIJ model of chapter 1. Our predictions of outbreak intensity and duration of travelling waves are in relatively good agreement with the corresponding approximations derived from the original SIJ model. Indeed, the equations predicting maximum infestation are structurally very similar. It is yet an open question whether or not it is possible to construct an analytic approximation (analogous to the sech-squared function for the non-spatial SIJ model) of the invasion wave profile generated by the spatial SIJ model.

With increasing temperatures caused by global climate change, we concluded in chapter three that univoltine MPB population growth rates can be expected to increase across certain elevational gradients in host areas. From our analysis of the non-spatial SIJ model in chapter two, we predict that these increasing growth rates will lead to significantly increased outbreak severity in terms of total tree mortality over the course of an outbreak. Similarly, the spatial SIJ model of chapter four predicts increasing peak infestation mortality as growth rates increase. Chapter four also showed us that the speed of a MPB invasion increases with increasing net reproductive rates. Furthermore, at some low elevation host areas, univoltine MPB may transition to bivoltine life cycles. This will likely lead to dramatic increases in yearly population growth rates and hence, outbreak mortality could be elevated to disastrous levels.

BIBLIOGRAPHY

Abatzoglou, J. T. (2013). Development of gridded surface meteorological data for ecological applications and modelling. *International Journal of Climatology*, (1):121–131.

Abatzoglou, J. T. and Brown, T. J. (2013). A comparison of statistical downscaling methods suited for wildfire applications. *International Journal of Climatology*, 32(5):772–780.

Abramson, G., Kenkre, V. M., Yates, T. L., and Parmenter, R. R. (2003). Traveling waves of infection in the hantavirus epidemics. *Bulletin of mathematical biology*, (3):519–534.

Amman, G. D. and Cole, W. E. (1983). Mountain pine beetle dynamics in lodgepole pine forests: Part ii population dynamics. *U.S. Department of Agriculture, General Technical Report INT-145*.

Amman, G. D. and Schmitz, R. F. (1988). Mountain pine beetle-lodgepole pine interactions and strategies for reducing tree losses. *Ambio*.

Anderson, R. M. and May, R. M. (1979a). Population biology of infectious diseases: Part i. *Nature*, (6):361–7.

Anderson, R. M. and May, R. M. (1979b). Population biology of infectious diseases: Part ii. *Nature*, (5722):455–461.

Anderson, R. M. and May, R. M. (1982). The logic of vaccination. *New Scientist*, (1332):410–415.

Aukema, B. H., Carroll, A. L., Zheng, Y., Zhu, J., Raffa, K. F., Moore, R. D., Stahl, K., and Taylor, S. W. (2008). Movement of outbreak populations of mountain pine beetle:influences of spatiotemporal patterns and climate. *Ecogeography*.

Aukema, B. H., Carroll, A. L., Zhu, J., Raffa, K. F., Sickley, T. A., and Taylor, S. W. (2006). Landscape level analysis of mountain pine beetle in british columbia, canada:

spatiotemporal development and spatial synchrony within the present outbreak. *Ecography*, (3):427–441.

Axelson, J. N., Alfaro, R. I., and Hawkes, B. C. (2009). Influence of fire and mountain pine beetle on the dynamics of lodgepole pine stands in british columbia, canada. *Forest Ecology and Management*.

Bentz, B. J. (2006). Mountain pine beetle population sampling: inferences from lindgren pheromone traps and tree emergence cages. *Canadian Journal of Forest Research*, 36(2):351–360.

Bentz, B. J., Duncan, J. P., and Powell, J. A. (2016). Predicting thermal refugia from mountain pine beetle outbreaks in a changing climate: A case study in the u.s. northern rocky mountains. *Forestry*.

Bentz, B. J., Logan, J. A., and Amman, G. D. (1991). Temperature dependent development of the mountain pine beetle (coleoptera: Scolytidae), and simulation of its phenology. *Canadian Entomologist*, (5):1083–1094.

Bentz, B. J. and Mullens, D. E. (1999). Ecology of mountain pine beetle (coleoptera: Scolytidae) cold hardening in the intermountain west. *Environmental Entomology*, (4):577–587.

Bentz, B. J., Régnière, J., Fettig, C. J., Hansen, E. M., Hayes, J. L., Hicke, J. A., and Seybold, S. J. (2010). Climate change and bark beetles of the western united states and canada: direct and indirect effects. *BioScience*, (8):602–613.

Bentz, B. J., Vandygriff, J., Jensen, C., Coleman, T., Maloney, P., Smith, S., Grady, A., and Schen-Langenheim, G. (2014). Mountain pine beetle voltinism and life history characteristics across latitudinal and elevational gradients in the western united states. *Forest Science*.

Berryman, A. A., Dennis, B., Raffa, K. F., and Stenseth, N. C. (1985). Evolution of optimal group attack, with particular reference to bark beetles (coleoptera: Scolytidae). *Ecology*.

Bjornstad, O. N., M. Peltonen, A. M. L., and Baltensweiler, W. (2002). Waves of larchbudmoth outbreaks in the european alps. *Science*.

Bleiker, K. P., O'Brien, M. R., Smith, G. D., and Carroll, A. L. (2014). Characterisation of attacks made by the mountain pine beetle (coleoptera: Curculionidae) during its endemic population phase. *The Canadian Entomologist*, 146(3):271–284.

Campbell, R. I. A. R., Hawkes, B. C., and Shore, T. L. (2004). Dendroecological reconstruction of mountain pine beetle outbreaks in the chilcotin plateau of british columbia. *Mountain pine beetle symposium: challenges and solutions, Kelowna, British Columbia*.

Crabb, B. A., Powell, J. A., and Bentz, B. J. (2012). Development and assessment of 30-m pine density maps for landscape-level modeling of mountain pine beetle dynamics. *Res. Pa RMRS-RP-96WWW. U.S. Department of Agriculture, Forest Service, Rocky Mountain Research Station, Fort Collins, CO*.

Curry, G. L., Feldman, R. M., and Sharpe, P. J. (1978). Foundations of stochastic development. *Journal of Theoretical Biology*, 74(3):397–410.

Duncan, J. P., Powell, J. A., Gordillo, L. F., and Eason, J. (2015). A model for mountain pine beetle outbreaks in an age-structured forest: Predicting severity and outbreak-recovery cycle period. *Bulletin of mathematical biology*, (7):1–29.

Gilbert, E., Powell, J. A., Logan, J. A., and Bentz, B. J. (2004). Comparison of three models predicting developmental milestones given environmental and individual variation. *Bulletin of mathematical biology*, (6):1821–1850.

Heavilin, J. and Powell, J. (2008). A novel method for fitting spatio-temporal models to data, with applications to the dynamics of mountain pine beetle. *Natural Resource Modelling*, 21(4):489–524.

Heavilin, J., Powell, J. A., and Logan, J. A. (2007). Development and parametrization of a model for bark beetle disturbance in lodgepole forest. *Plant Disturbance Ecology*.

Hethcote, H. W. (1994). A thousand and one epidemic models. *Frontiers in mathematical biology*.

Hethcote, H. W. (2000). The mathematics of infectious diseases. *SIAM review*, (4):599–653.

Houghton, J. T., Filho, L. G. M., Callander, B. A., and Kattenberg, N. H. A. Climate change 1995: the science of climate change.

Hrinkevich, K. and Lewis, K. J. (2011). Northern range limit mountain pine beetle outbreak dynamics in mixed sub-boreal pine forests of british columbia. *Ecosphere*, (10):116.

Jönsson, A., Appelberg, G., and Börring, S. H. L. (2008). Spatio-temporal impact of climate change on the activity and voltinism of the spruce bark beetle, ips typographus. *Global Change Biology*, 15(2):486–499.

Keeling, M. J. (1999). The effects of local spatial structure on epidemiological invasions. *Proceedings of the Royal Society of London B: Biological Sciences*, (1421):859–867.

Kermack, W. O. and McKendrick, A. G. (1927). A contribution to the mathematical theory of epidemics. *Proceedings of the Royal Society A*, (772):700–721.

Kot, M., Lewis, M. A., and van den Driessche, P. (1996). Dispersal data and the spread of invading organisms. *Ecology*, 77(7):2027–2042.

Kurz, W. A., Dymond, C. C., Stinson, G., Rampley, G. J., Neilson, E. T., Carroll, A. L., Ebata, T., and Safranyik, L. (2008). Mountain pine beetle and forest carbon feedback to climate change. *Nature*, (7190):987–990.

Leslie, P. H. (1945). The use of matrices in certain population mathematics. *Biometrika*, (3):183–212.

Logan, J. A. and Bentz, B. J. (1999). Model analysis of mountain pine beetle (coleoptera: Scolytidae) seasonality. *Environmental Entomology*, 28(6):924–934.

Logan, J. A. and Powell, J. A. (2001). Ghost forests, global warming, and the mountain pine beetle (coleoptera: Scolytidae). *American Entomologist*, 47(3):160.

Mattson, W. J. (1996). Escalating anthropogenic stresses on forest ecosystems: forcing benign plant-insect interactions into new interaction trajectories. *Congress report*.

Meddens, A. H., Hicke, J. A., and Ferguson, C. A. (2012). Spatiotemporal patterns of observed bark beetle-caused tree mortality in british columbia and the western united states. *Ecological Applications*, (7):1876–1891.

Neubert, M. G. and Caswell, H. (1996). Demography and dispersal: calculation and sensitivity analysis of invasion speed for structured populations. *Ecology*, 81(6):1613–1628.

Powell, J. A. and Bentz, B. J. (2009). Connecting phenological predictions with population growth rates for an outbreak insect. *Landscape Ecology*.

Powell, J. A. and Bentz, B. J. (2014). Phenology and density-dependent dispersal predict patterns of mountain pine beetle (dendroctonus ponderosae) impact. *Ecological Modelling*.

Powell, J. A., Jenkins, J. L., Logan, J. A., and Bentz, B. J. (2000). Seasonal temperature alone can synchronize life cycles. *Bulletin of mathematical biology*, (5):977–998.

Régnière, J. and Bentz, B. (2007). Modeling cold tolerance in the mountain pine beetle, dendroctonus ponderosae. *Journal of Insect Physiology*.

Régnière, J., Powell, J., Bentz, B., and Nealis, V. (2012). Effects of temperature on development, survival and reproduction of insects: experimental design, data analysis and modeling. *Journal of Insect Physiology*.

Reid, R. W. (1962). Biology of the mountain pine beetle, dendroctonus monticolae hopkins, in the east kootenay region of british columbia ii. behaviour in the host, fecundity, and internal changes in the female. *The Canadian Entomologist*, 90(6):605–613.

Reid, R. W. and Gates, H. (1970). Effect of temperature and resin on hatch of eggs of the mountain pine beetle (dendroctonus ponderosae). *The Canadian Entomologist*, 102(5):617–622.

Reid, R. W. and Gates, H. (1990). Growth response in a douglas-fir/lodgepole pine stand after thinning of lodgepole pine by the mountain pine beetle: A case study. *Journal of the Entomological Society of British Columbia*.

Ricker, W. E. (1958). Handbook of computations for biological statistics offish populations. *Bulletin of the Fisheries Resource Board Canada*.

Riley, S. (2007). Large-scale spatial-transmission models of infectious disease. *Science*, (5829):1298–1301.

Ruan, S. and Xiao, D. (2004). Stability of steady states and existence of travelling waves in a vector-disease model. *Proceedings of the Royal Society of Edinburgh: Section A Mathematics*, 134(5):991–1011.

Rupp, D. E., Abatzoglou, J. T., and Mote, K. C. H. P. W. (2013). Evaluation of cmip5 20th century climate simulations for the pacific northwest usa. *Journal of Geophysical Research: Atmospheres*, 118(19):10–884.

Safranyik, L. (2003). Mountain pine beetle epidemiology in lodgepole pine. *Mountain pine beetle symposium: challenges and solutions*.

Safranyik, L., Shrimpton, D. M., and Whitney, H. S. (1975). An interpretation of the interaction between lodgepole pine, the mountain pine beetle and its associated blue stain fungi in western canada. *Canadian Entomologist*.

Schmidt, W. C. and Alexander, R. R. (1985). Strategies for managing lodgepole pine. *Lodgepole Pine-The Species and Its Management, Office of Conferences and Institutes, Cooperative Extension, Washington State University*.

Sharpe, P. J. H., Curry, G. L., DeMichele, D. W., and Cole, C. L. (1977). Distribution model of organism development times. *Journal of Theoretical Biology*.

Sherratt, J. A. (1994). On the evolution of periodic plane waves in reaction-diffusion systems of - type. *SIAM Journal on Applied Mathematics*, 54(5):1374–1385.

Sherratt, J. A. (1998). Invading wave fronts and their oscillatory wakes are linked by a modulated traveling phase resetting wave. *Physica D: Nonlinear Phenomena*, 117(1):145–166.

Thomson, A. M., Calvin, K. V., Smith, S. J., Kyle, G. P., Volke, A., Patel, P., Delgado-Arias, S., Bond-Lamberty, B., Wise, M. A., and Clark, L. E. (2011). Rcp4.5: a pathway for stabilization of radiative forcing by 2100. *Climatic Change*, (1).

Tobin, P. C., Nagarkatti, S., Loeb, G., and Saunders, M. C. (2008). Historical and projected interactions between climate change and insect voltinism in a multivoltine species. *Global Change Biology*, 14(5):951–957.

Turchin, P. (1998). *Quantitative analysis of movement: measuring and modeling population redistribution in animals and plants*, volume 1. Sunderland: Sinauer Associates.

van den Bosch, F., Metz, J. A. J., and Diekmann, O. (1990). The velocity of spatial population expansion. *Journal of Mathematical Biology*, 28(5):529–565.

Vuuren, D. P. V., Edmonds, J., Kainuma, M., Riahi, K., amd K. Hibbard, A. T., and Rose, S. K. (2011). The representative concentration pathways: an overview. *Climatic Change*.

Weed, A. S., Bentz, B. J., Ayres, M. P., and Holmes, T. P. (2015). Geographically variable response of dendroctonus ponderosae to winter warming in the western united states. *Landscape Ecology*.

Yamanaka, T., Tatsuki, S., and Shimada, M. (2008). Adaptation to the new land or effect of global warming? an age-structured model for rapid voltinism change in an alien lepidopteran pest. *Journal of animal ecology*, 77(3):585–596.

APPENDICES

APPENDIX A
DISTRIBUTIONAL MODEL OF MPB PHENOLOGY

Not all individuals in a population of poikilothermic organisms progress through particular life stages at the same rate. This is primarily due to intrinsic genetic variation at the individual level. Therefore, we assume that developmental rates are randomly distributed across a population according to some probability distribution. Before describing the effects this assumption of rate variability on development times and hence adult MPB emergence distributions, we outline the general developmental model for physiological age of a single (or mean individual) beetle in a given life stage.

Phenology Preliminaries

MPB go through 8 life stages (oviposition, egg, larval instars 1-4, pupae, and teneral adult) throughout the course of their life history. Each stage has a unique developmental rate function that depends on the temperature of the medium surrounding the beetle (tree phloem or ambient air). We denote the developmental rate function for life stage j by $\rho_j(T(t))$ where $T(t)$ is the temperature as a function of time t. By rate we mean proportion of life stage completed per time (1 day). The time required to complete a life stage (developmental time) denoted by $\tau_j(T)$ for a constant temperature is therefore given by

$$\tau_j(T) = \frac{1}{\rho_j(T)}.$$

The physiological age of a beetle in life stage j is defined as the proportion of that life stage completed at time t and is denoted by $a_j(t)$. It is important to realize the distinction between insect physiological age and real time. Physiological age is a direct function of temperature, i.e. MPB complete fractions of the stage more or less rapidly depending on temperature. The range of $a_j(t)$ is the interval $[0, 1]$ where $a_j(t_{j-1}) = 0$ and $a_j(t_j) = 1$ implies that the life stage began at time t_{j-1} and ended at time t_j. We

formally define the relationship between physiological age and developmental rate as

$$\frac{d}{dt}a_j(t) = \rho_j(T(t)),$$

equivalently,

$$a_j(t) = \int_{t_{j-1}}^{t} \rho_j(T(s))ds$$

where the life stage j begins at time t_{j-1}. If t_{j-1} is known, the developmental time for stage j is $t_{j-1} - t_j$ where t_j is found by solving

$$a_j(t_j) = 1 = \int_{t_{j-1}}^{t_j} \rho_j(T(s))ds$$

given a known temperature signal $T(t)$ (for example, see Fig. 5.1).

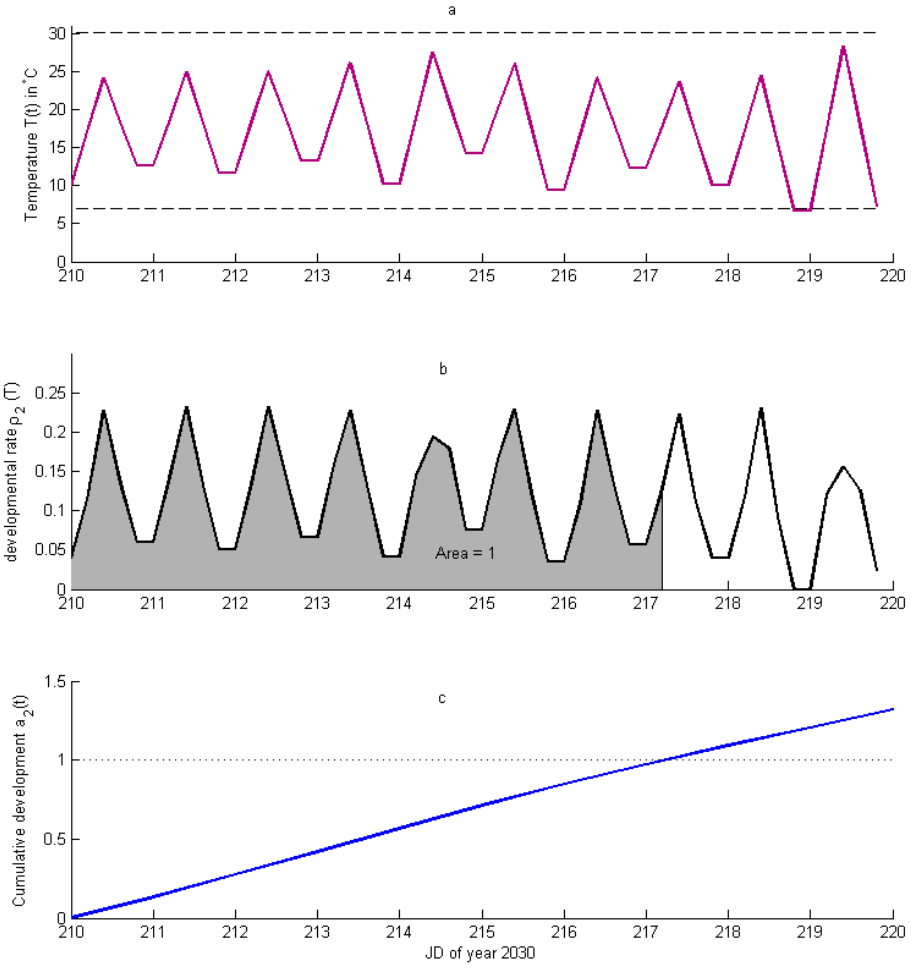

FIGURE 5.1: Life stage development response to temperature. The developmental time for the second stage of the MPB life history (egg, $j = 2$) using the temperature signal shown in (a) (daily high and low temps with interpolated midpoints) from latitude 44°N and longitude 115°W for the year 2030 projected by global climate model CanEsm2 with emissions scenario Rcp-4.5 is just over 7 days ($t_1 = 210$ and $t_2 = 217.2$). The dashed lines in (a) represent low and high developmental temperature thresholds, $7°C$ and $30°C$ respectively. Note that when the temperature is below the lower threshold at the end of day 218, the developmental rate in (b) is zero. Cumulative development for a day shown in (c) is calculated using Simpson's rule on developmental rates for that day. Rate curve and parameters are taken from Régnière et al. (2012).

Since we need to know how many adult beetles emerge from an infested tree each day to compute the number of newly infested trees (per old infested tree), we ultimately need to know the time of development of the adult life stage. We calculate the time of adult development t_8 (given oviposition time t_0) by daisy-chaining the 8 life stages as follows:

$$1 = \int_{t_0}^{t_1} \rho_1(T(s))ds,$$

$$
\begin{aligned}
1 &= \int_{t_1}^{t_2} \rho_2(T(s))ds, \\
&\vdots \\
1 &= \int_{t_{j-1}}^{t_j} \rho_j(T(s))ds, \\
1 &= \int_{t_7}^{t_8} \rho_8(T(s))ds.
\end{aligned}
\tag{5.1}
$$

Incidentally we must find all life stage development times t_1, t_2, ..., t_8 successively. In practice, this is done numerically since realistic temperature signals are vectors with temperatures given at certain points in time.

Developmental Rate Curves

Specific MPB life stage developmental rate functions and corresponding parameters are taken from Régnière et al. (2012). Figure 3.3 shows graphs of the 8 parameterized rate curves. While there is no true mechanistic basis underlying the derivation of the rate curves, they are an empirical mathematical description of the shape of developmental responses to temperature. In general, each curve has lower and upper temperature thresholds forming a range of temperatures outside of which no development occurs. Note that for the most part, developmental rate curves are increasing between the thresholds. Parameters were estimated by maximum likelihood using measured developmental times from samples of beetles for each life stage at various constant temperatures. See Régnière et al. (2012) for details of experiments, data collection methods, and parameterizations.

Population Variability

We now return to the notion of developmental rate variability. Let ε be a normal random variable with variance σ^2 and mean $\sigma^2/2$. Then $\delta \equiv e^{\varepsilon}$ is a lognormal random variable, $\delta \sim \ln\mathcal{N}(\sigma^2/2, \sigma^2)$. Let $r(T) = \delta\rho(T)$ for some constant temperature T and rate curve ρ. The lognormal random variable $r(T)$ represents the stochastic developmental rate of an individual beetle. Since $\eta \equiv \delta^{-1}$ has a lognormal distribution (with the same variance as δ, namely σ^2), the stochastic developmental time $t_d = \eta\tau(T)$ is also lognormal.

The parameters of the normal distribution for ε are chosen so that the expected value of η is 1 which ensures that the expected value of $t_d(T)$ is $\tau(T)$ for constant temperature T (Fig. 5.2). We force the expected value of $t_d(T)$ to be $\tau(T)$ since the parameterization of rate curves used laboratory developmental times (at various constant temperatures) transformed to developmental rates. Furthermore, we are interested in

predicting life stage development times in order to calculate MPB population growth rates. Thus, we want mean developmental time to be unbiased. It should be noted that the requirement for unbiased developmental time causes developmental rates to be biased. That is, the expected value of a developmental rate distribution $r(T)$ at some fixed temperature is not $\rho(T)$ but rather $e^{\sigma^2}\rho(T)$. This does not pose any significant problems, however, since σ is small for all life stages and ultimately we are only concerned with finding development times.

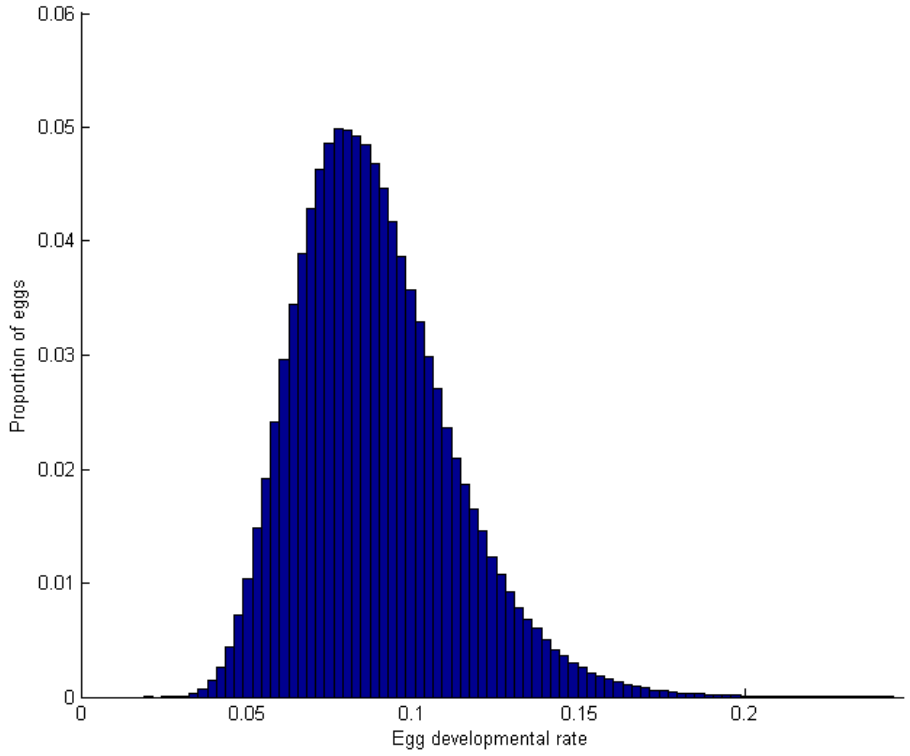

FIGURE 5.2: The lognormal distribution of developmental rates $r(T)$ for the MPB egg life stage (at constant temperature $T = 15°$ Celsius) using rate curve and corresponding parameters from Régnière et al. (2012). Note that the mean of this distribution is $0.09 = e^{\sigma^2}\rho(15°)$

.

The lognormal variance σ^2 was estimated for each life stage in the parameterization process using laboratory data on developmental times. Since it is believed that this variance may be significantly different in the field, we introduce a variance multiplier υ to account for rate variability amplification due to natural exogenous forces.

There are several reasons for assuming that developmental rates are lognormally distributed. First, individual-level traits subject to natural selection under changing

environmental conditions produce intrinsic variation within populations. This variation translates to random variability in the parameters of the rate curves. We assume this variability is normal (via the random variable ε) according to quantitative genetic theory. Régnière and Powell (2013) showed that this assumption of normality in the parameters leads to lognormally distributed developmental rates. Second, the positive skew of the lognormal distribution is a characteristic often observed in distributions of developmental rates and times of insects (Curry et al. 1978). Finally, a lognormal random variable cannot be negative and thus developmental rates and times are guaranteed to be nonnegative as in reality.

Cohorts and Emergence Distributions

Distributional models are sometimes called *cohort* models because they keep track of numbers of individuals entering and exiting the life stages of an organism's life cycle. A cohort is a group of individuals that enter a certain life stage at the same time. Cohort models calculate the proportion of a cohort that completes the life stage during each time step given a distribution of developmental rates. In our R-model, the time step is one day and we use lognormally distributed developmental rates. We may think of life stage development as a foot race. Just as in a race, individuals have varied natural speeds (developmental rates). A heat (cohort) at the starting line ($a_j(t_0) = 0$ for all individuals) is initially in a tight clump just after the race begins at time t_0. Gradually, the pack spreads out since some runners are faster than average and some are slower than average. If the time step were one minute, a cohort model would keep track of how many runners crossed the finish line ($a_j(t) = 1$) during each minute after the race began (Fig. 5.3).

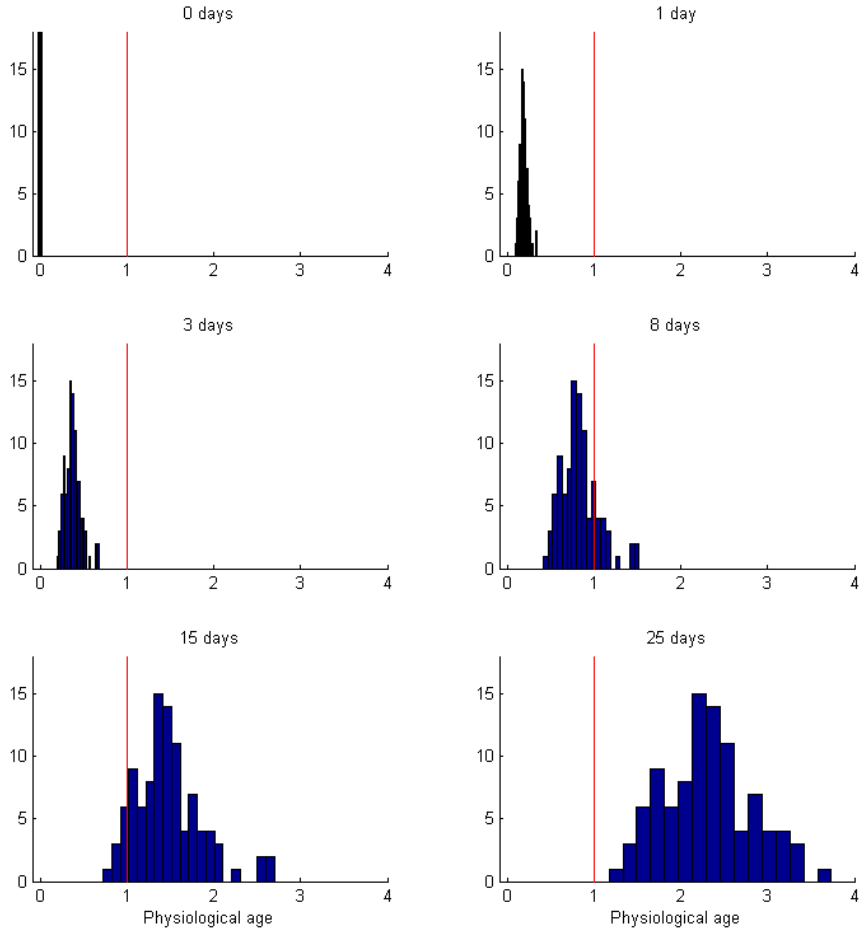

FIGURE 5.3: MPB egg stage development. In all graphs, the vertical axis represents percent of 100 eggs laid on a single day. Initially, we have a cohort of individuals starting the egg stage illustrated by the vertical bar (starting line) at age 0 (top left). The vertical line at age 1 (finish line) represents the age of life stage completion. With time, the cohort spreads out (in terms of development) due to the lognormal distribution of developmental rates (mean rate of 0.09/day). The cohort model keeps track of how many beetles from each cohort emerge from the life stage (cross the finish line) each day.

Each life stage has an associated function that gives the sizes of all starting cohorts at every point in time. The cohort model uses this starting function (which comes from the previous life stage) to calculate the total number of beetles from all cohorts that complete life stage j at time t. The result is the life stage *emergence function*, denoted by $N_j(t)$, which is used as the input starting function for the next life stage. This is the distributional model's version of equations (5.1), i.e. daisy-chaining.

To facilitate the mathematical implementation of the distributional model we define the *cumulative development function*

$$D(t) = \int_0^t \rho(T(s))ds \tag{5.2}$$

where time $t = 0$ corresponds to the start of the first life stage (oviposition). A beetle's time of development t for a life stage starting at time t_0 satisfies

$$1 = \int_{t_0}^t r(T(s))ds.$$

Replacing r with $\delta\rho$ and then dividing by δ gives

$$\eta = \int_{t_0}^t \rho(T(s))ds$$

which is equivalent to

$$\eta = D(t) - D(t_0)$$

where $\eta = \frac{1}{\delta}$ is the lognormal random variable used to distribute developmental times. The probability density function for η is

$$p(\eta) = \frac{1}{\eta\sigma\sqrt{2\pi}} e^{\frac{-\left(\ln(\eta)+\frac{\sigma^2}{2}\right)^2}{2\sigma^2}}$$

and thus the probability of a beetle emerging from the life stage at time t, given the starting time t_0, is

$$p(t|t_0) = \frac{1}{(D(t) - D(t_0))\sigma\sqrt{2\pi}} e^{\frac{-\left(\ln(D(t)-D(t_0))+\frac{\sigma^2}{2}\right)^2}{2\sigma^2}}.$$

Using the emergence function from the previous life stage $N_{j-1}(t)$ we find the starting number of beetles in a cohort that begin life stage j at time t_0 by evaluating $N_{j-1}(t_0)$. The number of beetles in that cohort that complete life stage j at time t is $N_{j-1}(t_0) \cdot p(t|t_0)$. The total number of beetles from all starting cohorts that complete the stage at time t is the emergence function for life stage j,

$$N_j(t) = \int_0^t N_{j-1}(t_0)p(t|t_0)dt_0 \ , \ j = 2, .., 8, \tag{5.3}$$

where t ranges from 0 (July 19, the start of the first life stage) to 407 (August 31 of

the following year). Note that the variable of integration is cohort starting time t_0. The emergence function $N_j(t)$ gives the number of beetles completing the life stage (emerging) on any given day between July 19 (the mean time when beetles begin attacking trees) of year $n-1$ and August 31 of year n. Figures 5.4 and 5.5 show the life stage emergence functions for all 8 MPB life stages generated by an example temperature signal with 408 daily temperatures.

The starting function for the oviposition life stage, $N_0(t)$, is called the *attack distribution* and gives the probability of a beetle attacking the tree on a given day. We assume this distribution is normal with mean July 24, based on data in Bentz (2006), and standard deviation 2 days.

Calculation of the oviposition life stage emergence function from the attack distribution is slightly different than that of the other stages. We assume that oviposition completion time for an individual beetle starting oviposition at time t_0 follows an exponential distribution with time varying rate parameter $r(T(t))$ (the temperature dependent oviposition developmental rate curve lognormally distributed across the population) and probability density function

$$f(t) = r(T(t))e^{-\int_{t_0}^{t} r(T(s))ds}.$$

The probability that a beetle completes oviposition before day t (but after day t_0) is given by the cumulative distribution function

$$F(t) = 1 - e^{-(D(t)-D(t_0))}$$

where $D(t) = \int_0^t r(T(s))ds$ is the cumulative developmental function. Thus, the probability that the beetle completes oviposition on day t given that it attacked the tree at time t_0 is the difference in exponential distribution cumulants for neighboring days,

$$p_e(t|t_0) = e^{-(D(t-1)-D(t_0))} - e^{-(D(t)-D(t_0))}.$$

If each attacking beetle has (mean) potential fecundity f_0, then the expected number of eggs laid by a beetle on day t given it began the oviposition life stage at time t_0 is

$$f_0 \; p_e(t|t_0).$$

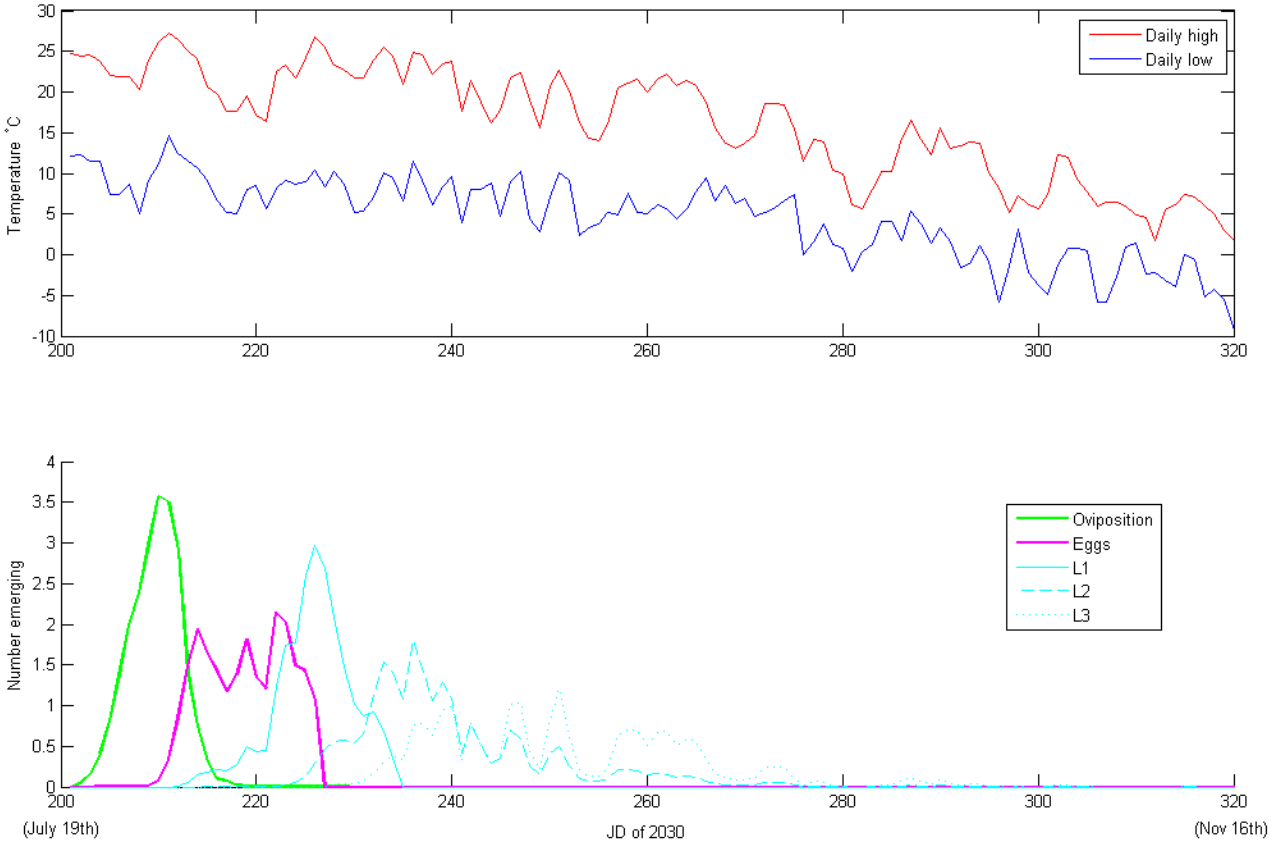

FIGURE 5.4: The first five MPB life stage emergence functions generated using a temperature signal from latitude 44°N and longitude 115°W for the year 2030 projected by global climate model CCSM4 with emissions scenario Rcp-4.5.

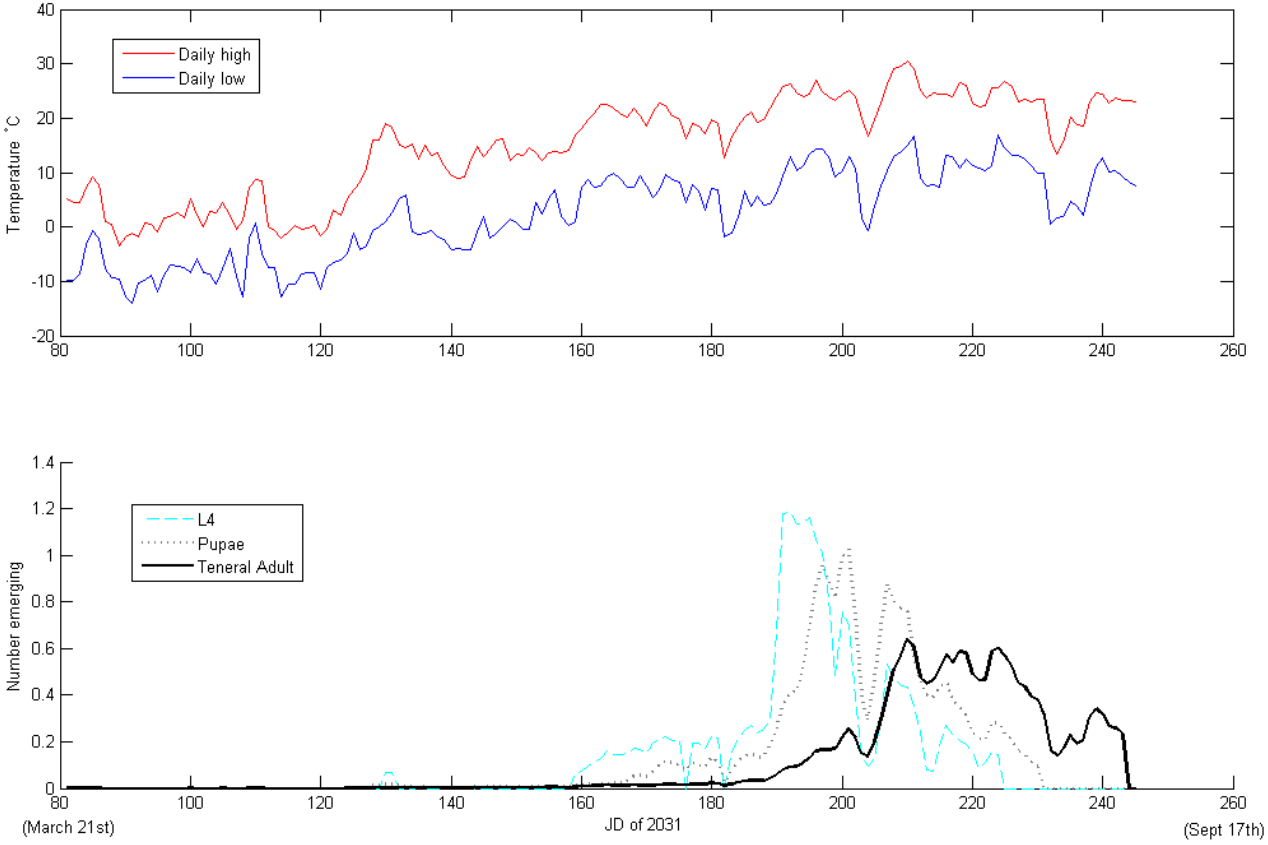

FIGURE 5.5: The last three MPB life stage emergence functions generated using a temperature signal from latitude 44°N and longitude 115°W for the year 2031 projected by global climate model CCSM4 with emissions scenario Rcp-4.5.

Since the probability that a beetle starts oviposition at time t_0 is given by the attack distribution $N_0(t_0)$, the number of eggs laid at time t by a cohort of beetles starting oviposition at time t_0 is $N_0(t_0) \cdot f_0\ p_e(t|t_0)$. The total number of eggs laid at time t by all starting cohorts is the oviposition emergence function,

$$N_1(t) = f_0 \int_0^t N_0(t_0) p_e(t|t_0) dt_0.$$

Since a female in the wild typically does not live up to its full potential fecundity and actually lay F_0 eggs, we introduce the parameter n_e to represent the true (mean) number of eggs laid by a female in the field. We then truncate $f_0\ p_e(t|t_0)$ when oviposition reaches n_e, that is, if $f_0\ p_e(t|t_0)$ reaches n_e at time t', then $f_0\ p_e(t|t_0) = 0$ for all $t > t'$. We note here that our version of the cohort model keeps track of all n_e individuals spawned by a single attacking female. Later we multiply by the number of attacking females to get the total number of individuals in the tree.

The next step in calculating the MPB population growth rate for year n involves integrating the adult emergence function $N_8(t)$ from June 30 of year n to August 31 of year n. The limits of this integration correspond to reasonable limits on seasonality; development of eggs laid earlier than June 30 or later than August 31 will not be in the proper life stage (larvae or brood adult) to survive fall and winter cold temperatures (Régnière and Bentz, 2007). Thus, the domain of a life stage emergence function, in particular $N_8(t)$, must be the time interval July 19 of year $n-1$ to August 31 of year n.

APPENDIX B

Permission Letter

SPRINGER LICENSE TERMS AND CONDITIONS

Feb 23, 2016

This is an Agreement between Jacob P Duncan ("You") and Springer ("Springer"). It consists of your order details, the terms and conditions provided by Springer, and the payment terms and conditions.

All payments must be made in full to CCC. For payment instructions, please see information listed at the bottom of this form.

License Number

3814820363120

License date

Feb 23, 2016

Licensed Content Publisher

Springer

Licensed Content Publication

Bulletin of Mathematical Biology

Licensed Content Title

A Model for Mountain Pine Beetle Outbreaks in an Age-Structured Forest: Predicting Severity and Outbreak-Recovery Cycle Period

Licensed Content Author

Jacob P. Duncan

Licensed Content Date

Jan 1, 2015

Volume number

77

Issue number

7

Type of Use

Thesis/Dissertation

Portion

Full text

Number of copies

1

Author of this Springer article

Yes and you are the sole author of the new work

Order reference number

None

Title of your thesis / dissertation

A SPATIOTEMPORAL MOUNTAIN PINE BEETLE OUTBREAK MODEL PREDICTING SEVERITY, CYCLE PERIOD, AND INVASION SPEED

Expected completion date

May 2016

Estimated size(pages)

90

Total

0.00 USD

APPENDIX C

Curricula Vitae

JACOB P. DUNCAN

Department of Mathematics and Statistics, Utah State University, Logan, UT 84321
(507) · 202 · 3809 ⋄ jacob.duncan@aggiemail.usu.edu

EDUCATION

Utah State University, Logan, UT

- Ph.D. Candidate, Mathematics — Defended November **2015**
- Dissertation: *A spatiotemporal mountain pine beetle outbreak model: predicting severity, cycle period, and invasion speed*
- Advisor: James Powell (Applied Mathematics/Mathematical Biology)

Minnesota State University, Mankato, MN

- M.A. in Mathematics — **2010**
- Thesis: *Ordinals and cardinals: An overview of properties and arithmetic*

Metropolitan State University, Saint Paul, MN

- B.S. in Applied Mathematics, *Honors* — **2006**

PROFESSIONAL EXPERIENCE

- **Graduate Teaching Assistant/Tutor** — **August 2012 - Present**
  - Department of Mathematics and Statistics, Utah State University, Logan, UT
  - Instructor of record for College Algebra, Calculus I, and Calculus II
  - Curriculum development for Calculus II (departmental collaboration)
- **Graduate Research Assistant** — **Summer and Fall 2014, Summer 2015**
  - Department of Mathematics and Statistics, Utah State University, Logan, UT
  - Funded by National Science Foundation and USDA Forest Service grants
- **Community Faculty Mathematics Instructor/Tutor** — **December 2010 - July 2012**
  - Metropolitan State University, Saint Paul, MN
  - Instructor of record for College Algebra, Precalculus, Statistics and Calculus I
- **Graduate Teaching Assistant** — **August 2007 - May 2010**
  - Minnesota State University, Mankato, MN
  - Instructor of record for College Algebra and Recitation Leader for Intermediate Algebra

AWARDS AND HONORS

- **Graduate Researcher of the Year** — **2015**
  Department of Mathematics and Statistics, Utah State University
- **Graduate Teacher of the Year** — **2014**
  Department of Mathematics and Statistics, Utah State University

- **SIAM Award for Outstanding Efforts and Accomplishments** **2014**
  SIAM Chapter at Utah State University
- **Graduate Student Leadership Award** **2013**
  Department of Mathematics and Statistics, Utah State University
- **Eagle Scout Award** **1998**

PUBLICATIONS

1. Bentz BJ, **Duncan JP**, Powell JA. 2016. Elevational shifts in thermal suitability for mountain pine beetle population growth in a changing climate. *Forestry* doi: 10.1093/forestry/cpv054.
2. **Duncan JP**, Powell JA, Gordillo LF, Eason J. 2015. A model for mountain pine beetle outbreaks in an age structured forest: predicting severity and outbreak-recovery cycle period. *Bulletin of Mathematical Biology* 77(7):1-29

MANUSCRIPTS IN REVIEW

1. **Duncan JP**, Powell JA. Analytic approximation of invasion wave amplitude predicts severity of insect outbreaks. *SIAM Journal on Applied Mathematics* (Submitted September 2015).

MANUSCRIPTS IN PREPARATION

1. **Duncan JP**, Nydegger R, Powell JA. Modelling the spread of invasive phragmites. (Target submission: *Theoretical Ecology*, February 2016)

FUNDING

- Research Assistantships (3) **2014/2015**
  Funding provided by National Science Foundation and USDA Forest Service grants
  Award amount of **$15,000.00**
- Utah State University School of Graduate Studies and Research Travel Grants **2014/2015**
  Award amount of **$1000.00**
- Society of Industrial and Applied Mathematics (SIAM) **2015**
  Travel Grants for 8th International Congress of Industrial and Applied Mathematics (ICIAM) and SIAM Conference on Applications of Dynamical Systems
  Award amount of **$2650.00**
- SIAM Travel Grant for Conference on the Life Sciences and Annual Meeting **2014**
  Award amount of **$1150.00**

INVITED TALKS

1. "Spatiotemporal IDE model predicts invasion rate and outbreak severity of mountain pine beetle epidemics" The Annual Meeting of the Canadian Applied and Industrial Mathematics Society (CAIMS 2016), University of Alberta, Edmonton, AB, June 2016.

CONTRIBUTED TALKS

1. "Spatiotemporal IDE model predicts invasion rate and outbreak severity of mountain pine beetle epidemics" The 8th International Congress on Industrial and Applied Mathematics (ICIAM), Beijing, China, August 2015.

2. "A model for mountain pine beetle outbreaks in an age structured forest: Approximating severity and outbreak-recovery cycle period" SIAM Conference on Applications of Dynamical Systems, Snowbird, Utah, May 2015.
3. "Predicting severity and periodicity of mountain pine beetle outbreaks: An age structured forest demographic model with temperature dependent MPB infestation," Mathematical Association of America (MAA) Intermountain Conference, Orem, Utah, March 2014.

POSTERS

1. "Predicting invasion rates of *Phragmites australis*," Society for Mathematical Biology Conference, Atlanta, Georgia, July 2015.
2. "Predicting severity and periodicity of mountain pine beetle outbreaks," SIAM Life Sciences Conference, Charlotte, North Carolina, August 2014.

MENTORING EXPERIENCE

- Graduate Student Research Mentor - Rachel Nydegger **2014 - Present**
  - Co-mentored with James Powell
  - Poster: "Predicting invasion rates of *Phragmites australis*"
    Presented at 2015 Annual Meeting of the Society for Mathematical Biology
- Co-mentor in USU Mathematical Biology Lab **2013 - Present**
  (graduate and undergraduate students)
- Undergraduate Student Research Mentor - Ethan Williams **Spring 2014**
  - Co-mentored with Brynja Kohler
  - Modeling stretch-reflex motoneuron pools and clonus
    Manuscript in preparation
- Undergraduate Student Research Mentor - Timothy Schaefer **Spring 2009**
  - Co-mentored with Namyong Lee
  - Poster: "Synchronization of coupled oscillators in space: A modified Kuramoto model"
    Presented at Undergraduate Research Conference 2009,
    Minnesota State University, Mankato, MN

PROFESSIONAL SERVICE

- President, Utah State University SIAM Student Chapter **January 2015 - present**
- Vice President, Utah State University SIAM Student Chapter **January 2014 - January 2015**
- Member, Society for Industrial and Applied Mathematics **2013 - present**
- Member, Society for Mathematical Biology **2013 - present**
- Manuscript Reviewer, *Bulletin of Mathematical Biology.* **2015**

COMMUNITY OUTREACH

- Science Unwrapped participant (USU's family friendly, science–community interface)
  - Contributed research talk/poster on Mathematical Modelling of Insect Outbreaks **2014**
  - Contributed research talk/poster on Invasive Species Spread Rate Prediction **2015**